UNIVERSIDAD NACIONAL AUTÓNOMA DE MÉXICO

POSGRADO EN CIENCIAS DE LA TIERRA
CENTRO DE GEOCIENCIAS

ANÁLISIS HIDRÁULICO-MECÁNICO DE FLUJO DE AGUA SUBTERRÁNEA Y RESPUESTA DE LA FASE SÓLIDA POR MEDIO DE MODELADO ACOPLADO

T E S I S

QUE PARA OPTAR POR EL GRADO DE:
DOCTOR EN CIENCIAS DE LA TIERRA
(Agua subterránea)

PRESENTA:
Gil Humberto Ochoa González

Directora de Tesis:
Dra. Dora Celia Carreón Freyre
Centro de Geociencias

JURIQUILLA, QUERÉTARO. ABRIL 2020

Declaro conocer el Código de Ética de la Universidad Nacional Autónoma de México, plasmado en la Legislación Universitaria. Con base en las definiciones de integridad y honestidad ahí especificadas, aseguro mediante mi firma al calce que el presente trabajo es original y enteramente de mi autoría. Todas las citas de, o referencias a la obra de otros autores aparecen debida y adecuadamente señaladas, así como acreditadas mediante los recursos editoriales convencionales.

I N D I C E

Resumen 2

Introducción 4

Capítulo I. “Modeling the deformation of faulted volcano-sedimentary sequences associated to groundwater withdrawal in the Querétaro Valley, Mexico” 8

Capítulo II. “Assessment of groundwater flow in volcanic faulted areas. A study case in Queretaro, Mexico” 16

Capítulo III. “Shearing along faults and stratigraphic joints controlled by land subsidence in the Valley of Queretaro, Mexico” 39

Capítulo IV. “Overexploitation of groundwater resources in the faulted basin of Queretaro, Mexico: a 3D deformation and stress analysis” 58

Discusión 74

Conclusiones 77

Agradecimientos 78

Referencias 79

RESUMEN

Durante el desarrollo del proyecto doctoral se publicaron cuatro trabajos de investigación que buscan mejorar la comprensión del flujo de agua subterránea y las condiciones de deformación en el subsuelo de la Ciudad de Querétaro. En los modelos presentados se considera la alta heterogeneidad estratigráfica y estructural del subsuelo que presenta alternancias de materiales volcánicos, vulcanosedimentarios y fallamiento regional. En una primera etapa el trabajo se centró en el estudio del flujo de agua subterránea y de la distribución del abatimiento de niveles piezométricos causados por la extracción excesiva. Se realizaron modelos numéricos para simular la deformación en el contexto geológico de Querétaro, acoplando el incremento del esfuerzo efectivo en materiales granulares (en la fase sólida) al disminuir la presión de poro. Los primeros análisis de deformación se realizaron en las secuencias someras fluvio-lacustres (Ochoa-González et al., 2013), estas secuencias fueron definidas al establecer los modelos y su geometría y distribución se mantuvo constante en cada modelo.

Posteriormente, se trabajó en la simulación de abatimientos piezométricos integrando las fallas geológicas y el truncamiento estratigráfico asociado. Los resultados obtenidos muestran que las fallas pueden funcionar como barreras limitantes del flujo transversal entre ambos lados, aun cuando la zona de falla podría funcionar como canal de flujo (Ochoa-Gonzalez et al., 2015). El incremento de esfuerzos efectivos se relacionó con la ruptura de pozos en discontinuidades geológicas a diferentes profundidades (juntas estratigráficas y fallas) (Carreón Freyre et al., 2016). La modelación geomecánica permitió determinar las concentraciones de esfuerzos y deformaciones en zonas de discontinuidad en tres dimensiones. En un trabajo final se relacionan los desplazamientos verticales con la subsidencia previamente reportada y las deformaciones horizontales con distintos sistemas de fracturamiento en el medio granular (Ochoa-González et al., 2018).

El trabajo desarrollado ha permitido integrar diferentes aspectos del fenómeno de subsidencia en un modelo que es coherente con las mediciones de abatimientos piezométrico y con deformaciones observadas en superficie, como hundimientos, desplazamiento de fracturas y cizallamiento de pozos. Se utilizó el código numérico de la Universidad de Padua para crear un modelo numérico que permite hacer una valoración adecuada de la subsidencia y fracturamiento causados por la extracción excesiva de agua subterránea en la Ciudad de Querétaro. El modelo puede ser utilizado también como una herramienta de gestión para estimar la posible afectación de la extracción excesiva de agua subterránea la infraestructura urbana.

ABSTRACT

During the development of the doctoral project, four research papers were published that seek to improve the understanding of groundwater flow and deformation conditions in the subsoil of the City of Querétaro. The models presented consider the high stratigraphic and structural heterogeneity of the subsoil, shown as alternations of volcanic and sedimentary layers crossed by regional faults. In the first stage, the work focused on the study of groundwater flow and the distribution of piezometric level depletion due to over-exploitation. Numerical models were made to simulate deformation according to the Queretaro geological context, by coupling the increase of the effective stress in granular materials (in the solid phase) with the decrease of the pore pressure. The first deformation analyzes were performed in the shallow fluvio-lacustrine sequences (Ochoa-González et al., 2013), these sequences were defined when establishing the models and their geometry and distribution remained constant in each model.

Subsequently, the work has been addressed to the simulation of piezometric withdrawal integrating geological faults and the associated stratigraphic truncation. The results obtained show that the faults can function as limiting barriers of the transverse flow between both sides; even though the fault zone may function as a flow channel (Ochoa-Gonzalez et al., 2015). The increase of effective stresses was related to the rupture of wells in geological discontinuities (stratigraphic joints and faults) at different depths (Carreón-Freyre et al., 2016). Geomechanical modeling allowed to determine stress concentrations, displacements and deformations in discontinuity zones in three dimensions. In a final work, vertical displacements are related to the previously reported subsidence and horizontal deformations with different fracturing systems in the granular materials (Ochoa-Gonzalez et al., 2018).

The developed work has allowed the integration of different aspects of the subsidence phenomenon in a model that is consistent with measurements of piezometric declines and with deformations observed in the surface, such as settlements, fracture displacements and shearing of wells. The numerical code of the University of Padua was used to create a model that allows an adequate assessment of the subsidence and fracture caused by excessive groundwater extraction in the City of Querétaro. The model can also be used as a management tool to estimate the possible impact of excessive groundwater extraction on urban infrastructure.

INTRODUCCIÓN

El fenómeno de subsidencia del terreno por extracción de agua subterránea se ha estudiado y documentado en diferentes partes del mundo (UNESCO, 1984). La relación entre la extracción de fluidos y el hundimiento se ha establecido desde hace varias décadas, de manera empírica o semi empírica (Wadachi 1940, Hwang y Wu 1969, Castle, Yerkes y Riley 1969) comparando mediciones o volúmenes de extracción de agua, gas y petróleo. En la literatura se reportan distintas relaciones entre ambos fenómenos, la primera explicación teórica (aún la más utilizada) se basa en la teoría de consolidación unidimensional de Terzaghi (1923), en la cual los esfuerzos efectivos se incrementan cuando la presión de agua de poro disminuye. El incremento de esfuerzos efectivos tiene como consecuencia la consolidación o compactación de los materiales que conforman los acuíferos granulares. Un modelo numérico desarrollado para simular este fenómeno es presentando por Hoffmann y colaboradores (2003) basado en el programa de diferencias finitas de simulación de agua subterránea MODFLOW (Harbaugh, 2000).

La hipótesis de este trabajo se basa en la teoría de consolidación que indica que, durante la extracción excesiva de agua subterránea, es decir cuando la descarga es mayor que la recarga y se genera una disminución de la presión del agua, las propiedades físicas y mecánicas de las secuencias que conforman un acuífero granular determinan el acomodo de la deformación asociada al incremento de esfuerzo efectivo. La subsidencia y fracturamiento observados en la superficie terrestre se deben a deformaciones acumuladas en diferentes profundidades y que dependen de las condiciones geológicas especificas en cada sitio de estudio. La distribución de la deformación debe entonces realizarse en tres dimensiones y evaluar su variación con el tiempo.

Cuando el basamento de los materiales granulares compresibles presenta una topografía irregular, como un basamento rocoso afectado por fallas, la compresión del sistema acuífero genera diferentes tipos de esfuerzos, así como hundimientos diferenciales en la superficie. Esto a su vez puede generar fracturas que pueden de dañar la infraestructura urbana, como se ha reportado en diferentes lugares del mundo y de México (Galloway y Burbey, 2011, Carreón 2010). La simulación en tres dimensiones de la deformación permite el análisis detallado de los hundimientos diferenciales y los esfuerzos generadores de fracturas que la teoría generalizada de consolidación unidimensional (Galloway y Sneed, 2013). En el análisis realizado en este trabajo se utilizaron técnicas de modelación numérica, como el método de elementos finitos (Teatini y colaboradores 2006) y la teoría de consolidación tridimensional de Biot (Biot 1941).

En México el fenómeno de subsidencia se ha reportado en diferentes estados y ciudades como la Ciudad de México; Abasolo, Celaya y Salamanca (en Guanajuato), Aguascalientes (en Aguascalientes), Ciudad Guzmán. Jocotepec y Ameca (en Jalisco) y Querétaro (en Querétaro). En la ciudad de Querétaro se han reportado fracturas desde hace un par de décadas por Trejo y Martínez (1991); y Rojas et al. (2002). En esta ciudad se ha recopilado información sobre la evolución de los niveles piezométricos medidos por el personal del organismo operador estatal de agua (CEA), con lo cual se puede calcular y evaluar el comportamiento de los abatimientos. También existe información sobre el hundimiento superficial y la aparición de fracturas durante las últimas dos décadas (Pacheco y colaboradores 2006, Chaussard y colaboradores 2014).

El objetivo general del trabajo es estudiar la relación que existe entre el abatimiento piezométrico y las deformaciones asociadas principalmente en medios granulares, así como sus variaciones espaciales y temporales. Se evalúa también la influencia de fallas geológicas mayores en las condiciones generales de flujo y deformación.

Para el análisis de la subsidencia en la ciudad de Querétaro, se estableció la configuración geológica del subsuelo tomando en cuenta el modelo conceptual reportado por Carreón Freyre et al. (2005) e integrando información de fallas y otras estructuras geológicas reportadas por Alaniz y colaboradores (2001), Xu y colaboradores (2011). Se definieron las unidades estratigráficas principales con características hidráulicas y mecánicas especificas como compresibilidad, conductividad hidráulica y capacidad de almacenamiento. Durante el desarrollo de los modelos propuestos se consideraron la interdigitación de unidades geológicas y la influencia de las fallas, que segmentan el sistema de manera hidráulica y localizan la deformación superficial.

El trabajo de investigación se desarrollo de la siguiente manera, en el primer trabajo se integró en un modelo numérico la información disponible piezométrica y geológica (Ochoa González et al., 2013). El primer modelo fue la base para entender la forma y distribución del sistema acuífero, así como el impacto o la influencia que tienen las discontinuidades en la respuesta a la extracción de agua. En el segundo trabajo (Ochoa González et al., 2015), se analiza el comportamiento hidráulico de las fallas y su repercusión en el flujo de agua subterránea y el abatimiento. Las fallas se analizaron como como unidades acuíferas independientes y no solo como truncamiento de unidades estratigráficas. En el tercer trabajo (Carreón Freyre et al., 2016) se integró información geológica e hidrológica así como resultados de modelos numéricos, para evaluar los mecanismos de falla de pozos de extracción de agua subterránea reportados en la zona de estudio. Se presenta un modelo conceptual sobre la distribución de esfuerzos de cizalla y de compresión a diferentes profundidades. En el cuarto trabajo (Ochoa González et al., 2018) se realizó la simulación numérica de la evolución de los esfuerzos y de las deformaciones en el tiempo y las variaciones de su distribución espacial. Los resultados obtenidos se correlacionaron con observaciones reales de abatimiento, hundimiento y fracturamiento para diferentes tiempos.

En los siguientes párrafos se describe brevemente cada capítulo.

En el **Capítulo I** (Ochoa González et al., 2013) se presenta una simulación numérica del abatimiento piezométrico y de la consolidación de las diferentes unidades que conforman el sistema para relacionarlos con el hundimiento y fracturamiento asociado. Se conformó un modelo con información geológica, geofísica y de abatimientos piezométricos incluyendo la unidad granular somera y las unidades inferiores a la unidad rocosa conformada por andesitas y basaltos del Mioceno Tardío (Tmt AB). El modelo acopla los fenómenos de flujo de agua subterránea y la deformación de los materiales debido a los cambios de presión de agua de poro durante un periodo de 30 años utilizando la teoría de poroelasticidad de Biot (1941). La correcta representación geométrica de las diferentes unidades geológicas fue fundamental para alcanzar resultados representativos. La simulación de la consolidación del sistema permitió evaluar las condiciones de hundimiento de la superficie del terreno, los resultados obtenidos coinciden en la distribución y en las magnitudes observadas en campo. Los campos de esfuerzos y deformaciones se calcularon para la superficie del modelo, los resultados muestran que las zonas de mayor hundimiento no necesariamente coinciden con las zonas de mayor abatimientos piezométrico y que la distribución de las fallas geológicas afecta a los patrones de abatimientos y de hundimientos, como ya había

sido reportado por Carreón Freyre et al. (2005). El análisis presentado en este capítulo se enfoca en el modelo numérico de la zona central del graben de Querétaro para definir las condiciones óptimas de frontera. Las propiedades principales de los materiales, conductividad hidráulica, almacenamiento y compresibilidad fueron calibradas con mediciones de campo y laboratorio. Los valores de almacenamiento y de compresibilidad están relacionados entre sí por lo que se ajustaron de manera iterativa. El modelo permitió definir valores preliminares de las propiedades hidráulicas del sistema.

En el **Capítulo II** (Ochoa González et al., 2015) se estudia la influencia de las fallas geológicas y de estructuras intrusivas en el flujo de agua subterránea y comportamiento hidráulico del sistema en una zona al norte del graben de Queretaro. En estudios previos se ha documentado que las fallas geológicas determinan patrones complejos en el flujo de agua subterránea (Caine, Evans y Forster, 1996; Allenaan y Michel, 1999; Rafini y Larocque, 2012). Los resultados del modelo fueron calibrados con el análisis de una prueba de bombeo. Se llevó a cabo una simulación de la misma prueba (descrita en el capítulo) con un modelo numérico de diferencias finitas que permitió mejorar su interpretación. En esta zona también se presenta una estratificación de materiales con propiedades contrastantes, además está afectada por dos fallas geológicas y se ha documentado la presencia de un cuerpo intrusivo. Todas estas estructuras fueron incluidas en el modelo desarrollado como unidades hidráulicas independientes. El periodo de tiempo simulado fue de 72 horas, igual a la duración de la prueba de bombeo que se monitoreó constantemente. En la simulación se incluyó el gradiente hidráulico regional como condición inicial y de frontera, se analizó la conductividad hidráulica horizontal y vertical del sistema, no se integró la compresibilidad de los materiales. En el proceso de calibración se utilizó el algoritmo PEST (Doherty 2005) que permitió identificar la sensibilidad del modelo a las propiedades de diferentes materiales y establecer los valores significativos de conductividad hidráulica. La simulación generó altos gradientes hidráulicos perpendiculares a los planos de falla debido a la diferencia de niveles piezométricos en las unidades adyacentes, que funcionan como barrera de flujo. También se observaron gradientes dentro de las fallas con la misma orientación y con magnitud suficiente para generar un flujo interno dentro de ellas, que funcionan como conducto preferencial. El uso de modelos 3D para simular el abatimiento piezométrico permitió analizar la distribución de gradientes bajo distintas condiciones estructurales. Se realizó también un análisis de las derivadas de los abatimientos, independiente de la simulación, con la finalidad de identificar tipos coexistentes de flujo entre las fallas y la matriz rocosa. Como resultado de este análisis se presenta la configuración de las tasas de abatimientos y se identifican posibles tipos de flujo en la matriz rocosa y dentro de las fallas. Los resultados de la simulación sugieren que un flujo regional puede ser canalizado a través de las fallas mayores.

En el Capítulo III (Carreón Freyre et al., 2016) se analiza la ruptura reportada de pozos de extracción de agua subterránea asociada a la localización de esfuerzos de cizalla y se estudia el rol de los gradientes hidráulicos en el incremento de esfuerzos durante un periodo de 11 años. Se proponen posibles mecanismos de desplazamiento de los materiales a los lados de fallas y de las interfaces estratigráficas. Asimismo, se relaciona la ubicación de los pozos y la profundidad de ruptura con los contactos entre distintas unidades geológicas. Se presenta un modelo conceptual 2D para analizar la distribución de esfuerzos, desplazamientos y deformaciones en diferentes profundidades; generados por el incremento de la presión efectiva al abatirse los niveles de agua subterránea de manera irregular. En este trabajo se simula el incremento de esfuerzos efectivos mediante un modelo equivalente de incremento diferencial de presión en superficie para estudiar la distribución

de esfuerzos en los contactos entre unidades y en las fallas. Los resultados muestran un relación directa entre la localización de esfuerzos de cizalla y las zonas de ruptura de los pozos. Para la realización de este trabajo llevé a cabo el modelo numérico y las secciones geológicas en dos y tres dimensiones, así como el análisis de abatimientos y de gradientes hidráulicos y de su relación con las fallas geológicas.

En el Capítulo IV (Ochoa González et al., 2015) se presenta un modelo con geometría similar a la presentada en el Capítulo I, con modificación de condiciones de frontera e incluyendo tasas variables de explotación del agua subterránea. También se ajustaron las propiedades físicas de los materiales para calibrar el modelo con las mediciones de hundimientos reportadas por Chaussard y colaboradores (2014) utilizando métodos de percepción remota. Asimismo, se utilizaron valores de compresibilidad de materiales representativos medidos en laboratorio y se integraron las conductividades hidráulicas reportadas por Carrera-Hernández y colaboradores (2016) para las mismas unidades geológicas. Con las nuevas condiciones de frontera y la calibración del modelo llevó a cabo una simulación de abatimientos y hundimientos con un mejor ajuste con las mediciones de campo. En este capítulo se utiliza un modelo geomecánico para analizar los campos de esfuerzos y deformaciones de manera tridimensional en toda la geometría del modelo. La distribución se analizó a diferentes profundidades y se relacionó las deformaciones y esfuerzos con las fracturas cartografiadas en superficie.

Capítulo I. "Modeling the deformation of faulted volcano-sedimentary sequences associated to groundwater withdrawal in the Querétaro Valley, Mexico". Publicado en proceedings 20th international congress of modelling and simulation, Adelaide, Australia, diciembre 2013, indexado en Web of Science's Conference Proceedings Citation Index (CPCI)

20th International Congress on Modelling and Simulation, Adelaide, Australia, 1–6 December 2013
www.mssanz.org.au/modsim2013

Modeling the deformation of faulted volcano-sedimentary sequences associated to groundwater withdrawal in the Querétaro Valley, Mexico

G.H. Ochoa-González [a], P. Teatini [b], D. Carreón-Freyre [c], and G. Gambolati [b]

[a] *Western Institute of Technology and Higher Education (ITESO), Jalisco, Mexico*
Email: gilochoa@iteso.mx
[b] *Dept. of Civil, Environmental and Architectural Engineering, University of Padova, Italy*
[c] *Centro de Geociencias, National Autonomous University of Mexico, Queretaro, Mexico*

Abstract: The City of Querétaro is located on a graben structure that formed a continental basin filled since the Oligocene time with volcanic and sedimentary materials. In the N-W direction two major normal faults are dipping to the West and the thicknesses of the filling materials vary many tens of meters in close distances. The filling materials include lacustrine and alluvial sediments, pyroclastic deposits, and interbedded fractured basalts. Hence, important differences of hydraulic and mechanical properties characterize the various units.

Groundwater was been strongly withdrawn over the last three decades in the study area, with a level decline exceeding than 100 m in some areas. Because of the high variability of the geological deposits, a space variable decrease of the piezometric levels, and consequently of the effective stress increase, has been observed. Piezometric variations are also due to faults that strongly impact on groundwater flow dynamics. The variable distribution of the effective stress increase has caused large differential subsidence causing ground fracturing that has damaged the urban infrastructures of the City of Querétaro.

The geological heterogeneities of the subsoil were integrated into a flow and geomechanical model to predict the deformation caused by fluid withdrawal. Initially the hydrodynamics of the pumped aquifer system was simulated by a 3-D groundwater flow model and then the subsidence was computed with the aid of a 3-D poro-mechanical model with the pore pressure field specified as an external distributed source of strength within the porous medium. The model is calibrated using observed groundwater and land settlement records, with the generated three-dimensional stress field that is compared with the distribution of the major fractures detected in the city.

The aim of this work is to predict the differential deformation of the faulted volcano-sedimentary sequences. The simulation is carried out by an advanced three-dimensional finite-element flowdynamic-geomechanical code. The conceptual model was accurately defined using the correlation of geological logs of extraction wells, field mapping of faults, fractures, and the integration of major structures reported in previous geophysical works. The stratigraphic sequences were simplified with seven mayor hydrogeological units with specific mechanical properties, hydraulic conductivity, and storage capacity. The 30 years records of piezometric level were used to simulate groundwater depletion and the resulting land subsidence.

The results of the geomechanical simulations show that the areas where large differential subsidence developed correspond to the portions of the city where earth fissuring have been observed. The spatial relationship between major withdrawals and the largest simulated subsidence is assessed.

Keywords: *Groundwater withdrawals, land subsidence, earth fissuring, modeling, Querétaro (Mexico)*

1. INTRODUCTION

Climate changes and, in particular, the decrease in precipitation and increase in temperature, are a very severe problem in desert and semi-desert populated environments, and even more when they are associated with a rapid urban development. This is a typical situation of several cities in the Transmexican Volcanic Belt (Karmalkar et al., 2011), such as Querétaro, Morelia, Celaya, and the most famous case of Mexico City. In this portion of the central Mexico, the groundwater extraction from local aquifers is the primary source of water supply and contributes more than 70% to the water needs of more than 100 million inhabitants (INEGI, 2011). Overdraft of groundwater resources and, secondarily, the reduction of the natural recharge, have led to a dramatic piezometric decline up to 100 m in some sites. The consequent consolidation of the sedimentary/volcanic basins resulted in land subsidence with rates of the order of 10 cm/yr associated with earth fracturing (Figure 1) (e.g., Pacheco et al., 2006; López-Quiroz et al., 2009; Carreón-Freyre, 2010). In Querétaro as well, the main concern is overexploitation of aquifers that, since the fifties, have provided water to the inhabitants of this Valley and are alarmingly experiencing large piezometric decline from a few meters to about 120 m. Withdrawal has been recently estimated at 110 million m^3/yr while the total recharge is around 70 million m^3/yr. The valley is composed by highly heterogeneous sand-and-silt sediments with intercalated pyroclastic layers. Failure of the sequence is caused by a differential compaction of the sedimentary deposits and the presence of a pre-existing buried fault scarp (Carreón-Freyre et al., 2005a).

The complexity of the geological system, the piezometric evolution due to groundwater pumping, and the related land subsidence are addressed in this study with the aid of advanced three-dimensional (3-D) finite-element (FE) flow and geomechanical models. The occurrence is reconstructed since 1970. The model is calibrated using observed groundwater and land settlement records with the three-dimensional stress accumulation compared with the distribution of the major fractures mapped in the city.

2. QUERÉTARO VALLEY

The study area is located in the southern part of the City of Queretaro, on a graben structure formed by orthogonal normal faults with approximate trending N-S and E-W within the regional geological unit named Transmexican Volcanic Belt (TMVB) (Alaniz-Alvarez et al. 2001). The N-S trending west-dipping Central fault is the eastern limit of the regional Queretaro graben (Figure 2). Other major faulting family (trending NE-SW) produced a nearly orthogonal pattern with the N-S system that has resulted in a mosaic formed by horsts, grabens, and half-grabens (Xu et al. 2011) with varying vertical displacements, in some areas up to 400 m. Both fault systems have been active at least since the Miocene (Alaniz-Alvarez et al. 2001and controlled the deposition of sediments and volcanic rocks.

Figure 1. Photo of Querétaro, Cayetano Rubio Street, showing the effect of differential land subsidence due to groundwater withdrawals. The large displacement gradients are responsible for earth fissuring producing significant economic losses and increasing the safety issues in the urban area.

2.1. Hydrogeological Setting

The sedimentary-volcanic basin of the Querétaro Valley is made from seven major geologic units (Figure 3). Some of them are mainly porous formations and other mainly fractured units. Porous deposits are thought to be the more compressible than fractured rocks, and therefore characterized by a larger capability to store water.

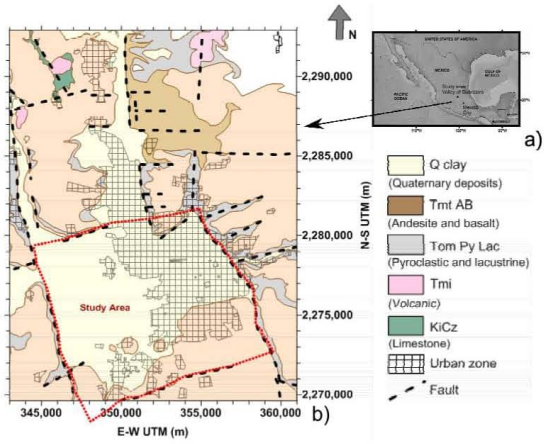

Figure 2. Location of the study site (a) and geological map of the Querétaro valley (b). The simulated area is highlighted by a dotted red line.

The units are listed in the following order from top to bottom: 1) Q clay: Quaternary clays: lacustrine, surficial and thin deposits with low permeability; 2) Tp Ar-Cg: sediments and volcanic rocks, the first main porous unit; 3) Tmt AB: Andesitic and Basaltic fractured unit; 4)Tom Py Lac: pyroclastic and lacustrine deposits forming the second main porous unit; 5) Tmm AB: older Andesitic and Basaltic fractured unit underlying TomPyLac; 6) To AB: another Andesitic and Basaltic fractured unit, adjacent to the TmmAB; it is characterized by a different degree of fracturing relative to Tmm AB, and hence has different hydrogeologic properties; 7) Base: even if probably other porous/fractured materials exist below To AB (Carreon-Freyre et al., 2005b), we assume that the base unit confines the compressible sequences from which groundwater is withdrawn; this unit was simulated in the model as a low permeability and rigid material.

2.2. Groundwater Resources Withdrawn and Land Deformation

Figure 4 shows the drawdown in some wells in Queretaro from 1970 to 2012. The average withdrawn trend deemed to be most representative for the Querétaro valley is marked in blue solid lines. Between 1970 and 1975 the average decline rate of these wells was less than 2 m/yr; after 1975 the slope increased to 3 m/yr. Some wells exhibit a different behavior: a significantly lower withdrawal (green dashed lines), a behavior similar to the average rate but presenting a slightly lower rate of depletion in the last measurements (yellow lines), and two wells with a drawdown higher than the average (gray dotted lines). Most of the wells other than the blue group are located in faulted zones.

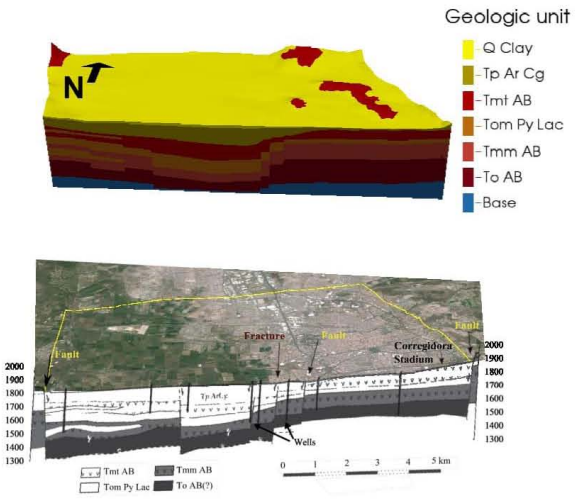

Figure 3. Comparison between the geological model used in the simulation and a geological section reconstructed by Carreon-Freyre et al. (2005b).

Earth fissuring due to groundwater withdrawal have been reported in Querétaro City since 1986. The occurrence is strongly affecting the urban infrastructures (Trejo and Martinez 1991). Particularly fracturing has been associated in Querétaro with the differential subsidence caused by the variations in thicknesses of the compressible layers (Rojas et al., 2002).

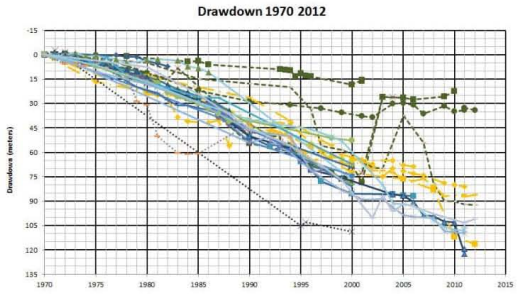

Figure 4. Historical drawdown from 1970 to 2012 in the Querétaro Valley. Blue colors indicate the average trend.

3. MODELLING SOIL DEFORMATION DUE TO GROUNDWATER PUMPING

3.1. Modelling Approach

The deformation of a porous medium caused by fluid withdrawal is theoretically described by the three-dimensional fully coupled poroelasticity model originally developed by Biot (1941). Typically, one-way coupling between the flow and the strain fields is assumed in the classical groundwater hydrology (e.g., Gambolati et al., 2000; Teatini et al., 2006), with the hydrodynamics of the pumped aquifer system first simulated by a 3-D groundwater flow model and the subsidence then computed with the aid of a 3-D poromechanical model with the pore pressure field specified as an external distributed source of strength within the porous medium.

For the sake of simplicity, the modelling approach is based on the assumption of a potential flow problem. Hence in the preliminary simulations that follow, the aquifer hydrodynamics is governed by the classical groundwater flow equation:

$$\nabla(K\nabla h) = S_s \frac{\partial h}{\partial t} + q \tag{1}$$

where h is the hydraulic head, t is time, q the source/sink, and S_s the specific elastic storage. Equation (1) is solved in space by linear finite elements (tetrahedra) and in time by a weighted finite difference scheme.

The incremental pressure $p = \gamma_w \Delta h$, with γ_w the specific weight of water, induced by water pumping is used in the geomechanical model to compute the medium displacements. The equilibrium equations for a mechanically isotropic elastic porous medium, in terms of incremental quantities, read (e.g., Verruijt, 1969):

$$G\nabla^2 u_i + (G+\lambda)\frac{\partial \varepsilon}{\partial i} = \frac{\partial p}{\partial i} \qquad i = x, y, z \tag{2}$$

where u_i is the displacement component along the i-th coordinate direction, λ and G are the Lamè constant and the shear modulus of the porous medium, respectively, and ε is the volume strain. The solution to equations (2) is obtained by finite elements using the same tetrahedral elements as the groundwater flow model.

The parameters S_s and G are linked through the following well-known relations:

$$S_s = \gamma_w (c_M + \phi\beta) \quad ; \quad c_M = \frac{1}{\lambda + 2G} = \frac{(1+\nu)(1-2\nu)}{E(1-\nu)} \quad ; \quad G = \frac{E}{2(1+\nu)} \tag{3}$$

with c_M the oedometric bulk compressibility, ϕ the medium porosity, β the water volumetric compressibility, E the Young modulus, and ν the Poisson ratio. The c_M used to form S_s or to compute E, λ, and G is the same in both the flow and the geomechanical models.

The numerical approach used in this preliminary modelling study does not address explicitly failure generation and fissure mechanics due to groundwater pumping, e.g. by the use of appropriate formulation such as the Interface Elements (Ferronato et al., 2008). However, the 3-D geomechanical analysis allows for the computation of the complete stress field:

$$\sigma_i = 2G\frac{\partial u_i}{\partial i} + \lambda\varepsilon \quad ; \quad \tau_{i,j} = G\left(\frac{\partial u_j}{\partial k} + \frac{\partial u_k}{\partial j}\right) \qquad i,j,k = x,y,z \tag{4}$$

with the fissure generation and/or activation that are more likely to occur where the normal stress component σ assumes negative (i.e., tensile) values or the tangential stress τ is relatively large with respect to compressive stress.

3.2. Model set-up

The simulated area (Figure 5) includes the oldest urban area and the surrounding farmland. This area is delimited by mayor geological structures (faults), but there are also faults inside the modeled domain. These latter cannot be observed at the ground surface but their geometry was defined with the aid of lithological well logs and geological and geophysical profiles.

The digital elevation model (DEM) represents the top surface of the domain. The thickness of the geologic units and discontinuities caused by faulting were obtained by analyzing 46 wells logs with varied depths, 11 gravimetric profiles (Pacheco et al., 2006), the geological profile showed in Figure 2 (Carreon-Freyre et al., 2005b), and geological profiles made for the purpose. The bottom boundary of the model, which is assumed to be a no flow surface, is represented by the top of the Base unit.

The model accounts for the seven main materials that compose the sedimentary-volcanic basin. A horizontal view of the mesh is shown in Figure 5. The mesh consists of 267,385 nodes and 1,520,244 tetrahedra, with each unit subdivided into 1 to 10 FE layers.

The flow model, which is solved in term of piezometric drawdown from 1970, uses an initial equilibrated condition with the water elevation fixed to a constant reference value. This is surely an approximation of the actual condition but it is quite effective for the computation of the forcing term for the geomechanical simulations. Fixed Dirichlet conditions are prescribed along the lateral boundaries assuming a zero piezometric change over time.

The model is stressed by the water extraction from 123 wells (Figure 4) over a period of 31 years (11500 days), i.e. from 1970 to 2001. Pumping rates are known for 21 wells. The remaining 102 well rates were estimated on the basis of other available information. Standard Dirichlet conditions are assumed in the geomechanical model. The basement is assumed to be fixed, the horizontal displacements of the outer boundaries are precluded and the top surface is left free to move both vertically and horizontally. The 1970 setting is assumed as the reference equilibrated state.

4. MODELING RESULTS

The modeling results show a maximum drawdown of 160 m to the East of the "Las Campanas" hill with a flux boundary associated to the "5 de Febrero" fault (Figure 6a). Contrasting hydraulic gradients can be observed in both East and West sides of the fault. On the other hand, surface deformation is localized in the West side of the fault (dark zone in Figure 6b) with a maximum vertical displacement equal to 2 m corresponding to a deformation rate of 6.5

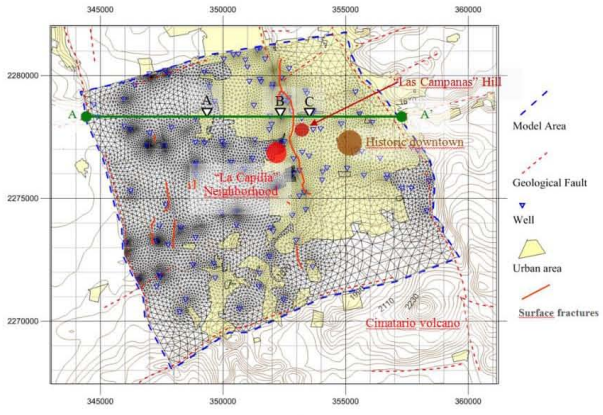

Figure 5. Horizontal projection of the 3D FE grid with the location of the main well fields used to withdraw water from the subsurface. The dashed red lines correspond to major normal faults delimiting the study area. The topographic elevation is represented by the brown curves.

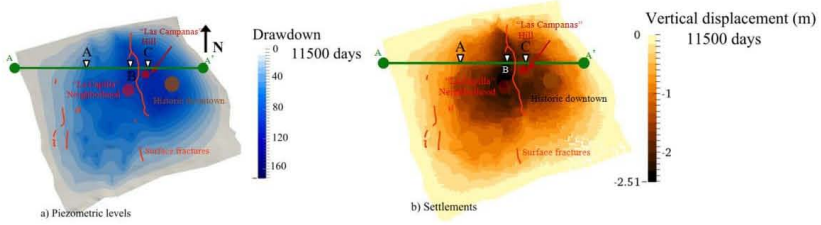

Figure 6. Simulated piezometric level and cumulative land subsidence between 1970 and 2001.

cm/yr. In the west side of the fault the deformation rate was less than 3 cm/yr.

These results provide evidence that land subsidence cannot be related to the piezometric change only. It appears that the variation of thickness and compressibility of the granular materials plays a major role. In the model section of Figure 7, the differences in subsurface structure and the relationship between the distribution of hydrostratigraphic units and water withdrawn are shown. On the ground surface (Figure 6) a higher drawdown within fractured volcanic rock units with a lower specific elastic storage and a lower deformability can be observed (**C zone,** nearby "Las Campanas" hill). At **B zone,** a thicker granular sequence and the "5 de Febrero" fault may influence the hydraulic behavior (Figure 6). The higher drawdown occurs at shallower depths (approximately 150 m) and is localized in the granular area with 100 m thickness. The **A zone** is located in an area with thicknesses similar to the other zones; the normal faulted bedrock (Figure 7) affect the piezometric variations versus depth. In this zone the surface deformation does not seem to reflect the deep structural variations but is mainly related to the surface drawdown.

Groundwater depletion and vertical deformation for the three studied zones of the section are provided in Table 1.

Table 1. Comparison between drawdown and surface settlement for the sites highlighted in Figures 6 and 7.

	A Point	**B** Point	**C** Point
Water drawdown at surface (m)	73.44 (min.)	106.93	122.06 (max.)
Surface settlement (m)	1.11 (min.)	2.25 (max.)	1.78

5. DISCUSSION AND CONCLUSION

This work presents a modeling investigation on the relationship between the variability of the geomechanical properties and the differential deformation of the Querétaro volcano-sedimentary sequences. This issue has not been addressed in the literature. Since the early 80s, the influence of bedrock topography on the deformation and fracture generation of overlying granular materials has been reported (Jaechens and Holzer, 1982) and many further studies were focused on this aspect. The modeling results presented here show that thickness variations of fractured volcanic and granular units directly affect the pressure changes in the deep layers and the deformation at the surface. Model outputs suggest that the larger land subsidence is not necessarily associated with the major withdrawn, as mentioned by Bell (2002). Model sections allow for a better understanding of groundwater depletion in zones B and C, which could not be achieved only with local piezometric measurements. The model can be further improved using the actual initial piezometric surface (instead of a flat one) and more realistic flow boundary conditions.

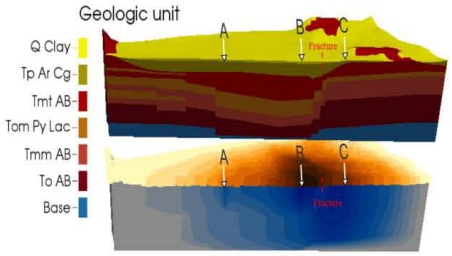

Figure 7. Vertical section of the model showing the subsoil structure and the variations of groundwater pressure in depth. Maximum depth is approximately 500 m.

REFERENCES

Alaniz-Alvarez S.A., Nieto-Samaniego A.F., Reyes-Zaragoza M.A. (2001) Estratigrafía y deformación extensional en la región San Miguel de Allende-Querétaro, México (Stratigraphy and extensional deformation in the San Miguel de Allende-Queretaro region, Mexico). *Revista Mexicana de Ciencias Geologicas* 18(2):129-148.

Bell, J.W., Amelung, F., Ramelli, A.R., Blewitt, G. (2002). Land Subsidence in Las Vegas, Nevada, 1935–2000: New Geodetic Data Show Evolution, Revised Spatial Patterns, and Reduced Rates. *Environmental & Engineering Geoscience*, 8 (3), 155-174.

Biot, C. (1941). General theory of three-dimensional consolidation. *Journal of Applied Physics*, 12(2), 155-164.

Carreón-Freyre, D., Cerca Martínez, M., and Hernández Marín, M. (2005a). Propagation of fracturing related to land subsidence in the Valley of Querétaro, Mexico. In: *Proc. 7th International Symposium on Land Subsidence* (SISOLS 2005, Shanghai, China), vol. 1, pp. 155-164. ISBN 7-5323-8209-5.

Carreón-Freyre, D., Cerca, M., Luna-González, L., and Gámez-González, F. (2005b). Influencia de la estratigrafía y estructura geológica en el flujo de agua subterránea del Valle de Querétaro. *Revista Mexicana de Ciencias Geológicas*, 22 (1), 1-18.

Carreón-Freyre, D. (2010). Land subsidence processes and associated ground fracturing in Central Mexico. In: *Land Subsidence, Associated Hazards and the Role of Natural Resources Development* (Proceedings of EISOLS 2010), edited by D. Carreón-Freyre et al., pp. 149-157, Red Book Series Publication 339, IAHS Press, CEH Wallingford. UK. ISBN 978-1-907161-12-4.

INEGI (2011). Censo Nacional de Poblacion, 2010, Mexico. Instituto Nacional de Estadistica, Geografia e Informatica.

Ferronato, M., Gambolati, G., Janna, C., and Teatini, P. (2008). Numerical modelling of regional faults in land subsidence prediction above gas/oil reservoirs. *International Journal for Numerical and Analytical Methods in Geomechanics*, 32, 633-657.

Gambolati, G., Teatini, P., Bau', D., and Ferronato, M. (2000). The importance of poro-elastic coupling in dynamically active aquifers of the Po river basin, Italy. *Water Resources Research*, 36(9), 2443-2459.

Jachens, R.C. and Holzer, T.L. (1982). Differential compaction mechanism for earth fissures near Casa Grande, Arizona. *Geological Society of America Bulletin*, 93, 998-1012.

Karmalkar, A.V., Bradley, R.S., and Diaz, H. F. (2011). Climate change in Central America and Mexico: regional climate model validation and climate change projections. *Climate Dynamics*, 37(3–4), 605-629.

López-Quiroz, P., Doin, M. P., Tupin, F., Briole, P., and Nicolas, J. M. (2009). Time series analysis of Mexico City subsidence constrained by radar interferometry. Journal of Applied Geophysics, 69(1), 1-15.

Pacheco, J., Arzate , J., Rojas, E., Arroyo, M., Yutsis , V., and Ochoa, G. (2006). Delimitation of ground failure zones due to land subsidence using gravity data and finite element modeling in the Querétaro valley, México. *Engineering Geology*, 84, 143-160.

Rojas, E., Arzate , J., and Arroyo, M. (2002). A method to predict the group fissuring and faulting caused by regional groundwater decline. *Engineering Geology*, 65, 245-260.

Teatini, P., Ferronato, M., Gambolati, G., and Gonella, M. (2006). Groundwater pumping and land subsidence in the Emilia- Romagna coastland, Italy: Modeling the past occurrence and the future trend. *Water Resource Research*, 42, W01406, doi:10.1029/2005WR004242.

Trejo-Moedano, A., Martínez-Baini, A. (1991). Agrietamiento de suelos zona de Querétaro. Agrietamiento de Suelos, Sociedad Mexicana de Mecánica de Suelos, A. C. 67-73.

Verruijt, A. (1969). Elastic storage of aquifers. In *Flow Through Porous Media*, edited by R. De Wiest, pp. 331-376, Elsevier, New York.

Xu, S., Nieto-Samaniego, A.F., Alaniz Alvarez, S.A., Cerca-Martinez, L.M. (2011). Structural analysis of a relay ramp in the Queretaro Graben, central Mexico: Implications for relay ramp development. *Revista Mexicana de Ciencias Geologicas,* 28(2), 275-289.

Capítulo II. “Assessment of groundwater flow in volcanic faulted areas. A study case in Queretaro, Mexico” Publicado en la revista de Geofísica Internacional junio de 2015

Geofísica Internacional (2015) 54-3: 199-220

Original paper

Assessment of groundwater flow in volcanic faulted areas. A study case in Queretaro, Mexico

Gil Humberto Ochoa-González, Dora Carreón-Freyre*, Mariano Cerca and Margarita López-Martínez

Received: January 15, 2013; accepted: September 24, 2014; published on line: June 30, 2015

DOI: 10.1016/j.gi.2015.04.016

Resumen

En este trabajo se integra la estratigrafía local y fallas como restricciones para un modelo numérico de flujo del agua subterránea en la parte norte del acuífero fallado del Valle de Querétaro. La información geológica de base fue establecida a partir de la reinterpretación de registros litológicos de pozos, fechamiento isotópico $^{40}Ar^*/^{39}Ar$ de rocas y cartografía de campo. En particular, la datación isotópica permitió obtener el tiempo de emplazamiento de un dique magmático a lo largo de la falla de El Nabo. El aumento de la tasa de flujo y la temperatura en el pozo El Nabo sugieren que la falla y el dique transportan un flujo regional. Un modelo numérico fue implementado para evaluar las contribuciones de fallas y estructuras volcánicas en el flujo general de agua subterránea. El modelo realizado con el software *Visual-Modflow* y código *Modflow* 2000 fue parcialmente restringido por los resultados de una prueba de bombeo en pozo "El Nabo", el pozo más profundo (Lat. 20 ° 42 '14 "N, Long. 100 ° 28'45" O, aproximadamente de 1000 m de profundidad) ubicado en la zona de Querétaro. La interpretación de los resultados del modelo y las observaciones de campo sugieren que las fallas reciben un flujo regional, compartimentalizan el sistema, y son responsables de un importante aumento del gasto, de 6 a 47 l/s, cuando se la perforación del pozo El Nabo bajo de 850 m profundidad. El estudio que aquí se presenta permite la evaluación de fallas normales e intrusivos que determinan el flujo del agua subterránea y podría ser relevante para el conocimiento de la dinámica de flujo en valles volcánicos cercanos. El modelo numérico implementado basado en información geológica, permitió una mejor comprensión de los sistemas acuíferos complejos, lo que no se puede evaluar por métodos analíticos. Por otra parte puede ser una aplicación útil para una mejor interpretación de pruebas de bombeo y para añadir datos complementarios de otras pruebas y/o de análisis de hidrogeoquímica.

Palabras clave: Flujo de aguas subterráneas, sistema acuífero fallado, modelación numérica, estructuras volcánicas, diques, México.

G. H. Ochoa-González
Posgrado en Ciencias de la Tierra
Centro de Geociencias
Universidad Nacional Autónoma de México
Campus Juriquilla
Blvd. Juriquilla 3001
Col. Juriquilla, Querétaro, C.P. 76230
Querétaro, México

D. Carreón-Freyre*
Laboratorio de Mecánica de Geosistemas
Centro de Geociencias
Universidad Nacional Autónoma de México
Campus Juriquilla
Blvd. Juriquilla 3001
Col. Juriquilla, Querétaro, C.P. 76230
Querétaro, México
*Corresponding author: freyre@geociencias.unam.mx

M. Cerca
Laboratorio de Mecánica de Geosistemas
Centro de Geociencias
Universidad Nacional Autónoma de México
Campus Juriquilla
Campus Juriquilla
Blvd. Juriquilla 3001
Col. Juriquilla, Querétaro, C.P. 76230
Querétaro, México

M. López-Martínez
Departamento de Geología
Centro de Investigación Científica y Educación Superior de Ensenada
Carretera Ensenada-Tijuana No. 3918
Zona Playitas C.P. 22860
Ensenada, B.C., México

Abstract

This work integrates local stratigraphy and faults to constraint a numerical model of groundwater flow in the North area of the Valley of Queretaro aquifer. Basic geological information was established from the reinterpretation of well logs, $^{40}Ar^*/^{39}Ar$ dating of rocks, and field mapping. In particular, dating allowed to obtain the timing of emplacement of a magmatic dyke inferred to be emplaced along the El Nabo fault. The increase of flow rate and temperature in the El Nabo well suggest that the fault and dike transport a regional flow. A numerical model was implemented to evaluate the contributions of faulting and volcanic structures in the overall groundwater flow. The model, accomplished with the *Visual-Modflow* software and *Modflow* 2000 code, was partially constrained by the results of a pumping test in the El Nabo well, the deepest well (Lat. 20°42'14"N, Long. 100°28'45"W, ca. 1000 m depth) located in the Queretaro area. The interpretation of the model results and field observations suggest that faults collect the regional flow, compartmentalize the reservoir, and are responsible of the dramatic increase of flow rate from 6 to 47 l/s when drilling the El Nabo well below a depth of 850 m. The study presented here allowed the assessment of normal faults and intrusives determining groundwater flow and might be relevant to the knowledge of flow dynamics in nearby volcanic valleys. The analysis of the pumping test suggest the presence of two different groundwater flow systems: (1) a flow related with the limestone and shale unit and (2) a regional linear flow through faults. The implemented numerical model, based on geological information, allowed a better understanding of complex aquifer systems that cannot be evaluated by analytical methods. Moreover it can be a useful application for a better interpretation of pumping tests and to add complementary data of other pumping tests and/or hydrogeochemical analysis..

Key words: Groundwater flow, faulted aquifers, numerical modeling, volcanic structures, dykes, Mexicos.

Introduction

Understanding groundwater flow systems is crucial for the management of groundwater resources in Mexico because many areas in arid zones depend on groundwater as the main source for urban, agricultural, and industrial development. In the Valley of Queretaro Aquifer (VQA), many wells are drilled near or along major faults and the high variability of piezometric levels in relatively short distances evidence changes on hydraulic properties (Carreón-Freyre *et al*., 2005; Figure 1). Furthermore, the spatial distribution of extraction wells and drawdown zones in the VQA during the last 30 years suggests that faults compartmentalize the aquifer system (Carreón-Freyre *et al*., 2005). In the VQA, groundwater is extracted from depths greater than two hundred meters; at this depth, geological heterogeneity should be considered for evaluating groundwater flow patterns to allow an accurate estimation of groundwater resources. Thus, the VQA could be considered a faulted aquifer, where faults and fracture zones strongly influence the overall flow dynamics of the system (Caine *et al*., 1996; Allen and Michel, 1999) and the assessment of the hydrogeologic behavior of major structures can be as important as obtaining the hydraulic properties of the stratigraphic sequences. This work examines the role of major structures (e.g., faults and volcanic or plutonic bodies) as hydrogeological independent units, rather than only as hydraulic boundaries, and presents a numerical modeling of the groundwater flow conditions in the faulted VQA. Integration of representative geological data in the model included: (a) vertical variations by assigning a hydraulic conductivity (K) to each geological unit; (b) faults; (c) lateral truncation of the hydro-stratigraphic units and; (d) the presence of intrusive rocks (Walton, 1970; Ingebritsen *et al*., 2006; Zoback, 2007), in particular dikes (Kulkarni *et al*., 2000).

The study area is located in the northwestern part of the VQA system (Figure 1). The Valley of Queretaro is located in the central part of the Miocene to Recent Trans Mexican Volcanic Belt (TMVB; Ferrari, 2000; Alaniz-Alvarez *et al*., 2002) and is delimited by groups of N-S and NE-SW trending faults active at least since the Miocene (Alaniz-Alvarez *et al*., 2001). We aim at having a better understanding on the role of major structures in groundwater flow patterns in the VQA by integrating them in a numerical model.

Faulted aquifer systems

Previous works have documented the variations in hydraulics properties induced by the complex architecture of regional faults (MaClay and Small, 1983; López and Smith, 1995; López and Smith, 1996; Caine *et al*.,

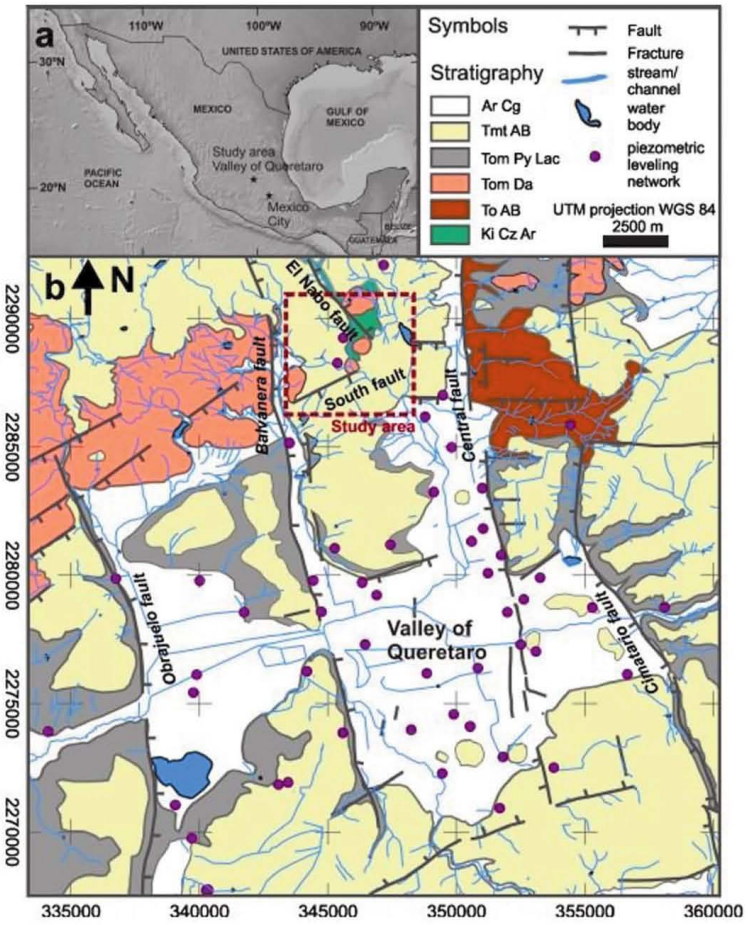

Figure 1. (a) The Valley of Queretaro is located in the central part of Mexico; (b) Geological map of the Valley of Queretaro. Dashed red square line on the geological map indicates the area considered in modeling, black lines are major faults. Green polygon represents the Cretaceous rocks exposed in the zone. Medium and light gray units represent Oligocene and Miocene volcanic rocks, respectively. (Modified form Carreon-Freyre *et al*., 2005).

1996; Allen and Michel, 1999; Carreón-Freyre *et al*., 2005; Anderson, 2006; Mayer *et al*., 2007; Delinom 2009; Rafini and Larocque, 2012). Anisotropy of hydraulic conductivity in faulted and stratified geological media determines groundwater flow patterns (Hsieh and Neuman, 1985). Regional faults represent an important heterogeneity influencing overall aquifer dynamics, not only determining preferential flow directions but also modifying their storage capacity (Pacheco, 2002; Burbey, 2008; Bense *et al*., 2013). Lithological changes and fractures in volcanic rocks, on the other hand, modify hydrogeological properties of geological units. A fault can be a preferential conduit for vertical flow, i.e., a "leaky fault", when the damaged zone is well developed and is laterally sealed (Zeidouni, 2012). Fault zones can also behave as leakage areas between aquifers by juxtaposing aquifers that would otherwise be separated by impermeable layers.

Major faults can behave as flow barriers or preferential channels depending on the hydraulic properties developed during deformation history (MaClay and Small, 1983; Caine *et al*., 1996; Carreón-Freyre *et al*., 2005; Mayer *et al*., 2007; Delinom, 2009, Rafini and Larocque, 2012), or they can only separate units of different hydraulic conductivity (Allen and Michel, 1999; Mayer *et al*., 2007); for instance, the vertical displacement of a fault can juxtapose permeable and impermeable layers in the direction perpendicular to the fault plane. In early models, faults were commonly considered as border conditions when assessing hydraulic parameters, even in stratified leaky systems (Rathod and Rushton, 1991).

The style of deformation and rupture of a fault zone strongly influences variations of its hydraulic properties. Caine *et al*. (1996) proposed four conceptual schemes for fault-related fluid-flow according to the distribution of conduits and barriers (localized and distributed) within fault plain. Anderson (2006) identified three essential hydraulic elements of a fault plane: (1) a low hydraulic conductivity core characterized by fault breccias, cataclastic rocks, and gouge; (2) an adjacent damaged zone characterized by an increase in the hydraulic conductivity caused by brecciation and fracturing and; (3) fresh unaltered rock with a characteristic hydraulic conductivity that can change in both sides of the fault because of the fault displacement.

A decrease in the hydraulic conductivity within a fault plane (flow barrier) can be associated with (Mayer *et al*., 2007; MaClay and Small, 1983): (1) cataclasis or grain size reduction; (2) juxtaposition of permeable and impermeable layers, displacements along the fault plane can decrease the possibility of flow through the fault and/or deviating flow along the fault; (3) rotation of plane and elongate detritus that became parallel to fault plane reducing the hydraulic conductivity in the orientation perpendicular to the plane; (4) presence of sedimentary materials with low hydraulic conductivity (e. g., clays) in the fault zone; and (5) chemical precipitation of mineral in the fault zone reducing permeability.

Furthermore, major faults often present associated or secondary planes and fractures that may cause contrasting hydraulic behaviors. In anisotropic media, each geological unit is represented by a hydraulic conductivity tensor considering three dimensional variations of hydraulic conductivity. In fractured rocks the tensor can align following the preferential orientation of fractures (Jourde *et al*., 2007).

Geology of the Study Area (Northwest of the Valley of Queretaro Aquifer, VQA)

The regional geology of the VQA has been extensively studied in the last decades (Trejo-Moedano, 1989; Valdez-Moreno *et al*., 1998; Aguirre-Díaz and Lopez-Martinez, 2001; Alaníz-Alvarez *et al*., 2001, 2002; Carreón-Freyre *et al*., 2005; Aguirre-Díaz *et al*., 2005; Xu *et al*., 2011). The Valley of Queretaro is a basin delimited by groups of N-S and NE-SW trending faults and volcanoes, located in the central part of the Trans Mexican Volcanic Belt (TMVB; Ferrari, 2000; Alaniz-Alvarez *et al*., 2002; Figure 1). The N-S trending west-dipping Central fault is the eastern limit of the regional Queretaro graben (Figure 1). The other major faulting family (trending NE-SW) produced a nearly orthogonal pattern with the N-S system that has resulted in a mosaic formed by horsts, grabens, and half-grabens (Alaníz-Alvarez *et al*., 2001, 2002; Carreón-Freyre *et al*., 2005; Aguirre-Díaz *et al*., 2005; Xu *et al*., 2011) with varying vertical displacements, in some areas up to 400 m. Both fault systems have been active at least since the Miocene (e. g., Alaniz-Alvarez *et al*., 2001; Zuñiga *et al*., 2003; Aguirre-Díaz *et al*., 2005) and both controlled the deposition of sediments and volcanic rocks in the VQA.

This study is focused on the northwestern part of the VQA (dashed square in Figures 1 and 2), a zone of groundwater recharge because of faulting (Conagua, 2003). The available information was compiled and integrated in a geological map with the hydrogeologic information of the VQA and surroundings. The local stratigraphy was established from the reinterpretation of well logs, $^{40}Ar^*/^{39}Ar$ dating of magmatic rocks, and geologic mapping. The structural and stratigraphic setting of this part of the basin can be defined with sufficient detail and indicates that the geological evolution is more complex than hitherto recognized (Figure 2a). In this area, the Cenozoic volcanic and colluvial sequences cover partially the Cretaceous units that were uplifted by a shortening episode and thus are well exposed in the hanging wall. A schematic W-E geological cross section AA' was constructed using the lithological logs of water extraction wells available in the zone (Mompani II, El Nabo, UNAM, and El Salitre) (Figure 2).

The oldest sequence (Cretaceous) consists of volcano-sedimentary rocks, documented here for the first time in the Valley of Queretaro (Ki MsV, see below), a thick Albian limestone and shale sequence (Ki Cz, of 800 m thick), and a late Cretaceous shale and sandstone interbedded with argillaceous limestone (Ki Cz-Ar). The Cretaceous sequence is pervasively folded by shortening deformation.

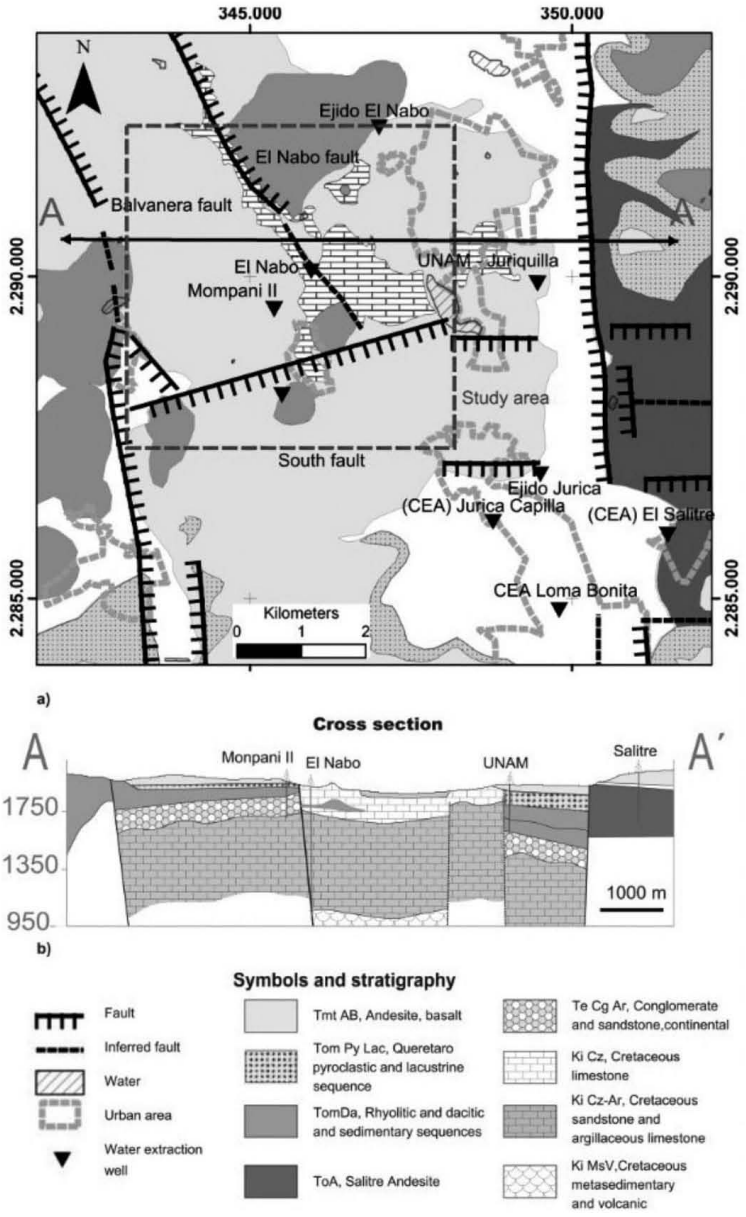

Figure 2. (a) Simplified geological map of the study area, the main structures considered in the model are the normal faults El Nabo, Balvanera and South. Logs of water extracting wells were projected to the A-A´ section shown in (b). The main stratigraphic units are presented in the cross section.

The Cenozoic sequence consists of a continental sedimentary unit with predominance of conglomerates and sandstone (Te Cg-Ar), overlain by a volcanic sequence with pyroclastic and sedimentary interbedded deposits. The Cenozoic sequence is fractured and affected by extensional faults. The Te Cg-Ar layer of probable Eocene age is present at the Mompani II well (at a depth of 200 m), and at the bottom of UNAM-Juriquilla and El Salitre wells (Figure 3a). The volcanic rock sequence includes lavas such as the Salitre Andesite (ToA) and silicic domes (Tom Da; Juriquilla dacite; Alaniz-Alvarez *et al*., 2002) of the Oligocene and early Miocene. An intrusive body of Oligocene age (ca. 30 Ma) is exposed in the zone of Juriquilla within the study area (Figure 2a). The pyroclastic and lacustrine sequences in the Queretaro area consist of tuffs and other pyroclastic deposits of 80 m in average of

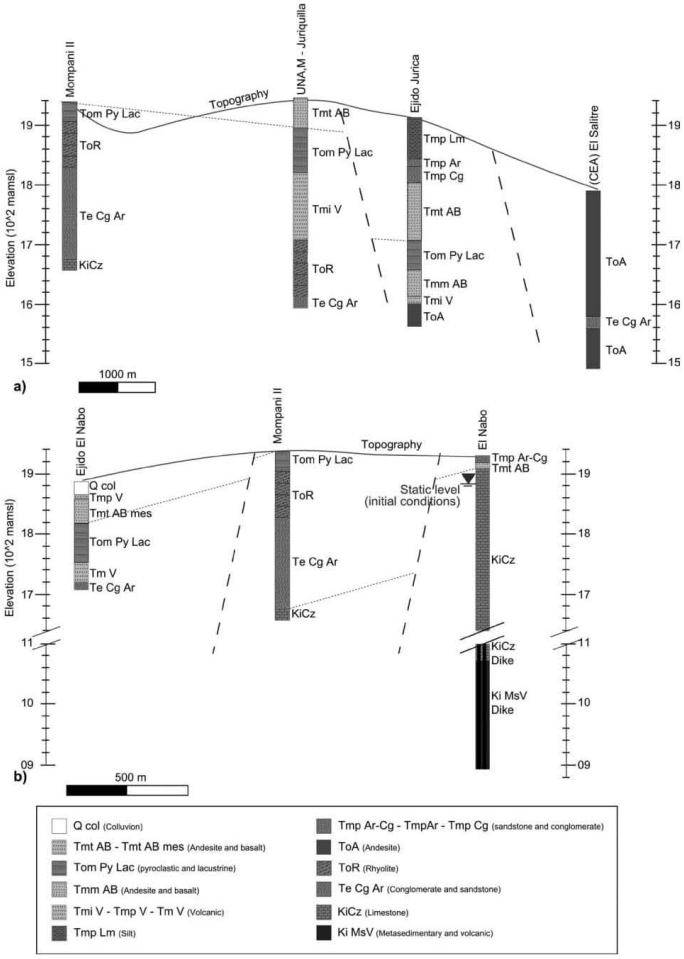

Figure 3. Stratigraphic correlation of the lithological logs of extraction wells used for the interpretation of the main structures and construction of the conceptual model. (a) Correlation of wells in the NW-SE direction including Mompani II, UNAM-Juriquilla, Ejido Jurica, and (CEA) El Salitre; (b) correlation in the N-S direction Ejido El Nabo, Mompani II, and El Nabo. The initial static water level in the El Nabo well is also shown.

thickness (Tom PyLac); and this unit includes the Ezequiel Montes Pumice, an important stratigraphic marker dated between 7.5 and 5.6 Ma (Aguirre-Díaz and López-Martínez, 2001). The coarse facies of this sequence (Tom PyLac) was the main hydrogeological unit exploited in the regional VQA, but is scarcely exposed in the study area, it is found in the upper part of the Mompani II log (Figure 3). Fissure basalts and lava flows (Tmt AB), ranging in age from 12 to 5 Ma (Aguirre-Díaz and López-Martínez, 2001) erupted from nearby volcanoes. The largest volcanic edifice, located 13 km to the NW from the studied area, is the La Joya Volcano ranging in age from 12 to 10 Ma (Valdez-Moreno *et al*., 1998).

The truncation and throw of the N-S trending extensional faults was inferred by the elevation differences among stratigraphic levels from the correlation of lithological logs presented in Figure 3. The vertical displacements are smaller than 200 m. From Figure 2b note that two additional buried faults nearby, and to west of UNAM well, were inferred in this work. Structurally, the study area is a block delimited by the major N-S trending *Balvanera* and *El Nabo* fault zones dipping to the northeast (Figure 4a). The South fault and other NE-SW trending fault segments delineate the limits of the block toward the south. Both faults systems have nearly vertical fault planes and their kinematics indicate dip-slip towards the center of the Queretaro Valley since Miocene time. These major faults include several parallel fault planes affecting areas with more than 50 m in width (Figure 4). Faults are partially exposed and their trace length was inferred by topography, field observations, and lithological correlations of well logs. The relative age of faulting in the region was analyzed in detail by Alaniz-Alvarez *et al* (2001); the older system corresponds to the South Fault that favors the emplacement of the Oligocene intrusive body. The Balvanera and El Nabo fault systems are younger and favor the Miocene volcanism through dykes emplaced along the faults planes (Figure 4). The *El Nabo Fault* is of particular relevance to this work, it is a nearly vertical fault partially exposed to the north of the study area where plateau lavas fill the hanging wall of the fault (solid line with thick marks in

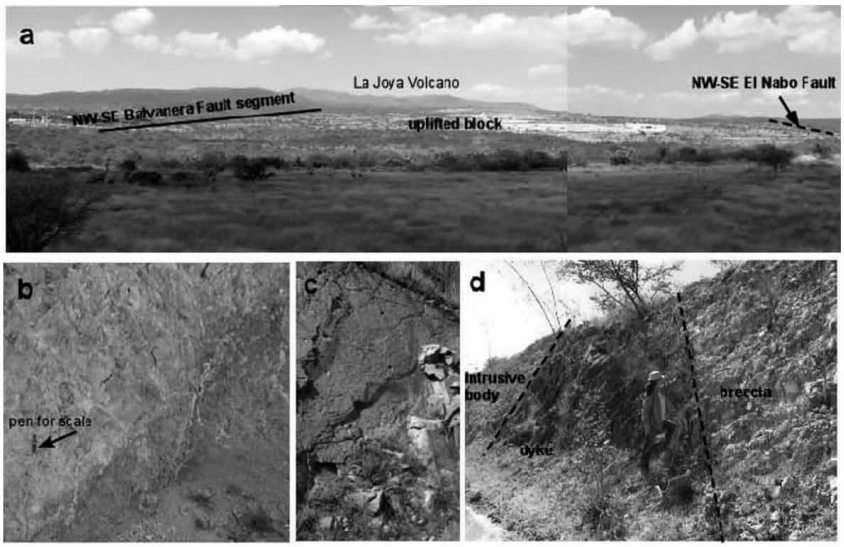

Figure 4. (a) General view to the NW of the study area, the escarp of the Balvanera fault can be observed, the trace of the El Nabo fault is inferred by a dotted line because it delimits NE side of the uplifted bock (horst). As reference the La Joya volcano is shown toward the NW of the study area; (b) close view in outcrop of the South Fault (pen for scale) showing the contact between the intrusive body at the left and evidence of hydrothermal activity; (c) outcrop of the intrusive body; (d) outcrop of a plane associated to the El Nabo fault zone, the contact with the intrusive body and the structure of a dyke with brecciated material are shown.

Figure 2a). Toward its southern part the fault is not clearly observed on surface but it can be inferred from the topographic relief and the interpretation of the stratigraphic records (dotted line in Figure 2a). A dyke emplaced along a fault plane parallel to El Nabo fault was observed at the surface northeastward of the El Nabo well (Figure 4b). All this information was integrated to constrain the numerical model.

Methodology

Stratigraphic correlation

The conceptual model of the study area is based on geological units with contrasting hydraulic properties, granular and fractured rock layers, truncated by major faults and volcanic edifices/bodies that may interrupt or favor lateral flows. Carreón-Freyre *et al*. (2005) correlated the hydrogeological units with lithostratigraphic units to describe the VQA and proposed a conceptual model of multilayer aquifer with groundwater flow varying from local to regional. The stratigraphic correlation of lithological logs for the Cenozoic was based on the reconnaissance of an andesitic-basaltic unit of late Miocene age, named Tmt AB, as an index layer. For instance, as shown in the record of the Ejido Jurica well (Figure 3a) the Tmt AB layer commonly is overlaid by a Miocene-Pliocene sedimentary unit, named Tmp Cg-Ar-Lm, and underlied by an Oligocene-Miocene pyroclastic and lacustrine unit, named Tom PyLac.

The Cretaceous units are more relevant to groundwater flow in this area and include sandstone and argillaceous sequences, limestone rocks, and a volcano-sedimentary sequence. These units were found during drilling of *El Nabo* well, which is the deepest in the study area and is located within a block where Tertiary sequences are partially eroded (Figure 3b). The contrasting stratigraphy and the vertical difference in elevation of the Ki Cz unit from 1680 to 1100 masl among the Mompani II and El Nabo records separated by approximately one kilometer suggested the presence of the El Nabo Fault at this location.

Drilling of the first 600 m depth of *El Nabo* well initiated in 2000 at this time the production of water was approximately 6 l/s. Extended drilling in *El Nabo* well from 600 to 1000 m depth was performed in 2007, the production of the well increased dramatically to 47 l/s after drilling at 850 m depth, that coincided with a lithological change from limestone to a volcano-sedimentary sequence (volcanic rocks and limestone) bearing biotite minerals). Further evidence of the fault and its relevance to groundwater flow was obtained by the geochronological data of rock samples from the El Nabo well presented below.

Biotite age determination

In order to define the age of the basal volcanic unit, rock samples collected each 3 m during drilling from 800 to 1050 m depth were classified by the use of a 20x-40x stereoscopic magnifier, and some samples of interest were selected for thin section description. Biotite concentrates were selected for dating at depths between 850 and 950 m. These biotite concentrates were analyzed by the $^{40}Ar^*/^{39}Ar$ technique at the Geochronology Lab in CICESE using a VG5400 mass spectrometer and a laser extraction system. The analytical details of the method can be consulted elsewhere (e.g., Cerca *et al*., 2007). Mineral concentrates were previously irradiated at the nuclear reactor of the University of McMaster in Hamilton, Ontario, Canada, using as monitor of irradiation two known-age samples of sanidine, FCT-2 of 27.84 ± 0.04 Ma and TCR-2 of 27.87 ± 0.04 Ma. All the experiments were made by step-heating by increasing the laser power from 0.2 to 8 watts and measuring the isotopic composition of argon released during each step. The reported age is calculated for each individual fraction and the integrated results adding individual steps in accordance to Hall (1981), and considering the corrections by discrimination, radioactive decay (Steiger & Jäger, 1977), the line background, and interference reactions from isotopes derived from Ca, Cl, and K. Results were grouped according to depth and size of the samples and are presented in a graph named age spectra. Correlation diagrams in which the relation ($^{40}Ar^*/^{39}Ar_K$) is given by the inverse of the intercept of the line defined by the data and is equivalent to the age in Ma are presented in a supplementary Figure (S1).

Integration of conceptual and numerical models

The conceptual model resulting from the interpretation of lithological logs, geological mapping, analysis of samples, and isotopic data is shown in Figure 5 (a, b). The wells integrated in the numerical model are El Nabo and Mompani II, 1100 and 250 m depth, respectively (Figure 5a). For the implementation of the numerical model, the volcanic sequences, sedimentary materials, and geological faults were considered as independent hydrogeological units; each one with a hydraulic conductivity tensor.

Groundwater simulation was accomplished with the *Visual-Modflow* software (Schlumberger Water Services, Inc) and the *Modflow* 2000 code (Harbaugh *et al*., 2000). In order to represent the hydraulic behavior of the mapped geological structures the numerical model was built with 100,000 cells, distributed in a horizontal grid of 100 x 100 cells in the N-S and E-W direction, each one represents a square of 2500 m^2. The model box is a square of 25 km^2 with a top surface with an average elevation of 1945 masl reproducing the actual topography and a flat surface at the bottom of the model (800 masl). The model box was divided in 10 horizontal layers of cells with variable thickness from the surface, according to the topography, to reach a bottom flat layer. Cells with similar hydraulic behavior were grouped to represent the geological units included in the model considering stratigraphic sequences and major structures. According to their physical characteristics, spatial distribution, and thickness, four geological units were defined in the conceptual model and represented in the numerical model shown in Figure 5a:

(1) *TomDa-Rhyolite*, this is the upper layer of the model, and groups the Cenozoic volcanic rocks including the volcanic and pyroclastic fractured sequences located above the piezometric level in the study area. These units, observed in the lithological records of the Ejido Jurica, UNAM-Juriquilla, and Ejido El Nabo wells, were not considered in the conceptual model because either they are located above the regional groundwater level (vadose zone) or are absent nearby the El Nabo well area (Figure 3). These units include: Late Miocene Andesites and Basalts (Tmt AB), Early Miocene Conglomerates and Sandstones Sandstones (Tmp Ar-Cg), and Quaternary Alluvium (Qal; Figure 2);

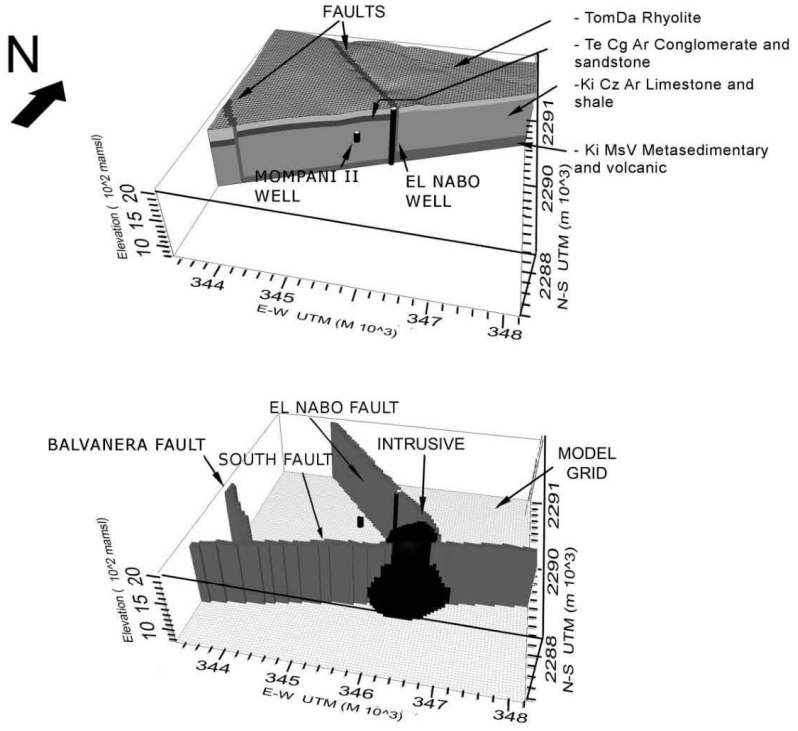

Figure 5. (a) Model box formed by an horizontal square grid of 25 km^2 and variable thickness layers. El Nabo and Mompani II wells were integrated in the model. Cells were grouped to represent hydro-stratigraphic layers with specific hydraulic properties. (b) Major geological structures in the model: (1) El Nabo fault-dyke, (2) Balvanera fault, (3) South fault and, (4) an intrusive body. The topographic surface is considered in the model.

(2) *Te Cg Ar Conglomerate and sandstone*, a sedimentary unit of conglomerate and sandstone found at the west of the El Nabo fault, was represented by a dark layer shown in the model of Figure 5a;

(3) *Ki Cz Ar Limestone and shale*, this unit includes Ki Cz and also the Ki Cz-Ar of sandstone and argillaceous limestone for modeling purposes, and;

(4) *Ki MsV Metasedimentary and volcanic* (Figure 5), located at the bottom of the model, corresponds in nature to the Cretaceous volcano-sedimentary unit (Ki MsV).

Faults are represented by groups of 50 m width vertically aligned cubic cells with specific hydraulic conductivity (gray cells in Figure 5b). The massive intrusive/subvolcanic body of 30 Ma is represented by a group of cells with a dome shape in the located central part of the model (black cells in Figure 5b). Major geological structures were considered as four individual units in the model: (5) the *El Nabo Fault*, (6) the *Balvanera Fault*, (7) the *South Fault* and, (8) the intrusive body placed in the lower part of the model (Figure 2 and Figure 5b).

Faulting and the intrusive body are thought to greatly influence groundwater by channelizing or arresting flow, or by interrupting the lateral continuity of the hydro stratigraphic units, such as the conglomerate and sandstone unit (*Te Cg-Ar)*. Truncation by faulting was suitable represented because each geological unit was composed by independent cells.

Once designed the geometry of the model, the initial and border conditions were established considering regional variations of the piezometric surface interpolated from 2004 and 2006 measurements (Figure 6). Previous work by Carreon-Freyre *et al*. (2005) indicated a regional gradient in the groundwater flow with a nearly north to south direction in the VQA. Regional piezometric were interpolated by krigging of the data from 40 water extraction wells located in the VQA, systematically monitored by the local agency of water (*Comisión Estatal de Aguas de Querétaro,* CEAQ) since 1996 (Carreón-Freyre *et al*., 2005). The interpolations show a persistent regional gradient with an approximate North-South trending. The wells located in the study area are El Nabo and Mompani II (Figure 1 and Figure 5a). A steady state numerical simulation was performed to establish the initial and boundary conditions (Figure 7b). Boundary effects were minimized by leaving a minimum radius of 2000 m from each well to the model borders.

Simulation of hydrodynamic conditions using the numerical model

A numerical simulation was performed to assess the hydrodynamic behavior of the system by the use of partial results of a pumping test. In the computational experiment the hydraulic properties were adjusted to correlate calculated and measured drawdown in the pumping and in one observation well.

A 260,000 s (72 hour) pumping test performed in the *El Nabo* well was simulated using the implemented numerical model. The location of the pumping test area is shown in Figure 2; the data record (water level and temperature) was made by a CTD Diver (*Schlumberger*) datalogger. This well is the single one in the region with about 1000 m in depth and therefore it was not possible to locate any observation well. The *Mompani II* well is located 1000 m to the SW, with a depth of 250 m. Because of the presence of the El Nabo Fault between the two wells no change in the hydraulic head during the pumping test was recorded at the Mompani II and thus, we assumed that groundwater flow in both wells were independent (possibly local and regional systems).

To accomplish the simulation, the hydraulic conductivities of the model and measured drawdown were closely fitted. We used a segment of the pumping test to simulate transient conditions generated by the pumping test. Continuous measurements of drawdown and temperature every 15 s are presented in Figure 8 (blue and green line respectively); blue squares indicate samples from the continuous measurements used for simulation. Because of the well depth only a part of the pumping test could be considered for adjustment. The first 10,800 s data (3 hours) were not considered because the pumping rate could not be maintained stable during this period and/or a well storage effect should be considered (Allen and Michel, 1999), the same issues were considered for the interpretation of the recovery data.

Simulated and observed drawdown in the segment between 10,800 and 250,000 s (3 and 69 hours) of the El Nabo test were fitted by adjusting the hydrogeological properties of the main units (e.g., Allen and Michel, 1999). The estimation of these properties was achieved using the PEST (*Parameter Estimation Software*) algorithm (Harbaugh *et al*., 2000; Doherty, 2005) trough *Visual-Modflow*. The finite differences *Modflow* algorithm solved groundwater flow by adjusting hydraulic

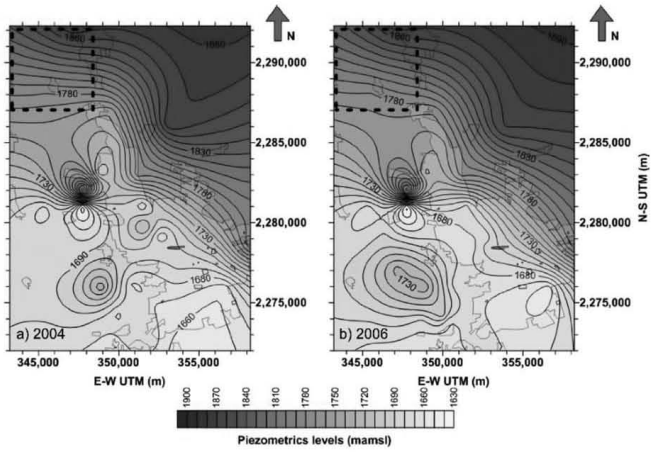

Figure 6. Piezometric levels measured in the Queretaro Valley for (a) 2004 and (b) 2006. The 2006 piezometric levels were used as initial condition for the model. Because the North-South hydraulic gradient, shown in the dashed square (modeled area), is persistent during 2004 and 2006 we considered steady state conditions.

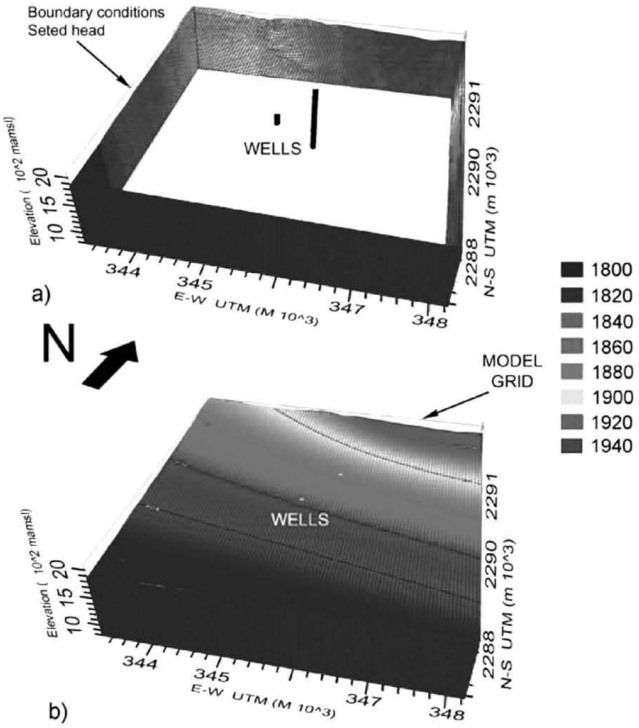

Figure 7. Piezometric conditions shown in the model box with (a) border and (b) initial conditions after the steady state measured in 2006 (see figure 6b).

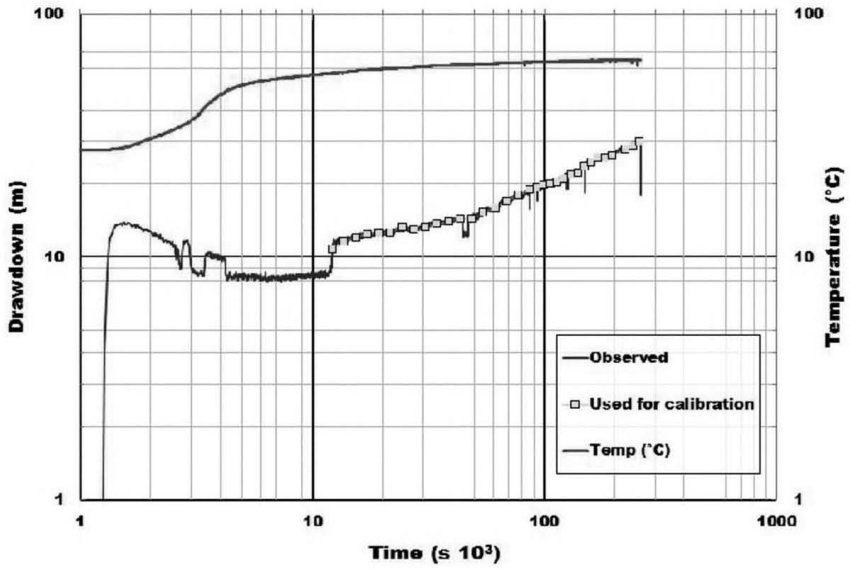

Figure 8. Drawdown measurements collected during the El Nabo pumping test. Blue line indicates continuous datalogger measurements, blue squares the sampled points for calibration. Green line indicates increasing temperature in the extracted water.

conductivities in three perpendicular directions, corresponding with the orientation of the grid to North-South, East-West, and vertically for this study case. The initial value of hydraulic conductivity (K) was established at 1e-04 m/s, corresponding to reported values for massive and fractured rocks (Walton 1970; Ingebritsen *et al*., 2006; Zoback, 2007).

The best fit of the observed and calculated drawdowns was achieved by using the hydraulic conductivities (K) values presented in Table 1, along two directions: horizontal E-W and vertically. The North-South values of K remained fixed at the initial value. The sensitivity values for the obtained hydraulic conductivities (Table 1) of the model vary with the distance between the geological units/faults and the pumping test zone. High sensitivity means a high influence of the geological unit in drawdown. The "limestone and shale" and "El Nabo fault" units show the highest sensitivity values (Table 1b). The high values in the El Nabo Fault are due to the fact that the pumping well is located along this fault. The lower obtained sensitivities correspond to the Balvanera and South faults, meaning that the conductivity values of these units did not affect the calculated drawdown.

The results of the pumping test were analyzed by the derivative of the data obtained by applying the fixed-end-point method proposed by Bourdet *et al*. (1989) (orange line in Figure 9). The use of the derivative allows analyzing in detail pressure changes in drawdown plots (Bourdet *et al*., 1989; Spane and Wurstner, 1993; Tiab, 2005). The derivative was smoothed by the use of the third point before and after the point of interest to reduce the sample rate noise. The intersection between dyke/fault and the El Nabo well was analyzed by the semi-analytical solution of Butler and Liu (1991).

Discussion of results

The implemented model allowed representing the faulted system of the study area by the hydraulic conductivities assigned to specified geological units, including faults. In order to constrain the overall flow conditions regional measurements of hydraulic heads and geological observations were integrated.

Table 1. (a) East-West and vertical hydraulic conductivities obtained from simulation. (b) Table of sensitivity variability for PEST analysis, higher sensitivity values of the model are related to the El Nabo fault. See text for details

Hydraulic conductivity (m/s)		
	E-W	**Vertical**
Rhyolite	2.8E-05	6.1E-06
Conglomerate and sandstone	3.4E-05	4.0E-05
Limestone and shale	5.6E-02	1.3E-05
Basement Limestone	9.9E-05	8.8E-06
Nabo-Fault NW-SE	4.4E-07	4.9E-04
South fault NE-SW	1.2E+02	6.1E-06
Balvanera-fault NW-SE	5.1E-04	9.7E-06
Intrusive	6.15E-05	1.39E-05
a)		
Sensitivity		
	E-W	**Vertical**
Rhyolite	4.0E-03	0.0E+00
Conglomerate and sandstone	4.0E-03	4.0E-03
Limestone and shale	1.2E-01	1.6E-02
Basement Limestone	8.8E-03	1.3E-02
Nabo-Fault NW-SE	1.0E+00	2.9E-01
South fault E-W	1.2E-01	0.0E+00
Balvanera-fault NW-SE	4.0E-03	0.0E+00
Intrusive	0.0E+00	0.0E+00
b)		

Geological constraints for the implementation of the model

The Cretaceous sequence drilled in El Nabo well, composed by a limestone and shale unit (Ki Cz-Ar) that overlies a volcano-sedimentary sequence (Ki Mvs), was of the most importance to establish the geological constraints of the model. The volcanic character of the basal volcano-sedimentary sequence was interpreted from the drilling samples and was confirmed by the isotopic ages. The overlying limestone and shale unit is more than 800 m thick and is inter-bedded both with sandstone or clay. In nearby superficial outcrops this unit is deformed by folding and contains calcite veins and fractures. Rock samples obtained from depths below 850 m at the El Nabo well of the volcanic sequence contained a large quantity of biotite. Differences in the size and aspect of biotite defined two size populations: (1) between 425 and 710 μm and (2) between 250 and 425 μm. The age spectra obtained for both sizes confirms that they correspond also to two different age populations.

Figure 10a shows the age spectra for the biotite population 1 indicating a Miocene age. The weighted average for argon fractions was made by considering the consecutive fractions with greater radiogenic argon content and more than 10% of the total ^{39}Ar released. A representative age of t = 9.5 ± 0.1 Ma was selected from the weighted average of 13 fractions from different experiments in the age spectra diagram. This biotite population is characterized by a ratio $^{37}Ar_{Ca}/^{39}Ar_{K} \leq 0.5$. The correlation diagrams obtained for these samples (Figure S1) show two isochron lines also converging at an age around 9.5 Ma. The Andesitic lava flows (Valdez-Moreno *et al*., 1998) cover most of the study area and have the same Miocene age obtained for biotite 1 population, the coincidence in age of the lavas and the biotite sampled at depth strongly support the interpretation that the lavas were feed by dikes emplaced along faults.

The biotite population 2 (Figure 10b) yielded older ages of ~100 Ma with age spectra diagram indicating a severe argon

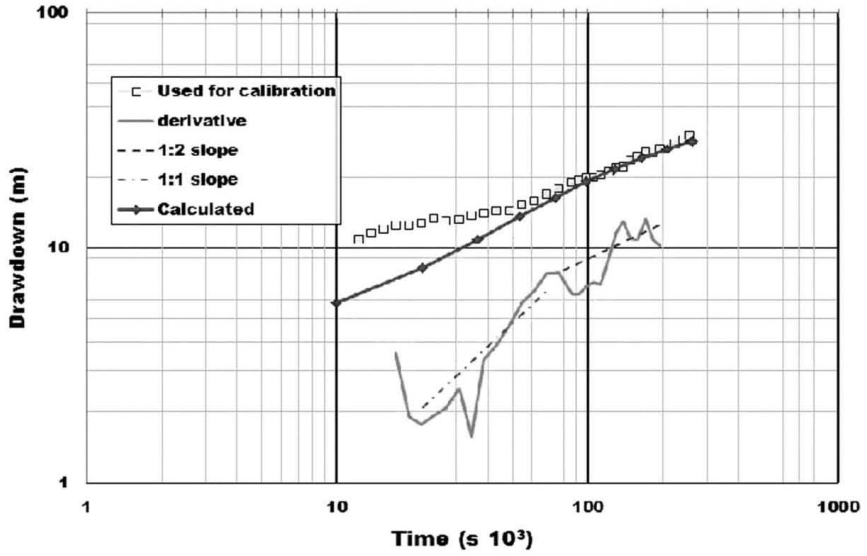

Figure 9. Measured drawdown during the pumping test at El Nabo (blue squares) and calculated curve using the implemented model. The derivative of the data obtained by applying the fixed-end-point method (Bourdet et al. 1989) is presented in a orange line. Derivative drawdown was analyzed by the semi-analytical solution of Butler and Liu (1991) obtaining 1:2 and 1:1 slopes.

loss. A reliable age cannot be obtained but the sequence is older than the minimum age obtained. This behavior was reproduced in the 855 m depth Biotite in duplicate experiments. A higher ratio of $^{37}Ar_{Ca}/^{39}Ar_{K}$ > 0.5 compared with biotite population 1 clearly indicates a different composition. Because of the different isotopic behavior of these samples the biotite populations were plotted separately in the correlation diagram (Figure S1), in which the equivalent age is shown in the abscissa axis. The correlation using the fractions from 3 to 6 of the 1st experiment and the fractions 3 to 8 of the duplicate experiment in the biotite 2 population also indicates an age of ~100 Ma, for the *Ki Ms V* rock sequence.

The documented difference in age of the biotite populations strongly supports our interpretation of the presence of a Miocene magmatic dyke intruding the Cretaceous sequence as shown in the schema of Figure 10c. The presence of this fault has important implications in groundwater flow by the increasing of the hydraulic conductivity within the fault plane that was observed during drilling.

It has been documented that dikes open weakened fractures to conduct magma toward the surface and during their emplacement they can cause further brecciation of the fractured zone and the increase of hydraulic conductivity (Zoback, 2007; Anderson, 2006). Beside the presence of the dike, further evidences supporting the circulation of hydrothermal fluids along the fault include the presence of hydrothermally altered calcite veins in exposures and in drilling samples of the El Nabo well (Figure 4b). Present day hydrothermal activity along the fault was confirmed by the increase from 25 to 63°C in the temperature records during pumping test (green line, Figure 8).

In order to consider the role of major faults in groundwater flow we integrated the *El Nabo, Balvanera* and *South* faults in the model. *El Nabo* and *Balvanera* are sub-parallel normal faults with NW-SE orientation (panoramic view, Figure 4a). The *Balvanera Fault* has a throw of more than 200 m after the Miocene lavas emplacement. The *El Nabo Fault* is located in a block delimited by the regional graben faults as shown in the cross-section of Figure 2b. Several faults and fractures with similar

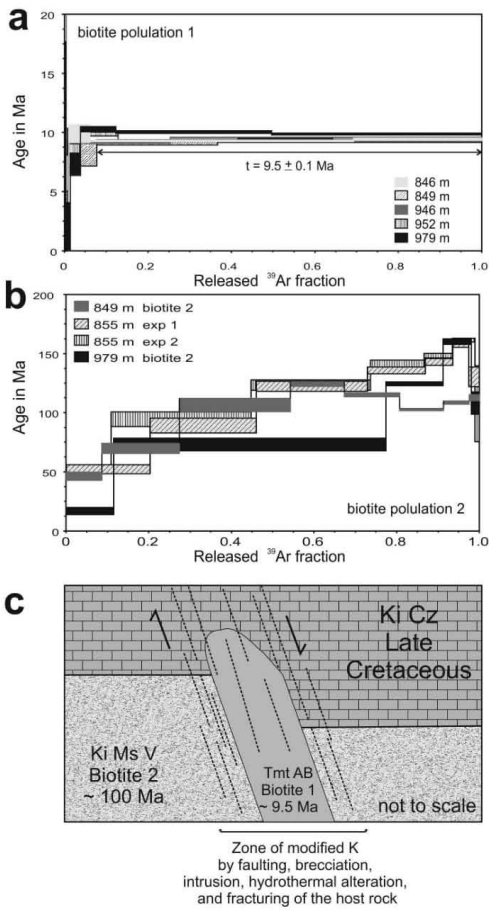

Figure 10. (a) $^{40}Ar/^{39}Ar^*$ age spectra obtained for the biotite population 1 (small size) collected at different depths between 846 and 979 m in El Nabo well. The age obtained for this population is interpreted as evidence for a Miocene dyke intrusion. (b) $^{40}Ar/^{39}Ar^*$ age spectra obtained for the biotite population 2 collected at the same depth interval of population 1. Although a reliable age cannot be assigned to the samples, a minimum age of 100 Ma is interpreted for the volcano-sedimentary sequence hosting the Miocene intrusion, (c) schematic section showing the intrusion of the volcanic dyke (Tmt AB, 10 Ma) within the Cretaceous sedimentary and volcanic units (host rocks: Ki Cz and Ki Ms V) that changes dramatically the hydraulic conductivity of the system by brecciation.

orientation were observed around the zone of the El Nabo well. The Cretaceous sedimentary sequences (Ki Cz-Ar) have a low hydraulic conductivity as shown by the low flow rate measured in the El Nabo well above 800 m depth (6 l/s). Nevertheless, flow rate increased to 47 l/s when drilling intersected the El Nabo Fault and dike at 850 m depth. We infer that the dike caused brecciation, fracturing, and hydrothermal alteration of the host rock and consequently an increase in the hydraulic conductivity. Evidence of other dikes emplaced on the *El Nabo Fault* area affecting other stratigraphic levels was observed in exposed parallel fault planes. For modeling purposes, the *Balvanera Fault* features are assumed to be similar to the *El Nabo Fault* and was calibrated as an independent unit.

The exposed plane of the older age *South Fault* (Figure 4b) contains open fractures filled with sediments and calcite that precipitated by the circulation of hydrothermal fluids. The *South Fault* favored the location of the Oligocene sub-volcanic body (30 Ma, TomDa) of silicic composition (Alanis-Alvarez *et al*., 2002) observed as a dome structure at the surface (Figure 2). Given its large spatial dimensions this structure was considered as an individual unit in the numerical model (Figure 5b).

The geological evidences suggest that groundwater flow through faults is significant in the study area: thus, the model integrated an increase of conductivity along the El Nabo fault.

Assessment of groundwater flow in faulted and high heterogeneous areas

The numerical model was constrained by the results of the pumping test in El Nabo well. The record of the test was sub-sampled and the obtained drawdown plot is presented in Figure 9 (blue squares) along whit its derivative (Bourdet *et al*., 1989). Considering an infinite linear strip embedded in a host material (matrix) with differing hydraulic properties Butler and Liu (1991) presented derivative curves with slopes varying from 1:2 and 1:4 for a case in which hydraulic conductivity is much larger than the host material (matrix). In their analysis these slopes corresponded to an initial linear flow within the strip that changed to bilinear flow when the flow from host material contributes to discharge. The slopes obtained from the drawdown derivatives of the El Nabo well pumping test are shown in Figure 9; a slope 1:1 (green dashed line) for the 20,000-70,000 s (5-19 hour) interval and a slope 1:2 (black dashed line) for the last part of the data. The first slope (1:1) corresponds to the primary flow drawdown that may be explained by two conditions: (a) groundwater flow contributed by the limestone unit presenting high K values in the E-W direction and (b) is enclosed within the fault walls (Table 1) or, (2) non lineal flow inside the fault walls and constrained by the regional gradient, which magnitude is large enough to oppose flow toward the well.

The 1:2 slope may be related either to discharge of a lineal regional flow within the El Nabo Dyke/Fault (i.e. strip unit, Butler and Liu, 1991) or a new source of regional flow. Support evidence of the contribution of a hydrothermal deep groundwater flow system through the fault was provided by the increase in temperature while pumping (25 to 63°C, green line in Figure 8). The initial increase of temperature in a time interval of 83 minutes suggests mixing of local fresh groundwater and hydrothermal flow, with the presence of a preferential conduct through the magmatic dyke/fault.

The calibrated hydraulic conductivities (obtained using PEST software) were used to simulate the pumping test in the numerical model (red line; Figure 9). The wellbore storage may have caused the rapid initial drawdown of the El Nabo pumping test (the well is more than 1000 m depth and 6 inches in diameter). Time required for pumping stabilization (10,000 s, or approximate 3 hours, Figure 8) was not considered in the model, drawdown initiated from a relative zero value. A pseudo-steady flow regime observed in the 10,800-35,000 s (3-10 hour) intervals (Figures 8 and 9) was not completely adjusted by the calculated drawdown. From 20 hour (75,000 s) the numerical solution converges with the data and the model results are better fitted (Figure 9). In spite of the initial differences, we consider that model curve captures the overall behavior of the pumping test suggesting a similarity of hydraulic behavior between model and test.

The model allows discussing the contribution of each geological element in the overall hydraulic behavior of the system. Faults were considered as vertical planar structures with varying hydraulic conductivities according to the E-W or vertical groundwater flow direction. The block model of Figure 11 summarize the main groundwater flow results using the K values presented in Table 1, and shows the piezometric levels reached at the end of the pumping test simulation. Colors indicate piezometric levels, which range from 1925 in the north area to 1820 masl toward the south. The higher gradient is obtained toward the east of the *El Nabo Fault*. Arrows, indicating flow directions, show clearly that major structures (El Nabo and South faults) favor ground-water flow patterns along planes and also delimit compartments with differences in hydraulic behavior. Field observations show that the hydraulic interaction of the fault with the El Nabo well starts at 850 m of depth and the presence of hydrothermal groundwater can be interpreted in terms of ongoing deep lateral flow facilitated by the heterogeneous permeability within the fault-zone probably due to the dyke intrusion (López and Smith, 1995; Lopez and Smith, 1996). Horizontal flow predominates in the model while the flow patterns deviate along the geometric boundaries of the intrusive body, interrupting the connection between El Nabo and South faults, and following the regional N-S gradient.

Figure 12 shows one horizontal and two vertical cross sections (in the E-W and N-S directions) of the model (Figure 11) that allow to analyze the influence of major structures (El Nabo and South faults and the intrusive body) in groundwater flow patterns. In the horizontal cross section at 1400 masl of Figure 12a the northern segment of the *El Nabo Fault* act as a barrier by interrupting groundwater flow from north to south within the limestone and shale unit, also shown in the vertical BB' profile

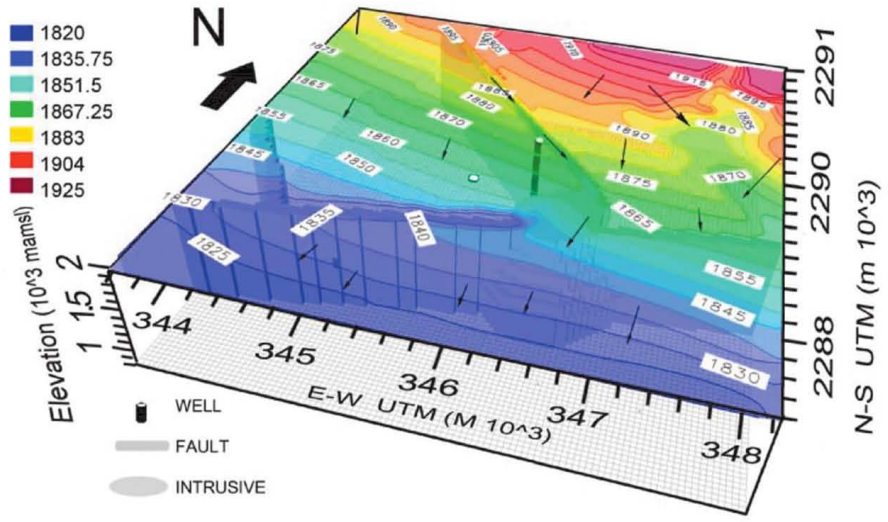

Figure 11. Model box of the study area presenting drawdown elevations and groundwater flow vectors after simulation of El Nabo pumping test using calibrated of hydraulic conductivity values shown in Table 1. Faults act as flow channel interfering with the regional flow gradient and compartmentalizing the aquifer system. Arrows show the direction and sense of flow. The large intrusive dome modifies flow in the fault. The El Nabo fault-dyke exerts a major influence in groundwater flow.

(Figure 12c). The hydraulic head observed at 1900 m north from the El Nabo fault decreases to 1840 m in the southern block. In the East-West cross section (AA´ in Fig. 12b) the color scale indicates a difference in piezometric elevations of 40 m at both sides of the fault. In the model the regional gradient is interrupted by the *El Nabo Fault* that acts as a lateral flow barrier in the east-west direction, the vertical equipotential lines indicate vertical flow within the fault. The NE-SW orientation of the *South Fault* seems to favor channelized lateral flow towards the SW along the main fault plane. The *South Fault* yielded the highest K value in the horizontal E-W direction (Table 1). The model is not sensitive to this structure and this high value may be an artifact produced in the model by the equalization of drawdown and regional gradient. However, field data suggest also a higher K for the *South Fault* than for *El Nabo Fault*.

The 1:2 slope of the derivative curve (orange line, Figure 9) was interpreted as lineal flow within a high permeability channel with semi-permeable walls, interpretation consistent with the presence of *El Nabo Fault-Dyke* (Figure 12 b, c). The semi-permeable walls condition in the model is represented by the equipotential lines at both sides of the faults. Smooth gradients within the stratigraphic units increase when crossing the fault indicating a high hydraulic gradient but with flow continuity. The limestone and shale unit also show hydraulic continuity with the fault to the west; whereas in the eastern part have a higher elevation suggesting a greater water contribution from the fault (Figure 12c).

Given that only one observation point could be considered, the El Nabo well is the deepest well drilled in the Queretaro area with most of the well depths about 300 m, analysis of representativeness of the obtained hydraulic conductivity was not possible to do. Nevertheless, the information yielded by the pumping test was useful for the calibration of the numerical model allowing simulating groundwater flow in the study area.

In summary, this work attempts to highlight the importance of integrating an accurate geological setting to understand groundwater flow dynamics in models of faulted aquifers in particular in cases were piezometric levels decrease constantly.

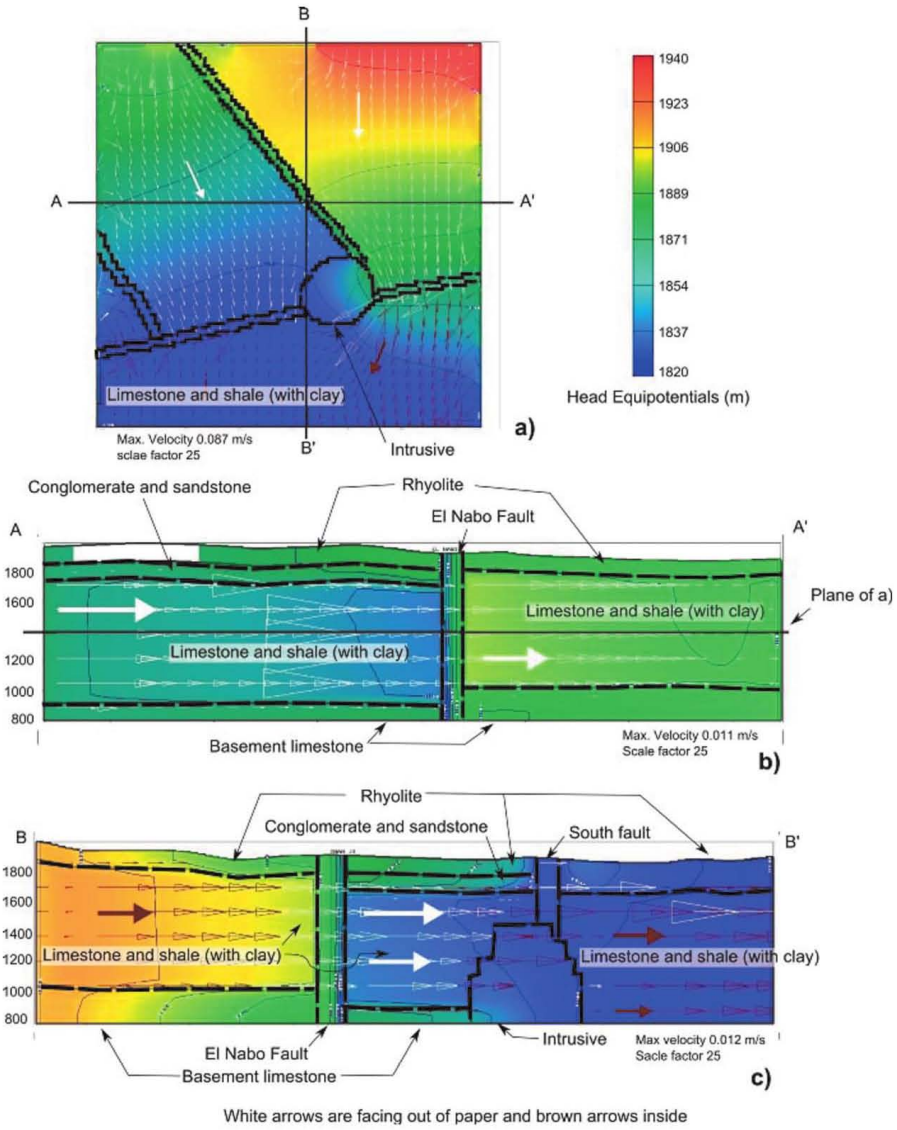

Figure 12. Horizontal and vertical sections of the model box are presented in Figure 11. Colors indicate variation of piezometric heads from 1940 to 1820 masl. (a) Horizontal cross section at 1400 masl (location shown in Figure 12b), the black lines represent the analyzed faults walls and intrusive body. (b) and (c) are two cross sections of the model box in the NS and EW directions respectively.

Fault zones in the study area have more than 50 m in thickness and several fault planes were observed where high and low K segments may coexist. Because the style and relative age of faulting determines variations in its hydraulic properties we consider that in faulted and deep aquifers (more than 200 m depth) the assessment of the overall flow dynamics is as, or more, important as obtaining specific hydraulic properties of the hydro-stratigraphic units.

Field evidences of present day hydrothermal water circulation within fault planes in the study area and the model results allow proposing that faults collect groundwater flow and explain the flow rate increase to 47 l/s at *El Nabo Fault*. Moreover, the Cretaceous sedimentary sequences show an overall low hydraulic conductivity. The magmatic dikes caused brecciation, open fractures, and hydrothermal alteration of the Cretaceous host rock and consequently enhancing its hydraulic conductivity (e.g., Zeidouni, 2012; Table 1). The South fault system favored the emplacement of the Oligocene intrusive body. Field observations suggest that this fault also favored fluid-flow over time along open fractures partially filled with sediments and secondary fault planes in a zone more than 50 m in width. We have observed precipitation of calcite in fractures (Figure 4b), and probably infiltration of superficial water. Correspondingly, after the simulation the higher K values obtained in the East-West direction of the South Fault allowed the hydraulic continuity of the system, according with the regional gradient (Figure 11).

Conclusions

Implementation of the geological structure in a numerical groundwater flow model, along with the estimation of hydraulic conductivities by a pumping test, produced relevant information about flow dynamics in the faulted aquifer system at the north of the Valley of Queretaro. This methodology can be applied to study groundwater flow in other areas of the Queretaro Valley and elsewhere in central Mexico, where water is extracted from depths greater than 200 m and high uncertainty exist about the influence of major structures in groundwater flow conditions.

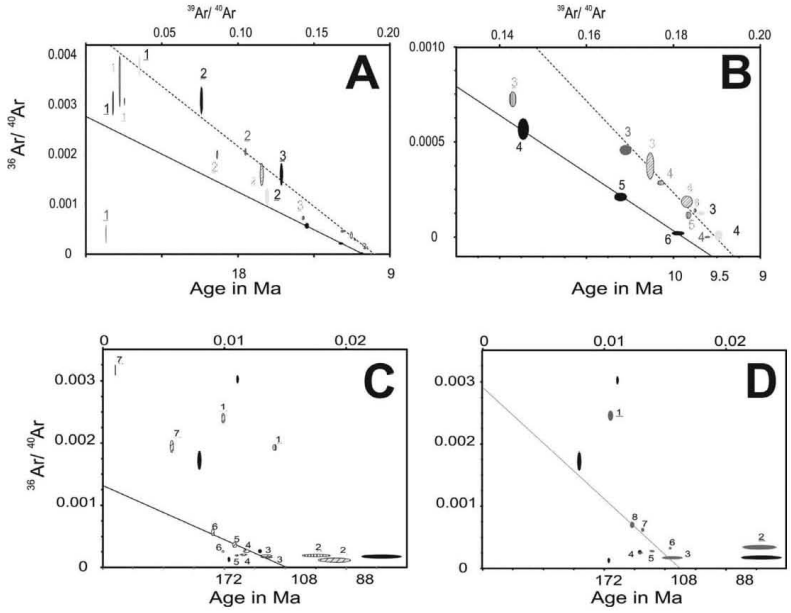

Figure S1. Correlation diagrams obtained for samples for Biotite Population 1 and 2. Isochron lines (A and B) yield an age around 9.5 Ma for samples of Biotite Population 1; whereas Biotite Population 2 (C and D) converge at an age around 100 Ma.

The study area is a block delimited by faults where the older geological units in the Queretaro Valley are exposed. Considering faults and truncation of hydrostratigraphic units in the sequence leaded to the reconnaissance of compartments in the aquifer system also reproduced in the model. The identification of groundwater flow patterns through the aquifer when modeling drawdown was consistent with measured piezometric levels. The derivative analysis of the pumping test suggests the presence of two different groundwater flow systems: (1) a flow, with slope 1:1, related to the limestone and shale sequence and, (2) a regional linear flow, with slope 1:2, transporting water through faults.

The numerical model along with the drawdown field observations allowed estimating relative values of hydraulic conductivity for eight geological units (Table 1). As expected, the model is sensitive to the fault located near the El Nabo well (Figure 1). Of importance to the study is the presence of volcano-sedimentary sequences below thick limestone units. Isotopic dating confirmed the presence of a Miocene magmatic dyke emplaced along the El Nabo Fault. Both the Balvanera and El Nabo fault systems favored the emplacement of Miocene volcanism through dykes along the faults planes (Figure 4). The presence of the fault-dyke was corroborated with stratigraphic correlation of a well log, and the results confirm its relevance to modify groundwater flow. The increased high flow rate in the El Nabo well pumping test (47 l/s) is an evidence of the high influence of the dike that allows groundwater to flow through the fault.

The obtained values agree with the conceptual model but connectivity between major faults cannot be evaluated only by the analysis of pumping tests. The numerical model allowed exploring the relevance of geological structures in the simulation of groundwater flow (Figures 11 and 12). In particular, the model results highlight how faults and intrusive bodies emplaced along faults modify groundwater flow by changing hydraulic properties and consequently flow direction. The model allowed improving the interpretation of the pumping tests. Numerical modeling is useful for a better understanding of complex aquifer systems that cannot be evaluated by analytical methods.

Acknowledgements

The project FOMIX CONACYT-Querétaro, Ref. QRO-2004-C01-39, supported this research in the Valley of Queretaro. Comision Estatal de Aguas de Queretaro (CEAQ), the local water management agency, is gratefully acknowledged for funding the isotopic dating and for the technical help provided during pumping tests. F.J. Gamez-González (Conagua), I. Barrón-Medellin (CEAQ), and J. Díaz Escarcega (CEAQ) provided useful discussions for the groundwater flow interpretation. G. Aguirre-Díaz and an anonymous reviewer helped to clarify the manuscript. R. Carrizosa-González (UNAM), I. Ortiz-Villaseñor (CEAQ), and J. Perez-Villarreal helped in the field campaign and data compilation.

References

Aguirre-Díaz G.J., López-Martínez M., 2001, The Amazcala caldera, Querétaro, México. Geology and geochronology. *Journal of Volcanology and Geothermal Research,* 11, 203-218.

Aguirre-Díaz G.J., Nieto-Obregón J., Zúñiga R., 2005, Seismogenic Basin and Range and intra-arc normal faulting in the central Mexican Volcanic Belt, Querétaro, México. *Geological Journal,* 40, 215-243.

Alaniz-Álvarez S.A., Nieto-Samaniego A.F., Reyes-Zaragoza M.A., Orozco-Esquivel M.T., Ojeda-García A.C., Vassallo F.L., 2001, Estratigrafía y deformación extensional en la región San Miguel de Allende-Querétaro, México (Stratigraphy and extensional deformation in the San Miguel de Allende-Queretaro region, Mexico). *Revista Mexicana de Ciencias Geologicas,* 18, 129-148.

Alaniz-Álvarez S.A., Nieto-Samaniego A.F., Orozco-Esquivel M.T., Vassallo F.L., Xu S., 2002, El sistema de fallas Taxco-San Miguel de Allende: implicaciones en la deformación post-eocénica del centro de México (The fault system Taxco-San Miguel de Allende: implications for post-Eocene deformation of central Mexico) *Boletin de la Sociedad Geologica Mexicana,* 55, 12-29.

Allen D.M., Michel F.A., 1999, Characterizing a Faulted Aquifer by Field Testing and Numerical Simulation. *Ground Water,* 37, 718-728.

Anderson E.I., 2006, Analytical solutions for flow to a well through a fault. *Advances in Water Resources,* 29, 1790-1803.

Bense V.F., Gleeson T., Loveless S.E., Bour O., Scibek J., 2013, Fault zone hydrogeology. *Earth-Science Reviews*, 127, 171-192.

Bourdet D., Ayoub J.A., Pirard Y.M., 1989, Use of pressure derivative in well-test interpretation. *SPE Formation Evaluation* June, 293-302.

Burbey T.J., 2008, The Influence of Geologic Structures on Deformation due to Ground Water Withdrawal. *Ground Water,* 46, 202-211.

Butler J.J., Liu W.Z., 1991, Pumping test in non-uniform aquifers - the linear strip case. *Journal of Hydrology*, 128, 69-99.

Caine J.S., Evans J.P., Forster C.B., 1996, Fault zone architecture and permeability structure. *Geology*, 24, 1025-1028.

Carreón-Freyre D., Cerca M., Luna-González L., Gámez-González F.J., 2005, Influencia de la estratigrafía y estructura geológica en el flujo de agua subterránea del Valle de Querétaro (Influence of the stratigraphy and geologic structures on groundwater flow, Querétaro Valley). *Revista Mexicana de Ciencias Geologicas,* 22, 1-18.

Cerca M., Ferrari L., López-Martínez M., Martiny B., Iriondo A., 2007, Late Cretaceous shortening and early Tertiary shearing in the central Sierra Madre del Sur, southern Mexico: Insights into the evolution of the Caribbean–North American plate interaction: *Tectonics,* 26, TC3007, doi:10.1029/2006TC001981.

Conagua, 2003, Plan de manejo del Acuífero Valle de Querétaro. *Comisión Nacional del Agua*, México, 234 pp.

Delinom R.M., 2009, Structural geology controls on groundwater flow: Lembang Fault case study, West Java, Indonesia. *Hydrogeology Journal*, 17, 1011-1023.

Doherty J., 2005, PEST Model-Independent Parameter Estimation User Manual: 5th Edition Watermark Numerical Computing, 336 pp.

Ferrari L., 2000, Avances en el conocimiento de la Faja Volcánica Transmexicana durante la última década. *Boletin de la Sociedad Geologica Mexicana,* 53, 84-92.

Hall C.M., 1981, The application of K-Ar and 40Ar/39Ar methods to the dating of recent volcanics and the Laschamp event. PhD Thesis. University of Toronto. Canada.

Harbaugh A.W., Banta E.R., Hill M.C., Mcdonald M.G., 2000, MODFLOW-2000, the U.S. Geological Survey modular ground-water model - User guide to modularization concepts and the Ground-Water Flow Process. U.S. Geological Survey Open-File Report 00-92, 121 pp.

Hsieh P.A., Neuman S.P., 1985, Field determination of the three-dimensional hydraulic conductivity tensor of anisotropic media, 1. Theory. *Water Resources Research,* 21, 1655–1665.

Ingebritsen S.E., Sanford W.E., Neuzil C.E., 2006, Groundwater in Geologic Processes. 2nd Edition.: *Cambridge University Press*, 536 pp.

Jourde H., Fenart P., Vinches M., Pistre S., Vayssade B., 2007, Relationship between the geometrical and structural properties of layered fractured rocks and their effective permeability tensor. A simulation study. *Journal of Hydrology*, 337, 117-132

Kulkarni H., Deolankar S.B., Lalwani A., Joseph B., Pawar S., 2000, Hydrogeological framework for the Deccan basalt groundwater systems, west-central India, *Hydrogeology Journal*, 8, 368–378.

Lopez, D.A., Smith, L, 1995, Fluid flow in fault zones: analysis of theinterplay of convective circulation and topographically driven groundwater flow. *Water Resources Research,* 31, 1489-1503.

Lopez D.A., Smith L., 1996, Fluid flow in fault zones: influence of hydraulic anysotropy and heterogeneity on the fluid flow and heat transfer regime. *Water Resources Research,* 32, 3227-3235.

Maclay R.W., Small T.A., 1983, Hydrostratigraphic subdivisions and fault barriers of the Edwards Aquifer, south-central Texas, U.S.A. *Journal of Hydrology,* 61, 127-146.

Mayer A., May W., Lukkarila C., Diehl J., 2007, Estimation of fault-zone conductance by calibration of a regional groundwater flow model: Desert Hot Springs, California. *Hydrogeology Journal,* 15, 1093-1106.

Pacheco F.A.L., 2002, Response to pumping of wells in sloping fault zone aquifers. *Journal of Hydrology,* 259, 116-135.

Rafini S., Larocque M., 2012, Numerical modeling of the hydraulic signatures of horizontal and inclined faults. *Hydrogeology Journal*. doi: 10.1007/s10040-011-0812-4.

Rathod K.S., Rushton K.R. ,1991, Interpretation of Pumping from two-zone layered aquifers using a numerical model. *Ground Water,* 29, 499-509.

Spane F.A., Wurstner S.K., 1993, DERIV: A computer program for calculating pressure derivatives for use in hydraulic test analysis. *Ground Water,* 31, 814-822.

Steiger R., Jäger E., 1977, Sub commission on Geochronology: Convention on the use of decay constants in Geo and Cosmochronology. *Earth and Planetary Science Letters,* 36, 359-362.

Tiab D., 2005, Analysis of pressure derivative data of hydraulically fractured wells by the Tiab's Direct Synthesis technique. *Journal of Petroleum Science and Engineering,* 49, 1–21.

Trejo-Moedano A., 1989, Estratigrafía y propiedades mecánicas del subsuelo del valle de la zona urbana de Querétaro (Stratigraphy and mechanical properties of the subsoil in the urban zone of Queretaro). Universidad Autónoma de Querétaro, México, 115 pp.

Valdez-Moreno G., Aguirre-Díaz G.J., López-Martínez M., 1998, El volcán La Joya, estados de Querétaro y Guanajuato; un estratovolcán miocénico del Cinturón Volcánico Mexicano (The volcano La Joya, states of Queretaro and Guanajuato, a Miocene stratovolcano from Mexican Volcanic Belt). *Revista Mexicana de Ciencias Geologicas,* 15, 181-197.

Walton W.C., 1970, Groundwater Resources Evaluation. Mc. Graw-Hill, New York. 185 pp.

York D., Evensen N., Lopez-Martinez M., De Basabe D.J., 2004, Unified equations for the slope, intercept, and standard errors of the best straight line *American Journal of Physics,* 73, 367-375.

Xu S., Nieto-Samaniego A.F., Alaniz-Alvarez S.A., Cerca-Martinez L.M., 2011, Structural analysis of a relay ramp in the Queretaro Graben, central Mexico: Implications for relay ramp development. *Revista Mexicana de Ciencias Geologicas,.* 28, 275-289.

Zeidouni M., 2012, Analytical model of leakage through fault to overlying formations. *Water Resources Research* 48, W00N02, doi:10.1029/2012WR012582.

Zoback M.D., 2007, Reservoir Geomechanics. Cambridge Press, 449 p.

Zuñiga F.R, Pacheco J.F., Guzmán-Speziale M., Aguirre-Diaz G.J., Espindola V.H., Nava E., 2003, The Sanfandila earthquake sequence of 1998, Queretaro, México: activation of an undocumented fault in the northern edge of central Trans-Mexican Volcanic Belt. *Tectonophysics,* 361, 229-238. doi:10.1016/S0040-1951(02)00606-6.

Capítulo III. “Shearing along faults and stratigraphic joints controlled by land subsidence in the Valley of Queretaro, Mexico”

Publicado en la revista Hydrogeology Journal en marzo 2016

Hydrogeol J
DOI 10.1007/s10040-016-1384-0

PAPER

Shearing along faults and stratigraphic joints controlled by land subsidence in the Valley of Queretaro, Mexico

D. Carreón-Freyre[1] · M. Cerca[1] · G. Ochoa-González[2] · P. Teatini[3] · F. R. Zuñiga[1]

Received: 12 August 2015 / Accepted: 10 February 2016

Abstract Slip of nearly vertical faults or horizontal stratigraphic joints has provoked the shearing of at least 16 well casings in a period of over 10 years in the Valley of Queretaro aquifer, Mexico. Evidence integrated from field observations, remote surface-deformation monitoring, in-situ monitoring, stratigraphic correlation, and numerical modeling indicate that groundwater depletion and land subsidence induce shearing. Two main factors conditioning the stress distribution and the location of sheared well casings have been identified: (1) slip on fault planes, and (2) slip on stratigraphic joints. Additionally, the distribution of piezometric gradients may be a factor that enhances shearing. Slip on faults can be generated either by the compaction of sedimentary units (passive faulting) or by slip of blocks delimited by pre-existing faults (reactivation). Major piezometric-level declines and the distribution of hydraulic gradients can also be associated with slip at stratigraphic joints. Faults and hydraulic contrasts in the heterogeneous rock sequence, along with groundwater extraction, influence the distribution of the gradients and delimit the compartments of groundwater in the aquifer. Analogue modeling allowed assessment of the distribution of stress–strain and displacements associated with the increase of the vertical stress. Fault-bounded aquifers in grabens are common in the central part of Mexico and the results obtained can be applied to other subsiding, structurally controlled aquifer systems elsewhere.

Keywords Geohazard · Aquifer compaction · Volcano-sedimentary sequence · Subsidence · Mexico

Published in the theme issue "Land Subsidence Processes"

✉ D. Carreón-Freyre
freyre@geociencias.unam.mx

[1] Laboratorio de Mecánica de Geosistemas, Centro de Geociencias, Universidad Nacional Autónoma de México (UNAM), 3001 Bvd. Juriquilla. Col Juriquilla, Queretaro C.P. 76230, México

[2] Posgrado en Ciencias de la Tierra, Centro de Geociencias, Universidad Nacional Autónoma de México (UNAM), 3001 Bvd. Juriquilla. Col Juriquilla, Queretaro C.P. 76230, Mexico

[3] Department of Civil, Environmental and Architectural Engineering, University of Padua, Padua, Italy

Introduction

Dependence on groundwater has provoked a dramatic decline of the piezometric levels in the wells supplying the city of Queretaro in Mexico over the last 40 years. The rapid exploitation of groundwater has caused a 2–5 m/y lowering of the piezometric level since the 1970s. Nowadays the depth of the water table below land surface in the lacustrine plain varies from point to point but averages about 160 m. Most of the water extraction wells (red circles in Fig. 1) are located within the Valley of Queretaro, and close to Miocene normal faults.

Rapid groundwater depletion in aquifers can induce compaction, land subsidence, soil fracturing, and faulting (Galloway and Burbey 2011; Carreón-Freyre 2010). Also, slip on pre-existing faults and ultimately horizontal shearing along weak lithological interfaces can be associated with groundwater or hydrocarbon depletion in particular cases (Dusseault et al. 2001). Faulting associated with land subsidence has been observed on the surface of the Queretaro plain, which has subsided 1–3 m over the last 40 years. The first fractures associated with land subsidence were observed in the early 1970s in Queretaro City (Rojas et al. 2002). Faulting of the recent sedimentary fill trends similarly to the regional north–south faults that have affected the region since the Miocene.

Published online: 02 March 2016

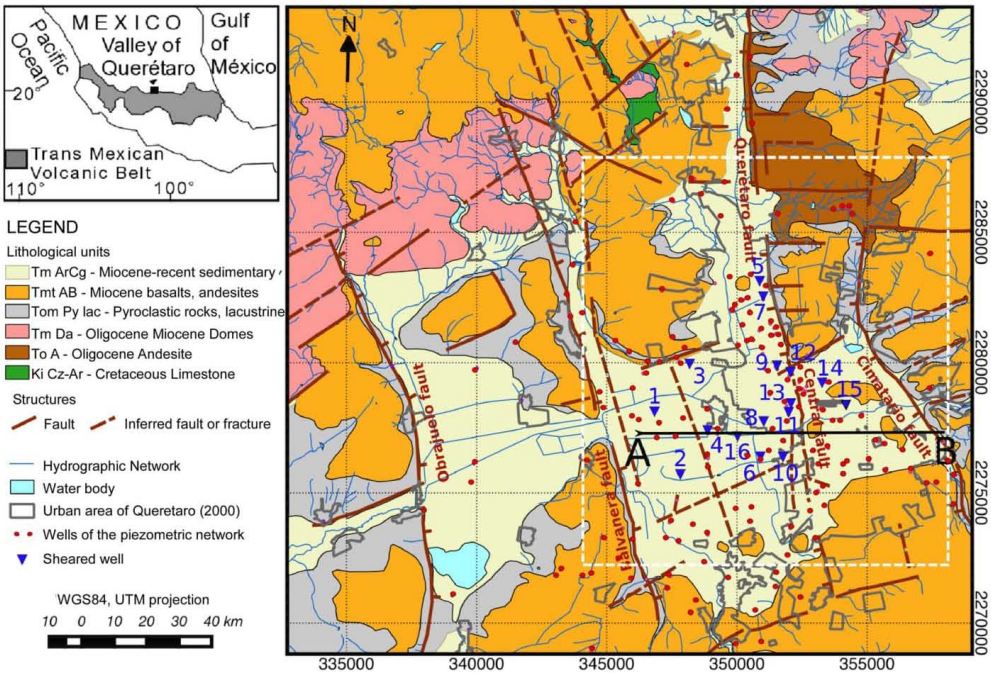

Fig. 1 Geological setting of the Queretaro Valley (modified from Carreón-Freyre et al. 2005). The study area is indicated with a *white dashed square*, groundwater extraction wells are marked with *red circles*, and sheared-casing wells with *blue inverted triangles*

For example, the Central Fault (CF) is a normal fault affecting the urban infrastructure of Queretaro City that links to the north with the trace of the regional Queretaro Fault (Carreon-Freyre and Cerca 2006). Nevertheless, fault slip is most likely caused by displacements at the edge of the buried tectonic scarps, which act as a rigid boundary localizing the deformation associated with groundwater depletion (Carreón-Freyre and Cerca 2009). The lack of seismicity reported in the area for the last 20 years does not support the hypothesis of *tectonic* fault displacements; there is only a single report of a small earthquake sequence about 20 km to the south of Queretaro City with normal fault mechanism similar to the regional faulting (Zúñiga et al. 2003). There is evidence of small along-dip displacements (less than 1 m) in the footwall of the regional faults such as in the Queretaro Fault (Fig. 1). Thus, the recent observed vertical slip of major faults is mostly related to land subsidence, in particular to differential compaction of variably thick sedimentary deposits generating zones of local shearing.

In many regions of central Mexico and Arizona in southern USA affected by land subsidence, it has been suggested that the buried scarps or sharp edges in the depth of the rigid basement can localize differential compaction of the overlying unconsolidated sediments (Jachens and Holzer 1982; Pacheco et al. 2006). In some cases, the ancient fault scarp was buried progressively as new rock sequences filled the topographic depressions, including the scarp, leading to important differences in thickness between the two sides of the fault. Long-term differential compaction of the thicker hanging-wall and thinner foot-wall sequences leads to the formation of a weak zone between these two parts and the propagation of the basement fault towards the surface. The compaction of the near surface sediments and the granular aquifers, interbedded with volcanic fractured aquifers, has been enhanced by intense groundwater exploitation in the region for several decades. Deformation in this complex system is attributed to predominantly vertical compaction following the trace of pre-existing faults and minor shearing along weak horizontal lithological interfaces.

A factor that may increase the localization of shearing forces is related to the distribution of hydraulic gradients due to groundwater withdrawal. Hydraulic gradients are formed where there is concentrated depletion of groundwater and may generate potential significant head differences in low-permeability zones and flow in high-permeability faulted zones. The modification of the stress state caused by hydraulic gradients can induce the slip of faults and joints. Groundwater

flow may lubricate permeable discontinuity planes. Shearing of the rock sequences also occurs when the seepage pressure exceeds the rock strength (Budhu 2011).

Previous works have documented the propagation of fractures from the subsoil to the surface in Queretaro (Carreón-Freyre et al. 2005; Carreon-Freyre and Cerca 2006). The piezometric evolution, ground deformation, and location of local faulting were correlated through a geomechanical model of the Valley of Queretaro (Ochoa-Gonzalez et al. 2013). The geological heterogeneities of the subsoil were integrated into this model to predict the deformation caused by water withdrawal within the sedimentary and pyroclastic granular materials. The results of the simulations showed that the areas where large differential subsidence had developed correspond to zones of the city with ground fractures. During the years 2000–2010, 16 casings of producing groundwater wells in the Valley of Queretaro were ruptured and displaced horizontally as shown in Fig. 2c. Besides the obvious damage to the wells and the production of groundwater (most of the ruptured wells were productive at the time of collapse), the damage suggests the formation of shearing planes associated with fault slip. The study area and location of the groundwater extraction wells that have been affected by shearing causing casing failure at different depths are presented in Fig. 1.

Compaction of aquifers in unconsolidated sediments results in the vertical protrusion of the well casing above land surface (Fig 2a), a common occurrence in the Valley of Queretaro (Pacheco et al. 2006) as in many other parts of the world; nevertheless, casing rupture in groundwater extraction wells has been poorly reported in the literature. The most detailed work on this subject was made by Borchers et al. (1998) who documented casing damage by a down-well television survey in 317 water wells in the Sacramento Valley, USA. Eighty-one wells were shown to be damaged by vertical compression of the well casing associated to land subsidence. Their results showed that the main cause of damage within the unconsolidated deposits was the compaction of clayey sediments related to a significant decrease of hydraulic heads, particularly when the resulting effective stresses exceeded the preconsolidation pressure of sediments (inelastic deformation). As sediments compact, they exert a frictional downward force on casings; when the contact between the casing and the deposits is weak, the well casing can be protruded but, if the frictional bond is strong enough, rupture occurs when the compressive stress exceeds the vertical compressive strength of the casing (Borchers et al. 1998).

In the afore-mentioned study, no case of casing rupture related to shearing was reported. However, shear failure of well casings in faulted reservoirs has been widely studied for oil extraction wells (Bo and Zhanghua 2004; Dusseault et al. 2001; Grasso 1992; Maury et al. 1992; Peng et al. 2007; Wang et al. 2011; Zoback and Zinke 2002). Casing failures due to compaction are common in reservoirs of high porosity and compressibility (Fredrich et al. 2000). In unconsolidated granular materials, non-uniform pressures may develop around the casing, and cavities may form and cause casing buckling and shear failure in the extracting wells. Casing shear failures caused by cavities in the unconsolidated sands of the Gudao reservoir, Shengli Oilfield in China, could be recorded and simulations showed that casing tends to bend toward discontinuities, with non-uniform small displacements (Peng et al. 2007). Within faulted rock masses, shearing has also been associated with the displacement of the rock strata along stratigraphic planes or along faults (Maury et al. 1992). Thus, casing-deformation mechanisms include localized horizontal shearing at weak lithology interfaces within the overburden. The shear failures can be triggered by stress concentrations generated by volume changes resulting from oil production or injection activity (Bo and Zhanghua 2004; Dusseault et al. 2001); moreover, the fault-dip variations also determine the maximum displacements of the casing and the axial strain (Wang et al. 2011).

In the Queretaro study case, both compressive and shearing mechanisms may coexist. Rupturing of a well casing may be due to the lateral displacement over weak stratigraphic or structural interfaces during compaction (Carreon-Freyre 2009). Evidence of ancient slip along the horizontal stratigraphic interfaces has been found elsewhere in the rock sequences exposed by regional faults (Xu et al. 2011). It is likely that the stress induced by pumping has reactivated these weak stratigraphic interfaces favoring shearing of the well casings. Photographs in Fig. 2 show evidence of land subsidence and differential deformation generating shear stresses that cause ground fracturing (Fig 2b), and horizontal (Fig. 2c) and vertical displacements of the near surface sequences (Fig 2d).

This work aims to integrate geological and hydrogeological evidence along with results from numerical models, to evaluate mechanisms of failure in granular and rock faulted aquifers caused mainly by groundwater withdrawal in intense extraction-rate regimes. Differential land subsidence and shearing of well casings along weak interfaces are evidence of the displacement along faults and stratigraphic joints in the Valley of Queretaro aquifer.

Geologic and hydrogeologic setting

The Valley of Queretaro is located within an extensional graben, Miocene in age, located at the border among the geological provinces of the Mesa Central and the Trans-Mexican Volcanic Belt (TMVB), in the central part of Mexico. The graben is delimited by two nearly orthogonal sets of structures (Alaniz-Alvarez et al. 2001; Carreón-Freyre et al. 2005; Aguirre-Diaz et al. 2005; Xu et al. 2011). Four north–south trending extensional faults associated with the larger scale Taxco San Miguel de Allende System define the main

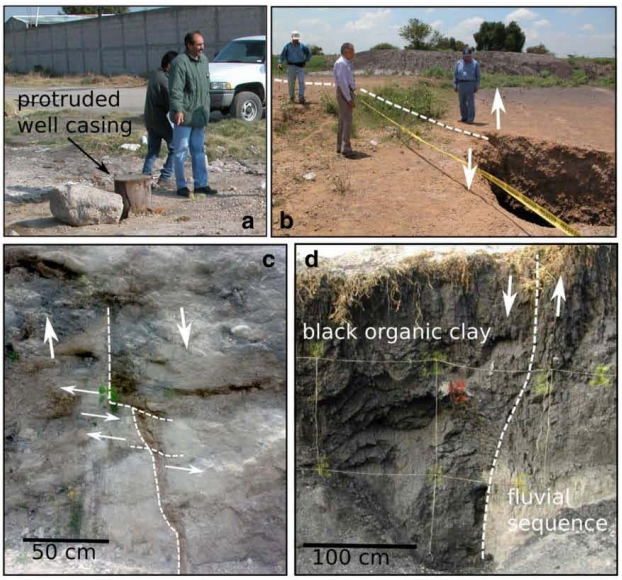

Fig. 2 Photographs of evidence of vertical and differential deformation within the near-surface sequences of Queretaro City: **a** Protruded well casing in the central part of the valley; **b** ground fracturing with differential vertical displacement; **c** displacements along horizontal discontinuities; **d** 1 m of vertical displacement of recent fluvio-lacustrine sequences (*rope squares* are 1 m^2)

extensional, nearly symmetric graben structure. The western flank of the graben is defined by the east dipping Obrajuelo and Balvanera Faults and the eastern flank by the west dipping Queretaro and Cimatario faults (Fig. 1). The block between the Balvanera and Queretaro Faults conforms the central basin of the graben. The Queretaro and Cimatario faults define the eastern part of the basin. The north–south trending extensional faults have three main periods of activity at about 10 million years (Ma), 7 Ma, and during the Quaternary, according to Alaniz-Alvarez et al. (2001). The Central Fault (CF) is the most important land-subsidence generated fault, with throws accumulating 2–3 m that continue at the south end of the trace of the Queretaro Fault. The analysis of well log records in the central part of the valley indicates that the Queretaro Fault is buried beneath a sedimentary cover along part of the trace of the CF. The regional Queretaro Fault has a total vertical throw of 172 m measured by Xu et al. (2011) in the north of the study area (near well No. 5, Fig. 1) accommodated in displaced blocks (steps), as is shown in the east–west geological section presented in Fig. 3. Throws of the Queretaro Fault in the zone of the buried trace, indicated by the differences in elevation of the same Miocene lava plateaus at both sides of the trace using the correlation of the lithological record of groundwater extraction wells, are of about 56 m in the central part near well No. 11, and 90 m to the south near well No. 6 (see location in Fig. 1 and vertical displacement of the Tmt AB unit near well No. 6 in Fig. 3). Because the trace of the Queretaro Fault is not evident south of the exposed area, Xu et al. (2011) proposed the existence of a relay ramp (overlapping zone) between the "5 de Febrero" and "Cimatario" Faults at the north of the city; the relay ramp has caused a basin-ward tilting of the horizontal layers. Quaternary slip in the CF has also been examined in trench excavations at two sites across the northernmost part of the fault where it displaces two Quaternary terraces of different ages. The trench exposures revealed a series of alluvial and pyroclastic deposits below a black organic clay deposit (Carreon-Freyre and Cerca 2006), ranging in age from ca. 25 to 1.75 thousand years (ka), that are vertically displaced across the steeply southeast-dipping fault (Fig. 2d). The trench data confirm that the fault has slipped within the last 25 ka but the vertical component of displacement of upper strata of 1.0 m (measured in the trench during year 2002) is equivalent to the surface subsidence recorded during the last ~30 years.

Besides the north–south trending faults, the geometry of the Valley of Queretaro is controlled by two other regional fault systems trending nearly orthogonal to the Queretaro fault and corresponding to the Chapala-Tula lineament ('Aguirre-Díaz et al. 2005; Suter et al. 2001). These faults are also extensional and along their trace there is evidence of aligned Oligocene domes (Alaniz-Alvarez et al. 2001) and recent volcanic activity (approx. 6 Ma, Aguirre-Díaz and López-Martínez 2001; Fig. 1). According to Alaniz-Alvarez et al. (2001) both fault systems were active contemporaneously in the Quaternary. The interaction among the two fault systems has produced the presence of a horst structure in the northern part of the Valley of Queretaro defined by south-dipping

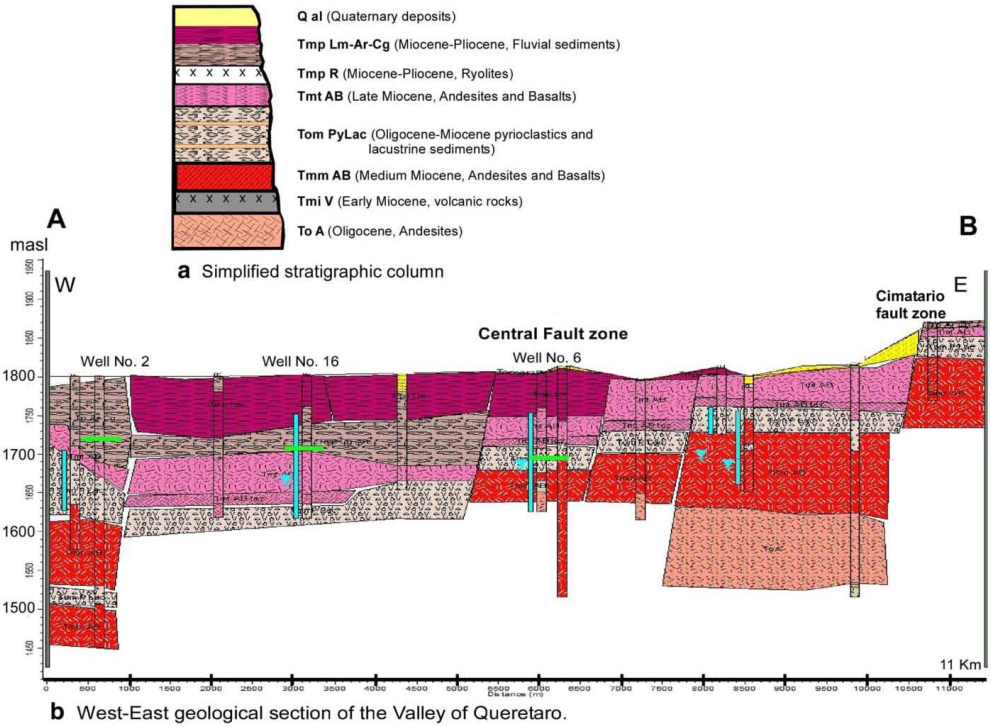

Fig. 3 **a** Representative stratigraphic column in the study area (adapted from Carreón-Freyre et al. 2005); **b** W–E geological section *A–B* (see Fig. 1) constructed by the correlation of lithologic well logs and highlighting the vertical dislocation between the main stratigraphic units by normal faulting. The location of the Central Fault (CF) and the *Cimatario Fault zone* is shown

faults, where the oldest rocks found in the region crop out; these structures control groundwater flow patterns (Ochoa-Gonzalez et al. 2015). In the southern part of the valley, there are north-dipping faults that delimit a horst, but in this case is mainly composed of late Miocene volcanic rocks of the Cimatario and other volcanoes. Other minor buried faults can be inferred from differences in the lithological logs in the central part of the valley that also determine groundwater patterns by delimiting compartments, as shown in the geological section of Fig. 3b. It is important to note that in this case, faults may behave either as hydraulic barriers or preferential channels, depending on the relative vertical displacements of the hydrostratigraphic units (Carreón-Freyre et al. 2005; Carrera-Hernández et al. 2015).

Queretaro City is partially placed above a plain composed of basaltic lava flows interbedded with an almost 100-m thick pyroclastic unit that was easily eroded by fluvial processes during the Tertiary. The near surface layers in the plain are composed of silt-sandy re-worked pyroclastic materials (also called volcaniclastic deposits) covered by organic silty and smectitic clay lacustrine materials. A detailed description of the stratigraphic sequence in the study area is presented elsewhere (Alaniz-Alvarez et al. 2001; Aguirre-Diaz et al. 2005; Carreón-Freyre et al. 2005; Xu et al. 2011; Ochoa-Gonzalez et al. 2015). The simplified stratigraphic column starting from the Oligocene (Fig. 3a) includes from bottom to the top: the lower-middle Tertiary volcanic rocks, mainly andesites and basalts but also dacite domes (units To A, Tmi V and Tmm AB); a granular sequence (50–80 m thick) composed of pyroclastic deposits (lapilli and ash) and lacustrine silt and clayey sediments (Tom Py Lac); the widespread volcanic unit of late Miocene composed of high fractured andesites and basalts (Tmt AB) that allowed the estimation of vertical displacements due to normal faulting; a thick fluvio-lacustrine unit normally graded that has coarse materials at the base (conglomerates and sands, Tmp Ar-Cg) and fine grain size materials at the top (silts and clays, Tmp Lm) corresponding to reworked pyroclastic and volcanic materials; and Quaternary alluvial and lacustrine deposits (Qal) that partially cover the study area. Below this sequence older, rock

sequences recognized in the Queretaro aquifer include a conglomerate of uncertain age, a limestone and shale sequence of the late Cretaceous, and a volcanic sedimentary unit of middle Cretaceous age (Ochoa-Gonzalez et al. 2015). The east–west geological section shown in Fig. 3b was constructed by the correlation of the lithological logs of water extraction wells. The variation of thickness and displacement of the geological units caused by normal faulting generates complex groundwater flow patterns.

Because of high contrast in the hydraulic properties of the stratigraphic sequence, the conceptual model of the Queretaro aquifer has been defined as a faulted, multilayer, semi-confined and compartmentalized system (Carreón-Freyre et al. 2005). Major faults in the area trace several kilometers long at surface and less than 10 km at depth, with a gouge zone typically of tens of meters; their hydraulic behavior may change abruptly at depth or in the surface depending on whether apertures are filled with low-permeability fault gouge or higher-permeability infill, and whether the fault offsets stratigraphic units of contrasting permeability (Ochoa-Gonzalez et al. 2015). Carreón-Freyre et al. (2005) proposed that the north–south and east–west faulting systems delimit compartments for local and intermediate groundwater flow systems based on the analysis of piezometric variations during the last 40 years. Recent isotopic data from groundwater samples provide evidence that these groundwater flow systems coexist in the Valley of Queretaro (G. Levresse, Centro de Geociencias-UNAM, personal communication, 2015): local and intermediate flow systems occur within the hydrostratigraphic units (approximately in the first 500 m in depth) and a regional flow system occurs through the two major faults systems, which may have horizontal and vertical components, frequently related to hydrothermal flows associated with the recent volcanic activity reported in the area (Aguirre-Díaz and López-Martínez 2001; Ochoa-Gonzalez et al. 2015).

In summary, groundwater flows through compartments delimited by the orthogonal north–south and east–west faulting systems as shown in the geologic model of Fig. 4 constructed with the software HydroGeoAnalyst (HGA, Schlumberger Water Resources). The three-dimensional (3D) geological model was realized by correlating 60 lithologic logs and field mapping.

Groundwater withdrawal began in Queretaro during the early 1970s. Since then, water depletion occurred with an approximate rate of 3–5 m/y (Conagua 2003). According to the piezometric historical records of Conagua (2003), during the decade 1980–1990, the shallow unconfined granular

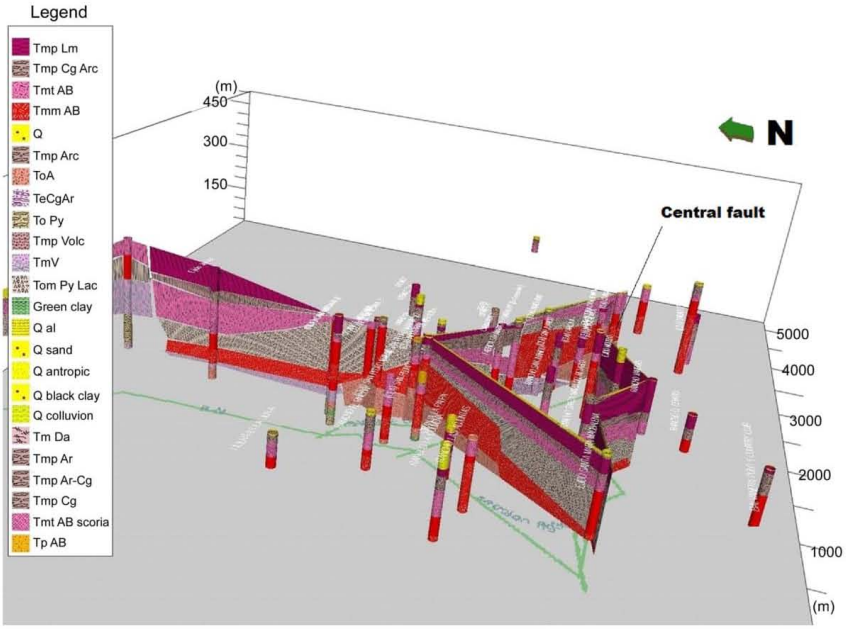

Fig. 4 Three-dimensional geological model showing the structure of the subsoil in the Queretaro area, faulting, and lateral and vertical variations of the main stratigraphic units (created using HGA)

aquifer, corresponding to the Tmp Lm-Ar-Cg stratigraphic unit, was exploited. The drawdown during this time was approximately from 40 to 70 m in depth below land surface. From the 1990s to the 2000s, groundwater was exploited from the underlying Tmt AB volcanic unit, a semi-confined fractured aquifer. At this time, the average depth of the extraction wells varied between 150 and 200 m. During the first decade of this century, the fractured aquifer was depleted and groundwater levels had declined to the elevation of the second granular aquifer, corresponding to the confined Tom Pylac unit, between 80 and 120 m in depth. Since then, the average depth of the new drilled extraction wells varies from 500 to 600 m. In many places in the Valley of Queretaro, the second granular aquifer has been already depleted and groundwater has been extracted from the second fractured volcanic unit Tmm AB. Nowadays groundwater flows mainly through this volcanic unit, the base of the granular aquifer and through major faults.

Modeling deformation due to groundwater pumping

The fault scarp of the Central Fault (CF) was measured at 0.75 m (Rojas et al. 2002) at the time of a decline of the groundwater level of about 60 m. Remote sensing measurements (InSAR) of the land subsidence rates in the Valley of Queretaro have yielded values up to 6.8 cm/y over the period 2003–2005 (Farina et al. 2007, 2008) with deformation patterns along the CF but with a wider influence in the central part of the fault; and an average rate of 5 cm/y over the period 2007–2011 (Chaussard et al. 2014), with land subsidence predominantly localized at the northern part of the CF where it intersects a SW–NE trending fault. Chaussard et al. (2014) classified the vertical deformation as a rapid fault-limited subsidence. Differences in the deformation and geometry observed along the CF seem to be related to lateral variations of the geological properties of sediments (Carreon-Freyre and Cerca 2006). For instance, Pacheco et al. (2006) reported a subsidence rate of 60 cm during year 2001 westward of CF and a relative stability to the east. The differences in reported land subsidence rates along the CF points to differential compaction of the sediments that is associated with localized ground fracturing and faulting. The temporal variations in the spatial distribution of subsidence suggest that deformation is controlled by changes in the localization of the drawdown zones. In the long-term, the CF controlled the thickness variations of the sedimentary filling in the study area and presently affects groundwater flow and deformation (Carreon-Freyre and Cerca 2006). Land subsidence is consistent with the average groundwater depletion rate of 3 m/y reported since 1975 (Conagua 2003); this rate has increased to 5 m/y in localized places over the last few years.

In order to assess the deformation due to the compaction of granular materials and the increase of effective stress associated with groundwater withdrawal, a flow and mechanical model has been developed previously using the 3D finite-element geomechanical simulator GEPS3D (Geomechanical Elasto-Plastic Simulator; Gambolati et al. 2001; Teatini et al. 2006). The major faults associated with land subsidence and seven lithologic units were included in the static model (Fig. 5; Ochoa-Gonzalez et al. 2013). From top to bottom the lithologic units are consistent with the simplified stratigraphic column of Fig. 3a and were integrated in the model as follow: (1) The Q Clay unit (Quaternary Clays), which is the same unit as Q al; (2) The Tp Ar-Cg unit (granular-fluvial sediments), which is the same unit as the Tmp Lm-Ar-Cg unit; (3) The Tmt AB unit (fractured andesites and basalts); (4) The Tom Py Lac unit (granular-pyroclastic and lacustrine deposits); (5) The Tmm AB unit (fractured andesites and basalts); (6) The ToA unit (andesites), and (7) a low permeability basal unit as the hydrologic basement.

The simulation approach included two phases: the hydrodynamics of the pumped aquifers is first simulated by a 3D groundwater flow model and then the subsidence is computed

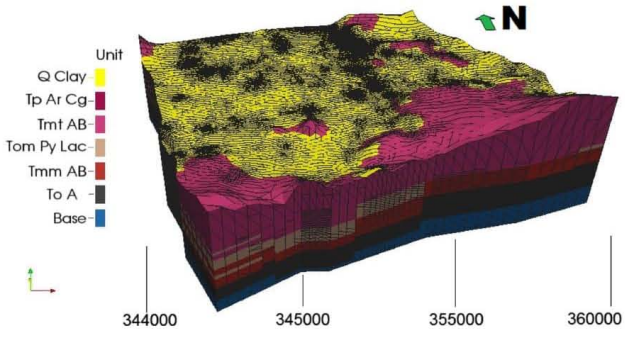

Fig. 5 3D finite element mesh of the geological structure of the Queretaro valley (modified from Ochoa-Gonzalez et al. 2013)

by the use of a 3D poro-mechanical model with the pressure variation considered as an external distributed source of strength within the porous media (for further details see Ochoa-Gonzalez et al. 2013). Failure generation was not explicitly simulated; nevertheless, the complete stress field was computed and the activation of discontinuities occurred when the normal stress (σ_1) became negative and/or shear stress increased above the bound $c+\sigma_1 \tan\varphi$, where c and φ are the cohesion and the friction angle of the fracture/formation, respectively.

The modeling results showed a total drawdown of 160 m and contrasting piezometric levels across the CF that agree with the hydrographs reported by Carreón-Freyre et al. (2005). The model was calibrated using the measured piezometric levels over the 31 years from 1970 to 2001. The output of the subsidence model presented in Fig. 6 agrees with field measurements and with the remote sensing (InSAR) records of land subsidence reported previously (Farina et al. 2007, 2008; Chaussard et al. 2014), thus allowing prediction of differential deformation of the volcano-sedimentary sequences and correlation with the development of earth fissures. The similarity in magnitude and subsidence patterns of the model developed by Ochoa-Gonzalez et al. (2013) and the InSAR results of Farina et al. (2007, 2008) and Chaussard et al. (2014) confirms the relevance of the CF to localize the surface vertical displacements (settlements; see red colors corresponding to more than 20 cm of settlements near CF, Fig. 6).

The results of the previous model (Ochoa-Gonzalez et al. 2013, 2014) show that thickness variations of fractured volcanic and granular units directly affect the effective stress changes in the deep layers and the distribution of the surface movements, with the larger land subsidence not necessarily directly above the most depleted zones of the aquifer system, as mentioned by Bell et al. (2002). The unequal distribution of the geological units in the valley of Queretaro causes complex patterns of groundwater flow and a highly variable distribution of pore pressure, with the major withdrawal zones that are not necessarily related in space with the largest subsidence areas. The surface deformation associated with land subsidence depends on the vertical compaction, and thus on the increase of effective stress, the thickness of the granular sequences (sedimentary and pyroclastic materials), and the location of major faulting.

The groundwater modeling results reported by Ochoa-Gonzalez et al. (2013) show major drawdown zones within the fractured volcanic units (see Tmt AB unit in the geological section of Fig 3b) in the CF footwall (at the east of the trace in surface) over the period 1970 to 2001 considering the piezometric values presented by Carreón-Freyre et al. (2005). The same model simulated a 2.25-m land subsidence, consistent with the scarp measurements available for the period (Rojas et al. 2002; Pacheco et al. 2006) over the hanging wall, at the west side of the CF, where compressible sedimentary materials of unit Tmp Lm-Ar are located (Fig 6).

In contrast with the previous piezometric evolution, the groundwater piezometric levels for the past 11 years (2003–2014) show that the major drawdown cone migrated to the west of the CF in the central part of the valley (dark blue zone in Fig. 7) and increased to about 60 m (5.45 m/y). A recovery of the former drawdown zone to the east of the CF is also observed but information is not available to explain this behavior. The highest depletion zone for the period 2003–2014 is located in the central block of the graben delimited by the two orthogonal systems of regional faulting, with minor

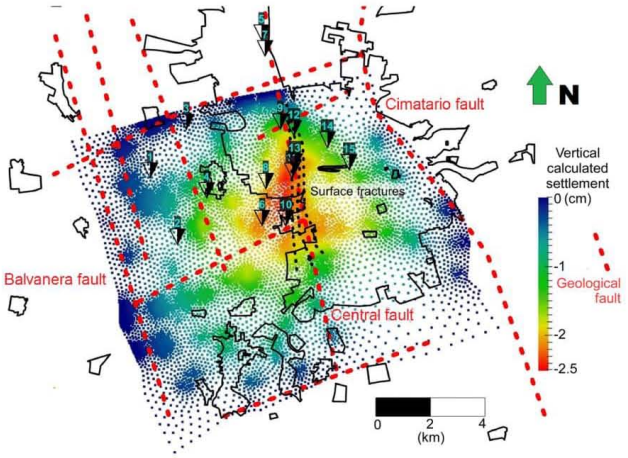

Fig. 6 Cumulative land subsidence in the study area as obtained from the 3D geomechanical model over the period 1970–2001 (modified from Ochoa-Gonzalez et al. 2014). The obtained vertical displacements correspond with the InSAR results reported by Farina et al. (2007, 2008) and Chaussard et al. (2014). The *numbered inverted triangles* indicate the location of the studied sheared-casing wells (as in Fig. 1). The *black polygons* correspond to the jurisdictional boundaries of Queretaro City. *Red dotted lines* indicate the trace of the major reported faults.

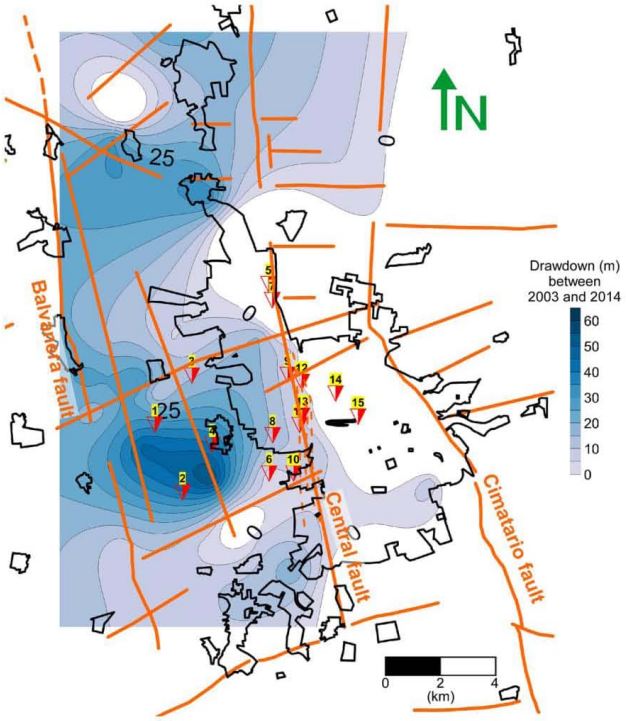

Fig. 7 Groundwater drawdown calculated from piezometric measurements over the period from 2003 to 2014. *Orange lines* indicate the trace of the major reported faults. The major zone of depletion (60 m) can be observed to the west of the Central Fault and is delimited by two E–W faults. The *numbered inverted triangles* indicate the location of the studied sheared-casing wells (as in Fig. 1). The *black polygons* correspond to the jurisdictional boundaries of Queretaro City

depletion recorded to the north and south in correspondence with other fault-delimited compartments of this aquifer system. The change in the hydraulic gradient across the CF for the two analyzed time periods suggests that the fault impedes groundwater flow causing the increased hydraulic gradient observed there. In the north of the Queretaro aquifer, simulated flow through regional faults suggests that these structures might represent either preferential channels or flow barriers (Ochoa-Gonzalez et al. 2015). In the case of the CF the number of sheared casing wells (5, 7, 10, 11, 12, 13) located along its trace are consistent with fault slippage. Wells 1, 2, and 4, in contrast are located within the major depletion zone. The remaining wells are located along other fault zones.

Shearing of pumping well casings

Shearing of well casings has been reported for oil production wells (Dusseault et al. 2001; Grasso 1992; Ferronato et al. 2008; Peng et al. 2007) but few cases have been reported for water extraction wells (Borchers et al. 1998). In the Queretaro study area, at least 16 productive groundwater wells have been ruptured by shearing at different times during the period from 2000 to 2010. Their locations evidence the spatial relation with faulting (particularly with respect to the CF), vertical deformation (Fig. 6), and groundwater drawdown (Fig. 7). Most of the wells have a steel casing of 35.6 cm in diameter (14 in. and 0.7 cm thick (1/4 in). Because of the proprietary nature of some of the well data (Queretaro Agency of Water, or CEA for its Spanish acronym) the details of well coordinates and rupturing dates are not available. Probably other wells ruptured but either they are not reported or were already abandoned for water production at the time of shearing.

The lithologic record of representative wells and the rupture depths are presented in Fig. 8 (well Nos. 2, 16, 6, 11, 3 and 5, ordered approximately from south to north). Most of the ruptures (marked with a green line in Fig. 8) correspond to depths characterized by a change in sedimentary facies from fine to coarse grain-size materials within the sedimentary units or directly at the contact between relatively stiffer volcanic rocks and more compliant granular materials, i.e. where higher mechanical strength contrasts are located. Deformation of the ruptured wells has been monitored in selected wells of the Valley of Queretaro by the use of a video camera that is able

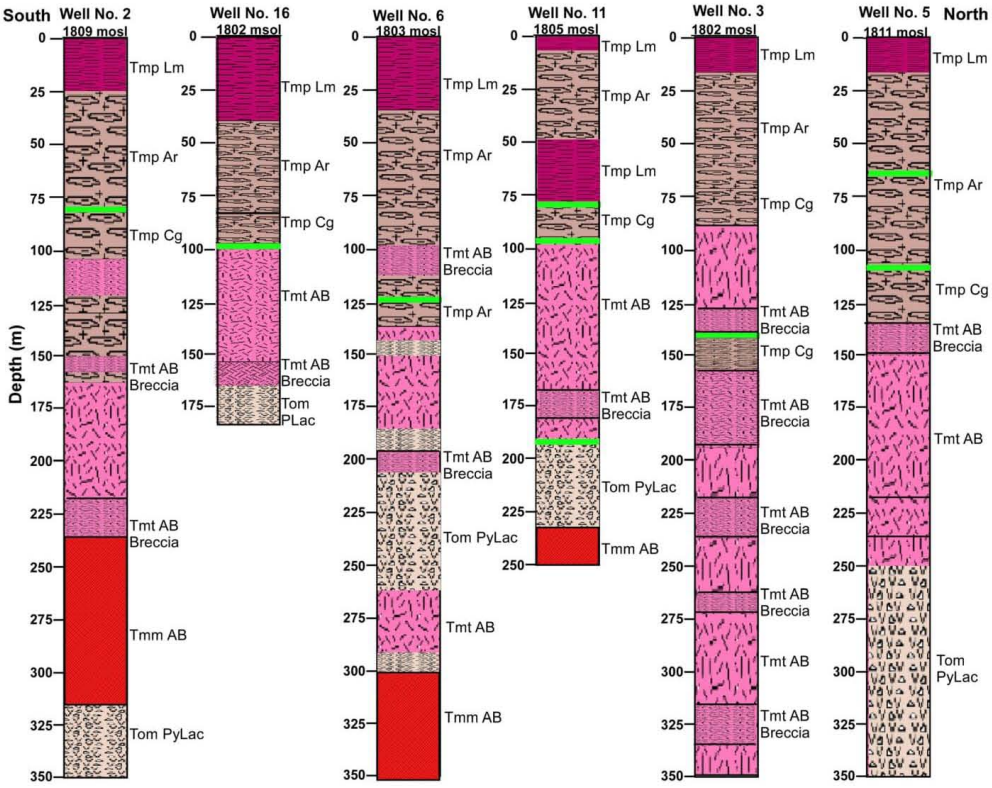

Fig. 8 Stratigraphy of six representative sheared groundwater extraction well casings. The wells are approximately aligned from south to north. Wells *5*, *6*, and *11* are located along the Central Fault (CF) (see Fig 1). The *green lines* indicate the depth of rupture during the period 2000–2010. Note that wells 5 and 11, located near the CF, sheared at different depths

to measure the casing diameter accurately. Video camera logs are mainly made for monitoring casing shapes and locations of shearing ruptures in casings and to provide images of the damage in the extraction wells. Damage recorded with this technique includes casing bending due to compressive stress, diameter variations along the casing due to deformation, cavities associated to the loss of material due to collapse of unconsolidated sedimentary formations, and rupture of the well. Figure 9 shows the casing images for normal and rupture conditions, as well as schematic longitudinal sections, for the two modes of shearing ruptures observed in the area: fault slip and stratigraphic joint slip.

An example of an extraction well steel casing broken by near vertical shearing caused by fault slip is presented in Fig. 9a. The rupture extends from 79 to 90 m depth. This well is located near the CF. Note that in Fig. 9a the vertical dashed lines outline the shape of the longitudinal fracture that has a significant aperture between the fracture planes. Along the aperture of the fracture, the unconsolidated fault gouge entered the casing. Figure 9b presents an image of an interval of borehole without casing that displaced laterally along a stratigraphic joint between coarse breccia and volcanic rocks in a well located west of the well 7. The figure shows a high rugosity slip plane at 260 m depth. Analysis of the video recording shows that several slip planes and rock collapses occurred between 244 and 270 m in depth. It is important to mention that static water level in this well was encountered at 98 m depth. The well ruptures present in the Queretaro aquifer evidence the activation of pre-existing faults by subsidence and the horizontal slip caused by shear stresses associated to groundwater exploitation.

Xu et al. (2011) also reported horizontal displacements along stratigraphic contacts associated with Miocene normal faulting in the Queretaro. These displacements occur when the

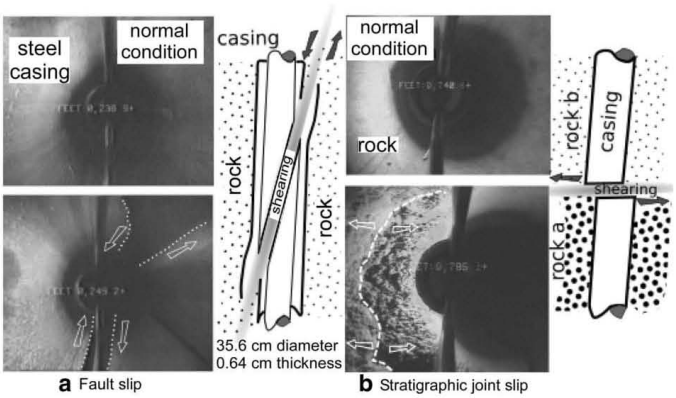

Fig. 9 Examples of well-casing shearing modes in the Valley of Queretaro as imaged from video camera monitoring: **a** slip on fault planes and, **b** slip at stratigraphic joints

lithostatic loads exceed the strength of the stratigraphic joints. From compressibility experimental data, Dusseault et al. (2001) reported a 5 % porosity reduction for a granular oil reservoir under drawdown conditions that represented 5 m of sediment compaction for a 100-m-thick reservoir. This is the same order of magnitude of the vertical deformation of the sedimentary and pyroclastic deposits in Queretaro nearby the CF. In the case of high angle normal faults such as CF, a narrow drawdown zone and the increase in effective stress may lead to shear-stress concentration and horizontal displacements along the strata and fault interfaces.

In the published literature, shearing related to land subsidence is mentioned to be produced by the horizontal displacement of layers along stratigraphic joints related to contacts, changes in sedimentary facies (grain size), or steeply inclined faults planes, where the extensional stress associated with hydraulic gradients can exceed the shear strength of the rocks or their interfaces (Burbey 2002, 2008; Hernandez-Marin and Burbey 2009). Dusseault et al. (2001) proposed that displacements are generated by volume changes resulting from fluid extraction where the main deformation is localized as shearing at the interfaces of geological materials and are directly related to the pore pressure and stress changes induced by fluid extraction.

Land subsidence and shearing in the Valley of Queretaro

Land subsidence in the Valley of Queretaro has been shown to be related to piezometric drawdown and to the variation of thickness and compressibility of granular materials (Ochoa-Gonzalez et al. 2013). In faulted and highly heterogeneous aquifer systems such as the Queretaro aquifer system, a close relation exists among the structure of the subsoil, the depositional conditions, the grain size distribution (hence hydraulic and geomechanical properties), and the spatial variation of piezometric gradients. Two main factors conditioning the stress distribution and the susceptibility of well casings to shearing have been identified: (1) slip on fault planes, and (2) slip on stratigraphic joints. Additionally, the distribution of piezometric gradients may be a factor that enhances shearing.

Subsidence-triggered slip on fault planes

The first order effect of subsidence in the Valley of Queretaro is the localization of settlements at the hanging wall of normal faults. Displacements of the order of meters can be generated either by the presence of steps in the buried basements below the compressible sedimentary units (passive faulting) or slip along relatively weak planes of pre-existing faults. The influence of the structural anisotropy produced by major faulting on the groundwater flow patterns in a horst block of the Queretaro aquifer has been analyzed by Ochoa-Gonzalez et al. (2015), using a numerical model implemented with the Visual-MODFLOW software. Their results showed how passive faults and volcanic structures compartmentalize the aquifer system and may transmit high-rate regional flows. An attempt to analyze the mechanical response of the multilayered and faulted Queretaro aquifer system to pumping was reported by Ochoa-Gonzalez and Carreón-Freyre (2010) using an elastic model implemented with Code_Aster (Fernandes 2009), a finite element simulator developed by EDF (Electricite de France). Their study suggested that, in the presence of faults, subsidence simulations must consider not only the superficial compressible geological deposits but the sum of the whole structure of the sequence affected by piezometric level variations.

For this work, a new 2D model is presented using Code_Aster, to include the geological features that may

condition the groundwater flow patterns and stress–strain relationships, i.e. the contrasting geomechanical layers related to stratigraphic variations and their lateral truncation by faulting (the setup is presented in Fig. 10a). The model domain is 4, 000 m long, 590 m high, and comprises four blocks (B_a, B_b, B_b and B_d) that are assumed to be separated by three normal faults (similar to the central part of geological section of Fig. 3b). The model addresses the five layers representing the main unconsolidated granular and rock geological units presented in Fig. 3a. Normal faults are not explicitly accounted for, and thus they do not have any specific property, but are defined by the vertical offset of the stratigraphic units. Two groups of elastic parameters were established to characterize both granular and fractured rock geological units. A Young modulus (E) equal to 1 GPa and a Poisson ratio (ν) of 0.3 were assigned to the granular units (Tmp LmArCg and Tom PyLac), according to the average values reported by Gercek (2007) for medium-dense silty sands and by Gregory (1976) for medium-porosity sedimentary rocks. For the fractured volcanic rocks (Tmt AB, Tmm AB), $E=10$ GPa and $\nu=0.25$ according to the values reported by Gercek (2007) for middle-jointed andesites and basalts. The ToA unit is a volcanic breccia as observed in several outcrops in the study area and was modeled with elastic parameters similar to granular materials ($E=1$ GPa, $\nu=0.3$). The code accounts for elastic deformation with boundary conditions that may impose displacements, and forces or stresses. The bottom boundary is fixed and horizontal displacements are precluded laterally (Fig. 10a). In the selected modeling approach, the increase of effective stress due to piezometric decline is approximated by the application of an external vertical load on the top of the model. The increase on effective stress is considered to be equivalent to the decrease of pore pressure ($d\sigma' = -dp$) due to drawdown as shown in Fig. 7. From the drawdown analysis, the maximum and minimum between piezometric levels for the 2003–2014 period amount to 80 and 10 m, respectively. Therefore, the corresponding applied load was estimated by computing the equivalent decrease of the hydraulic head to show how contrasting layers modify the stress and strain distribution when groundwater levels decline in a segmented aquifer. The applied load differs between the compartments delimited by faulting. The estimated applied load in the blocks B_b and B_c is 0.8 MPa, where major pore pressure depletion has been localized, and in the blocks B_a and B_d, it is 0.1 MPa (Fig. 10a). This procedure simulates a greater depletion in the blocks B_b and B_c; higher vertical stress is localized along the "fault plane" and lower horizontal stresses along stratigraphic joints, as shown in Fig. 10b. Major vertical displacements are localized on the top of the sequence (Fig. 10d).

Note that the order of magnitude of the vertical displacements equal to 25 cm agrees with that of the subsidence measured by remote sensing (Chaussard et al. 2014) in the compartment delimited by the CF (see Fig. 6) and previously simulated by Ochoa-Gonzalez et al. (2013). The distribution of the strain in Fig. 10e shows a clear increase of strain localized within the contact between the Tmt AB and Tom PyLac units. Small but significant horizontal strain values are distributed along the layer contacts in this equivalent model result.

Slip at stratigraphic joints

A second effect of subsidence in the study area is the horizontal slip along stratigraphic joints with an order of magnitude of centimeters as measured in ruptured wells. Similarly, the model results (Fig. 10c) show localization of the horizontal stresses at the intersections of faulting and stratigraphic joints with a value as much as 0.3 MPa (a third of the applied load). The horizontal strains are small but enough to induce shearing (Fig. 10f). For instance, a slip of 20 cm is produced along a stratigraphic contact considering a strain equal to 5×10^{-5} over the 4,000-m length of the model. This value is comparable with shearing observed in the rupture of wells casings (Nos. 11 and 5 in Fig. 8) and at outcrops (Fig. 2c).

Lithologic variations such as the degree of cementation in alluvium or other preexisting discontinuities (Budhu 2011), play an important role in the development and location of shearing (Hernandez-Marin and Burbey 2009). Budhu (2011) has analyzed shearing of the soil mass induced by the increase of vertical effective stresses caused by groundwater pumping. Similar cases of rock mass shearing leading to well-casing rupture were reported by Dusseault et al. (2001) in the Willmington oil field at Long Beach California, USA, where bedding planes slipped both seismically and aseismically over a 15-year period, and by Peng et al. (2007) for unconsolidated sands in the Gudao reservoir of the Shengli Oilfield, China, caused by induced cavities due to erosion.

The results of this study point out the strong effects exerted by the geological discontinuities on the stress and strain distribution in subsiding basins, with the potential for inducing localized formation shearing associated with horizontal displacements along weakening planes such as stratigraphic joints. It is documented here, that in Queretaro City, the depths of shearing in well casings reported in the period between 2000 to 2010 varied from 70 to 150 m depth in most of the cases. This depth interval corresponds with the variation in grain size of the Tmp normally graded fluvio-lacustrine unit, specifically with the change from basal conglomerates to silt and sandy materials (e.g., well Nos. 2, 6 and 5 of Fig. 8) or with the granular-rock contact between this unit and the underlying Tmt Andesitic and Basaltic rock (e.g., well Nos. 16, 11 and 3 of Fig. 8).

Distribution of piezometric gradients

At the beginning of the year 2000, piezometric levels were on average about 100 m below land surface (Conagua 2003) and

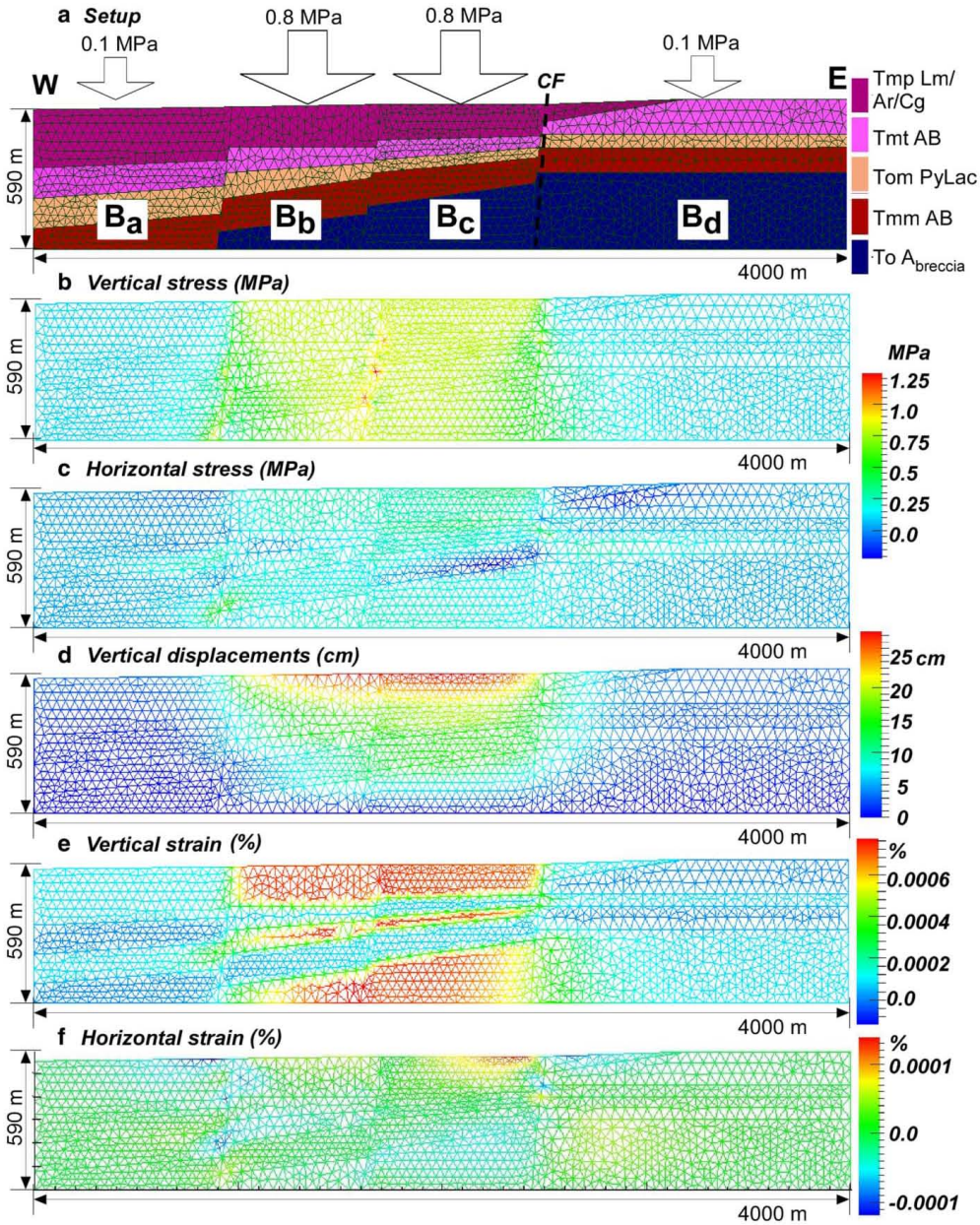

Fig. 10 Results of the 2D elastic simulation of stress–strain development in the faulted and heterogeneous basin of Queretaro for vertical applied loads equal to 0.8 MPa in blocks B_b, B_c, and 0.1 MPa in blocks B_a and B_d. **a** Geological setting and finite element mesh; **b** vertical stress distribution; **c** horizontal stress distribution; **d** vertical displacements; **e** vertical strain distribution; and **f** horizontal strain distribution

presently are more than 160 m below land surface. That means that steep piezometric gradients may be a factor in enhancing slip on fault planes and stratigraphic joints and shearing of the well casings by inducing hydraulic stresses on weak interfaces (faults and stratigraphic joints). The distribution of piezometric gradients gives further support to the importance of faulting to define groundwater compartments in the multilayer aquifer system of Queretaro. The analysis of groundwater depletion in the Queretaro aquifer during the period 1970–2001 reported by Carreón-Freyre et al. (2005), compared with the 2003–2014 period presented in this work, evidence an important change in the distribution of the drawdown cone mainly controlled by the CF. The highest drawdown values during the period 1970–2002 were located at the footwall of the CF at the central part of the valley and at the north zone (Carreón-Freyre et al. 2005) and migrated to the hanging wall, also at the central part of the valley, during the period 2003–2014 (Fig. 7). In particular, the shearing of well casings occurred during the time when the direction of the hydraulic gradient reversed from westward to eastward.

An analysis of the variation of the piezometric gradients (PG) in 2003, 2006, 2009, and 2014 is presented in Fig. 11. For comparative purposes, the actual surface topography (Fig. 11d), the trace of major faults, and the top morphology

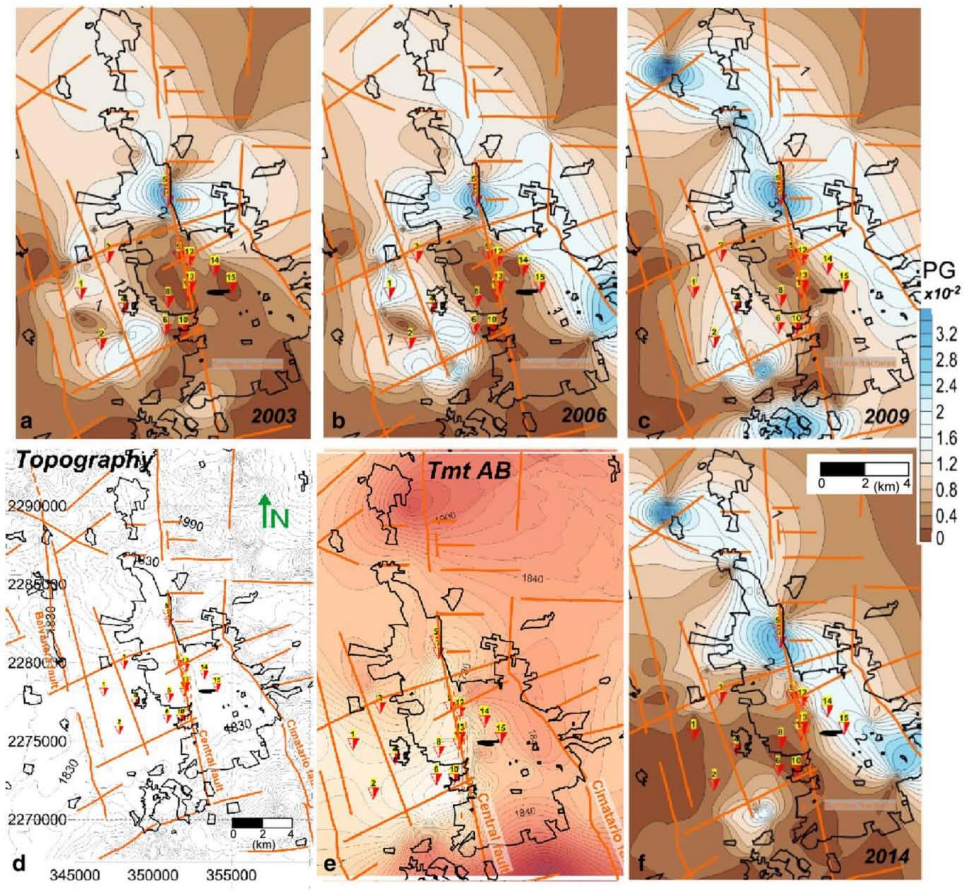

Fig. 11 Piezometric gradients (PG) in the Valley of Queretaro in **a** 2003, **b** 2006, **c** 2009 and **f** 2014. The current topographic elevation of the Queretaro Valley and the morphology of the top of the Tmt AB volcanic unit (andesites and basalts) are presented in parts **d** and **e**, respectively. The location of the sheared-well casings is shown as *red* or *yellow inverted triangles*. The main faults are represented by *orange* alignments

of the volcanic Tmt AB unit underlying the near surface granular sequence (Tmp Lm-Ar-Cg; Fig. 11e) are also presented. The steepest PGs for all periods developed near well Nos. 5 and 7 near the Queretaro Fault that displaces vertically the Tmt AB high permeable fractured rock units. In the Valley of Queretaro, average PG values were estimated near wells No. 1, 2, 3 and 4 in 2003 and 2006 (Fig. 11a,b), when the exploited aquifer was a middle permeable granular semi-confined unit and with an average piezometric level less than 100 m below land surface (Conagua 2003). In 2006 (Fig. 11b), the piezometric levels continued to decrease and a new high-PG zone appeared to the south-east, near the Cimatario Fault, also associated with faulted volcanic rocks. Besides faulting, buried topographic features also influence the distribution of the PG. For instance, the ruptured wells 12, 14, and 15 are located above a buried ramp zone of the Tmt AB volcanic unit (Fig. 11e) influencing the pattern of gradient contours from 2009 to 2014 (Fig. 11c,f). The most recent configuration (2014, Fig. 11f) shows that the steepest PGs align with faulting in a north–west direction. At present, the exploited aquifer consists mainly of the Tmm AB unit located beneath the Tom Py Lac granular unit (see Fig. 3a). The morphology of the Tmt AB unit (Fig. 11e) and the piezometric level, on average 140 m deep, coincide at about the same elevation. Although the precise dates of well ruptures are unknown, a spatial relation between location, the exploited hydrostratigraphic unit, and PG distribution was observed.

The conceptual model of Fig. 12 summarizes the ideas discussed above. Land subsidence in the Valley of Queretaro is related to groundwater extraction but differential compaction is influenced by faults and stratigraphy. InSAR data confirm that the zones of rapid deformation are controlled by pre-existing faults resulting in vertical displacement as much as 6 cm/y (Farina et al. 2008; Chaussard et al. 2014). Groundwater is pumped from different aquifer layers with depths ranging from 200 to 500 m causing differences in the hydraulic head as much as 70 m (Fig. 11a). Piezometric gradients might also have played a role in inducing casing ruptures; however, well-casing ruptures documented between 70 and 190 m depth suggest that deformation is accommodated by compaction and slip at pre-existing fault planes and stratigraphic joints. Pre-existing faults play an important role in the vertical displacement field, by controlling differential compaction (differential compaction develops between the two sides of a fault due to hydraulic barrier effects causing large head contrasts on opposite sides of the fault and/or the unequal thickness of the compressible sedimentary deposits), or by reactivation of slip along low cohesive and low friction planes. The slip along a stratigraphic contact needed to produce shearing is apparently small. Because the aquifer structure is composed of layers of interbedded granular materials and rock, the mechanical contrast may enhance slip. This might be the case when there is a lateral difference in compaction and a tilted stratigraphic contact resulting in downward shearing (Fig. 12b).

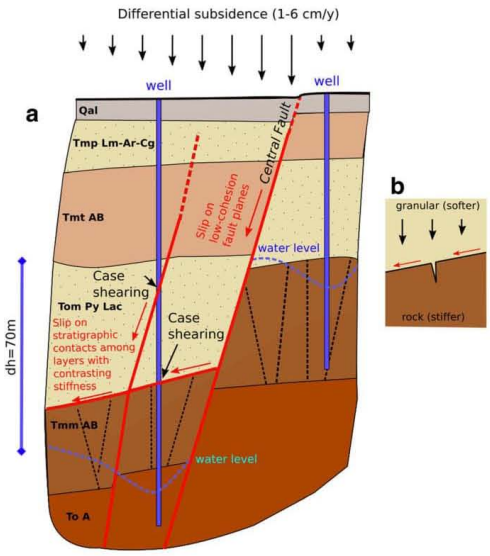

Fig. 12 Conceptual model for shearing in groundwater extraction wells associated with land subsidence in faulted and heterogeneous sedimentary basins: **a** shearing along high-dip-angle pre-existing faults by large differential compaction (local stresses) and **b** slip along low-dip-angle weakness planes

The results of the study suggest that when deformation is analyzed the potential slippage of faults and joints at depth should be considered. The shear mechanism documented in this work does not preclude the occurrence of the more conventional compaction mechanism for casing rupture. Both mechanisms can act during the accommodation of deformation in heterogeneous and faulted systems when groundwater (or oil) is exploited.

Conclusions

Several lines of evidence presented in this work suggest that well-casing shearing documented in the Valley of Queretaro aquifer is induced by groundwater withdrawal and land subsidence. To the authors' knowledge, this is the first study case to associate well-casing shearing with groundwater depletion and structural geology in a multilayer aquifer. Previously the occurrence has been only documented in detail for oil or gas extraction/injection wells. Groundwater depletion deformation and hydraulic gradients are controlled structurally by the two nearly orthogonal sets of regional faults and by the morphology of volcanic units. The variation in the distribution of piezometric gradients induces local variations in the state of stress of the aquifer system leading to the shearing of well casings. Slip on near vertical fault planes or at stratigraphic joints can be induced by differential compaction. The analysis presented in this work, based on field observations, remote surface deformation monitoring, in situ monitoring, stratigraphic correlation, and numerical modeling identified two main factors inducing shearing triggered by land subsidence:

- Structural features such as pre-existing regional faulting and/or buried bedrock topography
- Weak planes located in lithological interfaces (contrasts of stiffness at the geological contacts)

Additionally, other factors may enhance potential slip on weak interfaces:

- The distribution of piezometric gradients and drawdown patterns controlled by the geological structure
- Morphology of the hydraulic basement, mainly related to vertical displacements of regional faults delimiting aquifer systems in grabens. This aquifer structure is common in Mexico and the results obtained here can be applied to other similar subsiding aquifer systems
- Differential compaction between the two sides of a fault due to hydraulic barrier effects of the fault causing contrasting head changes on either side of the fault and/or unequal thickness of the compressible sedimentary deposits on either side of the fault

The shear mechanism documented in this work for fault-controlled aquifers does not preclude the occurrence of the more conventional compaction mechanism for casing rupture. The results of this work can be highly relevant because many of the developed aquifer systems in central Mexico are located in regional graben structures and groundwater depletion continues increasing daily. Numerical and analytical geomechanical models are critically important to improve understanding of groundwater flow patterns conditioned by geological structures and the hydromechanical implications of the associated subsidence, ground fracturing and potential slip of local and regional faults in order to reliably forecast infrastructure damage in developing urban areas.

Acknowledgements The authors are grateful to the Mexican Agency of Water (CONAGUA, Dirección Local en Queretaro) and the Agency of Water in Queretaro (Comision Estatal del Agua Queretaro) for the information provided and field support during mapping, particularly to Javier Gamez, Ignacio Barron, Ignacio Ortiz and Jesus Diaz. A part of this work was supported by the CONAGUA project No. SGT-OCLSP-QRO-13-EP-085-RF-CC. The comments from two anonymous reviewers and from Devin Galloway (US Geological Survey) were very helpful for the improvement of the manuscript. The authors also thank the members of the UNESCO Working Group on Land Subsidence for the discussions on the subject developed in this manuscript. The international collaboration is supported by UNESCO IGCP Project No. 641 (M3EF3 – Deformation and fissuring caused by exploitation of subsurface fluids).

References

Aguirre-Díaz GJ, López-Martínez M (2001) The Amazcala caldera, Queretaro, Mexico: geology and geochronology. J Volcanol Geotherm Res 111:203–218

Aguirre-Díaz GJ, Nieto-Obregón J, Zúñiga R (2005) Seismogenic basin and range and intra-arc normal faulting in the central Mexican Volcanic Belt, Querétaro, México. Geol J 40:215–243. doi:10.1002/gj.1004

Alaniz-Alvarez SA, Nieto-Samaniego AF, Reyes-Zaragoza MA (2001) Estratigrafía y deformación extensional en la región San Miguel de Allende-Querétaro, México [Stratigraphy and extensional deformation in the San Miguel de Allende-Queretaro region, Mexico]. Rev Mex Cien Geol 18(2):129–148

Bell JW, Amelung F, Ramelli AR, Blewitt G (2002) Land subsidence in Las Vegas, Nevada, 1935–2000: new geodetic data show evolution, revised spatial patterns, and reduced rates. Environ Eng Geosci 8(3): 155–174

Bo T, Zhanghua L (2004) Effect of the in-situ stress field on casing failure. In: 2004 International ANSYS Conference, Paper no. 35, Pittsburgh, PA, May 2004

Borchers JW, Gerber, Martin, Wiley, Jeffrey, Mitten HT (1998) Using down-well television surveys to evaluate land subsidence damage to water wells in the Sacramento Valley, California. In: Borchers JW (ed) Land subsidence: case studies and current research, Proc. of the Dr. Joseph F. Poland Symposium on Land Subsidence: Assoc. of Engineering Geologists Spec. Publ. 8, AEG, Zanesville, OH, pp 89–105

Budhu M (2011) Earth fissure formation from the mechanics of groundwater pumping. Int J Geomech ASCE 11:1–11. doi:10.1061/ASCEGM.1943-5622.0000060ok

Burbey TJ (2002) The influence of faults in basin-fill deposits on land subsidence, Las Vegas Valley, Nevada, USA. Hydrogeol J 10:525–538. doi:10.1007/s10040-002-0215-7

Burbey TJ (2008) The influence of geologic structures on deformation due to ground water withdrawal. Groundwater 46(2):202–211. doi:10.1111/j.1745-6584.2007.00395.x

Carreon-Freyre D (2009) Rupture of ground water pumping wells related to ground fracturing propagation in Queretaro City, Mexico. 2009 Ground Water Summit, NWGA, Westerville, OH

Carreón-Freyre D (2010) Land subsidence processes and associated ground fracturing in Central Mexico. In: Carreón-Freyre D et al (eds) Land subsidence, associated hazards and the role of natural resources development. Red Book Series Publ. 339, IAHS, Wallingford, UK, pp 149–157

Carreon-Freyre DC, Cerca M (2006) Delineating the near-surface geometry of the fracture system affecting the Querétaro Valley, Mexico: correlation of GPR signatures and physical properties of sediments. Near Surf Geophys 2006:49–55

Carreón-Freyre D, Cerca M (2009) Integration of geological properties in the estimation of subsidence in two urban areas of Mexico. In: Culshaw MG, Reeves HJ, Jefferson I Spink T (eds) Engineering geology for tomorrow's cities. Engineering Geology Special Publ., vol 22, Geological Society, London, 317 pp. doi:10.1144/EGSP22.I

Carreón-Freyre D, Cerca M, Luna-González L, Gámez-González FJ (2005) Influencia de la estratigrafía y estructura geológica en el flujo de agua subterránea del Valle de Querétaro [Influence of stratigraphy and geological structure on the groundwater flow in the Valley of Querétaro]. Rev Mex Cienc Geol 22(1):1–18

Carrera-Hernández J, Carreon-Freyre D, Cerca M, Levresse G (2015) Groundwater flow in a transboundary fault-dominated aquifer and the importance of regional modeling: the case of the city of Querétaro, Mexico. Hydrogeol J. doi:10.1007/s10040-015-1363-x

Chaussard E, Wdowinski S, Cabral-Cano E, Amelung F (2014) Land subsidence in central Mexico detected by ALOS InSAR time-series. Remote Sens Environ 140:94–106

Conagua (2003) Plan de manejo integrado del Acuífero del Valle de Querétaro [Integrated management plan of the aquifer of the Valley of Queretar]. Technical report, Qro. Comisión Nacional del Agua, Querétaro, Mexico, 150 pp

Dusseault MB, Bruno MS, Barrera J (2001) Casing shear: causes, cases, cures. Soc Petrol Eng (SPE) Drill Complet SPE 72060, pp 98–107 SPE, Richardson, TX

Farina P, Avila-Olivera JA, Garduño-Monroy VH (2007) Structurally-controlled urban subsidence along the Mexican Volcanic Belt (MVB) monitored by InSAR. In: Proc. Envisat Symposium 2007, Montreux, Switzerland, 23–27 April 2007

Farina P, Avila-Olivera JA, Garduño-Monroy VH, Catani F (2008) DInSAR analysis of differential land subsidence affecting urban areas along the Mexican Volcanic Belt (MVB). Riv Ital Telerilevam 40(2):103–113

Fernandes R (2009) Intégration du comportement mécanique élastoplastique de Drucker-Prager et post-traitements. Documentation de reference du Code_Aster [Integration of the Drucker-Prager elasto-plastic mechanical behaviour and post-processing. CODE-ASTER Reference Manual] [R7.01.16]. CODE_ASTER. http://www.code-aster.org/spip.php?rubrique2. February 2016

Ferronato M, Gambolati G, Janna C, Teatini P (2008) Numerical modelling of regional faults in land subsidence prediction above gas/oil reservoirs. Int J Numer Anal Methods Geomech 32:633–657

Fredrich JT, Arguello JG, Deitrick GL, de Rouffignac EP (2000) Geomechanical modeling of reservoir compaction, surface subsidence, and casing damage at the Belridge field. Paper SPE 65354, SPE Reservoir Evaluation and Engineering, SPE, Richardson, TX

Galloway DL, Burbey TJ (2011) Review: regional land subsidence accompanying groundwater extraction. Hydrogeol J 19:1459–1486. doi:10.1007/s10040-011-0775-5

Gambolati G, Ferronato M, Teatini P, Deidda R and Lecca R (2001) Finite element analysis of land subsidence above depleted reservoirs with pore pressure gradient and total stress formulations. Int J Numer Anal Methods Geomech 25(4):307–327

Gercek H (2007) Poissons ratio values for rocks. Int J Rock Mech Min Sci 44:1–13. doi:10.1016/j.ijrmms.2006.04.011

Grasso JR (1992) Mechanics of seismic instabilities induced by the recovery of hydrocarbons. Pure Appl Geophys 139:507–533

Gregory AR (1976) Fluid saturation effects on dynamic elastic properties of sedimentary rocks. Geophysics 41(5):895–921

Hernandez-Marin M, Burbey TJ (2009) The role of faulting on surface deformation patterns from pumping-induced groundwater flow (Las Vegas Valley, USA). Hydrogeol J 17:1859–1875. doi:10.1007/s10040-009-0501-8

Jachens RC, Holzer TL (1982) Differential compaction mechanism for earth fissures near Casa Grande, Arizona. Geol Soc Am Bull 93:998–1012

Maury VMR, Grasso JR, Wittlinger G (1992) Monitoring of subsidence and induced seismicity in the Lacq gas field (France): the consequences on gas production and field operation. Eng Geol 32:123–135

Ochoa-Gonzalez, G, Carreón-Freyre D (2010) Integration of geological and hydrogeological features for subsidence modeling in volcanic zones. In: Carreón-Freyre D, Cerca M Galloway DL (eds) Land subsidence, associated hazards and the role of natural resources development. Red Book Series Publ. 339, IAHS, Wallingford, UK, pp 114–119

Ochoa-Gonzalez G, Teatini P, Carreon-Freyre D, Gambolati G (2013) Modeling the deformation of faulted volcano-sedimentary sequences associated to groundwater withdrawal in the Queretaro Valley, Mexico. In: Piantadosi J et al (eds) MODSIM 2013: adapting to change—the multiple roles of modelling. Modelling and Simulation Society of Australia and New Zealand, Canberra, Australia

Ochoa-Gonzalez G, Carreón-Freyre D, Teatini P, Cerca M (2014) Urban structure damaged by differential land level lowering in the lacustrine plain of Queretaro City, Mexico. Geophysical Research Abstracts vol 16, EGU2014-16632, 2014. EGU General Assembly, 27 April–02 May 2014, Vienna

Ochoa-Gonzalez G, Carreón-Freyre D, Cerca M, Lopez-Martinez M (2015) Assessment of groundwater flow in volcanic faulted areas: a study case in Queretaro, Mexico. Geofis Intl 54(3):199–220, doi:10.1016/j.gi.2015.04.016

Pacheco J, Arzate J, Rojas E, Arroyo M, Yutsis V, Ochoa G (2006) Delimitation of ground failure zones due to land subsidence using gravity data and finite element modeling in the Querétaro Valley, México. Eng Geol 84:143–160

Peng S, Fu J, Zhang J (2007) Borehole casing failure analysis in unconsolidated formations: a case study. J Pet Sci Eng 59:226–238

Rojas E, Arzate J, Arroyo M (2002) A method to predict the group fissuring and faulting caused by regional groundwater decline. Eng Geol 65:245–260

Suter M, López-Martínez M, Quintero-Legorreta O, Carrillo-Martínez M (2001) Quaternary intraarc extension in the central Trans-Mexican volcanic belt. Geol Soc Am Bull 113:693–703 doi:10.1130/0016-7606(2001)113<0693:QIAEIT>2.0.CO;2

Teatini P, Ferronato M, Gambolati G, Gonella M (2006) Groundwater pumping and land subsidence in the Emilia-Romagna coastland, Italy: modeling the past occurrence and the future trend. Water Resour Res 42, W01406. doi:10.1029/2005WR004242

Wang P, Zhu Q, Bu X (2011) Finite element analysis on casing failure based on ADINA. Syst Eng Procedia Elsevier 1:42–47. doi:10.1016/j.sepro.2011.08.008

Xu S, Nieto-Samaniego AF, Alaniz-Alvarez SA, Cerca-Martinez M (2011) Structural analysis of a relay ramp in the Queretaro graben, central Mexico: implications for relay ramp development. Rev Mex Cienc Geol 28(2):275–289

Zoback MD, Zinke JC (2002) Production-induced normal faulting in the Valhall and Ekofisk oil fields. Pure Appl Geophys 159:403–420

Zúñiga FR, Pacheco JF, Guzmán-Speziale M, Aguirre-Díaz GJ, Espíndola VH, Nava E (2003) The Sanfandila earthquake sequence of 1998, Queretaro, Mexico: activation of a non-documented fault in the northern edge of central Transmexican Volcanic Belt. Tectonophysics 361:229–238

Capítulo IV. "Overexploitation of groundwater resources in the faulted basin of Queretaro, Mexico: a 3D deformation and stress analysis". Publicado en la revista Engineering Geology en noviembre 2018

Engineering Geology 245 (2018) 192–206

Contents lists available at ScienceDirect

Engineering Geology

journal homepage: www.elsevier.com/locate/enggeo

Overexploitation of groundwater resources in the faulted basin of Querétaro, Mexico: A 3D deformation and stress analysis

G.H. Ochoa-González[a,b], D. Carreón-Freyre[c,*], A. Franceschini[d], M. Cerca[c], P. Teatini[d]

[a] Instituto Tecnologico y de Estudios Superiores de Occidente (ITESO), Jalisco, Mexico
[b] Posgrado en Ciencias de la Tierra, Centro de Geociencias, Universidad Nacional Autónoma de México, Blvd. Juriquilla 3000, col. Juriquilla, Queretaro 76230, Mexico
[c] Lab. de Mecánica de Geosistemas, Centro de Geociencias, Universidad Nacional Autónoma de México, Blvd. Juriquilla 3000, col. Juriquilla, Queretaro, 76230, Mexico
[d] Dept. of Civil, Environmental and Architectural Engineering, University of Padova, Italy

ARTICLE INFO

Keywords:
Groundwater withdrawals
3D deformation and stress fields
Land subsidence
Ground ruptures
Numerical modeling
Querétaro (Mexico)

ABSTRACT

The City of Querétaro is located on a continental basin filled since the Oligocene with lacustrine and alluvial sediments, pyroclastic deposits, and interbedded fractured basalts. The graben structure of the basin was formed by two major North-South trending normal faults, among which the thicknesses of the filling materials vary many tens of meters in close distances. Hence, important differences of hydraulic and mechanical properties characterize the various geologic units. Groundwater has been strongly withdrawn over the last three decades in the study area, with a decline of the piezometric level exceeding 100 m. Because of the high variability of the geologic deposits, the piezometric decrease and consequently the effective stress increase are characterized by a large spatial variability. Piezometric variations are also due to faults that strongly impact on groundwater flow dynamics. The deformation and effective stress variability has caused large differential subsidence causing ground fracturing that has damaged the urban infrastructure of the City of Querétaro. This complex geological setting has been properly accounted into a three-dimensional (3D) flow and geomechanical modeling approach to quantify the displacement, deformation, and stress fields caused by water withdrawal. The static geologic model was accurately defined using geological logs from extraction wells, field mapping of faults, fractures, and the integration of major structures reported in previous geophysical works. The model has been calibrated using observed groundwater levels and land settlement records. The simulations have spanned the period from 1970 to 2011. The modeling results highlight that the areas where large differential subsidence and horizontal displacements developed correspond to the portions of the city where ground fractures are observed. Normal and shear components of the stress field changes accumulate along the discontinuity surfaces at depth, providing evidence that large piezometric declines can be a key factor triggering the fault reactivation. The spatial relationship between major withdrawals, discontinuities of the geologic structure, and accumulation of large stress and strain fields clearly emerged from the outcomes of the 3D geomechanical model.

1. Introduction

Cities in the central Trans-Mexican Volcanic Belt (TMVB) are example of zones where millions of people live, and the effects of climate change in terms of variation in the distribution and timing of precipitation have significantly threaten the availability of freshwater resources. Several cities, such as Mexico City, Aguascalientes, Morelia, and Querétaro, use groundwater as the primary source of water supply and contributes > 70% to the water needs of > 100 million inhabitants (Conagua, 2003; INEGI, 2011). Aquifer overexploitation has caused a significant decline of the piezometric head up to 100 m in these sites. The following consolidation of the sedimentary/volcanic basins has caused land subsidence with rates on the order of 10 cm/yr associated with ground ruptures, the most documented case is Mexico City, where land subsidence may reach 40 cm/s (e.g. López-Quiroz et al., 2009; Cabral-Cano et al., 2008; Carreón-Freyre, 2010).

In Querétaro, the over-use of groundwater to provide water to the inhabitants of the valley has caused an alarmingly piezometric decline to about 120 m and, consequently, land subsidence. The cumulative pumping rate was quantified in 110 million m^3/yr while the total recharge amounts to 70 million m^3/yr (Carrera-Hernández et al., 2016). The aquifer is characterized by a highly heterogeneous geologic system, with sand-and-silt sediments intercalated with pyroclastic layers and fractured volcanic rocks. Because of the largely different geomechanical

* Corresponding author.
E-mail address: freyre@geociencias.unam.mx (D. Carreón-Freyre).

https://doi.org/10.1016/j.enggeo.2018.08.014
Received 12 January 2018; Received in revised form 24 August 2018; Accepted 28 August 2018
Available online 30 August 2018
0013-7952/

Fig. 1. Photographs showing some of the effects of differential land subsidence due to groundwater withdrawals in Querétaro: a) panoramic view of the 5 de Febrero Avenue (looking North), with the ground fracture displacements that have affected both the street and the bridge built originally horizontal between I and II; b) ground fractures have produced differential vertical displacements larger than 1.5 m; c) recent displacements (2016–2017) on 5 de Febrero avenue (looking south) along the trace of the Central Fault. The photographs were taken in the highest subsidence area defined by Chaussard et al. (2014).

properties of these materials and the presence of pre-existing buried faults (Carreón-Freyre et al., 2005a, 2016), land subsidence is accompanied by ground ruptures that damage the urban infrastructures of the City of Querétaro (Fig. 1).

An advanced three-dimensional (3D) finite element (FE) flow and geomechanical modeling approach is used in this work to investigate the relationships between the piezometric evolution due to groundwater pumping, land subsidence, and the complex geological system of the Querétaro Valley. The study is based on the consolidation theory by Biot (1941) and a 3D modeling approach is used. Indeed, only 3D models allow investigating the patterns of the vertical and horizontal components of the land displacements, the stress and strain fields at depth, and the possible generation of earth fissures and fault reactivation (Gambolati and Teatini, 2015). Galloway et al. (2008) observed that horizontal strains may be locally large near pumping wells where large hydraulic gradients developed, at locations where the aquifer system thins abruptly above inflections in the basement topography, and near the boundaries of hydrogeologic units with contrasting hydraulic and (or) mechanical properties.

Historically, horizontal strains (and displacements) in subsidence studies were ignored for various reasons. A main reason of a wider application of one-dimensional (1D) subsidence models (e.g., Hoffmann et al., 2003; Hung et al., 2012; Mahmoudpour et al., 2016) is because "many researchers argue that horizontal strains are much smaller than vertical strains in most subsidence investigations and can therefore be ignored" (Galloway and Burbey, 2011). Second, the paucity of regional horizontal-displacement measurements and the larger computation burden of 3D models have contributed to their limited use.

Usually, 3D geomechanical models were used to develop theoretical analyses (e.g., Yang et al., 2015) or to investigate the deformation field due to exploitation of groundwater resources at local scale. For example, Burbey (2006) used horizontal and vertical GPS measurements during a 60-day aquifer test to calibrate a 3D groundwater flow and deformation model with water-level measurements from the pumping well. A regional-scale investigation has been carried out by Ye et al. (2016). An explicitly coupled 3D groundwater flow and displacement model was developed for downtown Shanghai, China. The simulated horizontal displacements peak at about 10 mm, i.e. < 10% of the maximum land subsidence. The pseudo-tabular setting of the hydrogeologic units composing the sedimentary sequence beneath the Yangtze River delta and the scattered distribution of the pumping/recharging wells were responsible for small and uniformly-distributed horizontal movements (Ye et al., 2016).

The geologic architecture of the Querétaro basin strongly differs from that of deltaic plains. For this reason, the three-dimensionality of the deformation and stress patterns caused by aquifer overexploitation is expected to be much larger in the study area. The models are calibrated using observed groundwater and land settlement records and then the 3D strain accumulations and stress changes compared with the distribution of the major ground ruptures mapped in the city.

A preliminary description of the model used in this study was published by Ochoa-González et al. (2013). The static/geologic model is kept from the previous work, but the modeling set-up is updated in relation to the boundary conditions, the parameter calibration, and the simulated time interval. A complete analysis of the 3D model outcome in terms of displacement, stress, and strain fields is presented and discussed here.

2. Geological setting

2.1. Structural geology

The Querétaro basin is a topographic depression filled by sediments formed by the normal displacement of regional faults since the Miocene (Alaniz-Alvarez et al., 2001) and volcanic activity. Two regional-scale fault systems cross the zone: 1) the N-S extensional fault system known as Taxco-San Miguel de Allende (Alaniz-Alvarez et al., 2001) and, 2) an E-W trending fault system, known as Chapala-Tula system (Sutter et al., 2001). The two systems divide the valley in a mosaic forming horsts, grabens, and half-grabens (Xu et al., 2011). The study area is located in the central depression of Querétaro City, formed by the interaction of the fault systems (Fig. 2). To the north, the central graben is delimited by two segments of an E-W trending south dipping normal fault with throws estimated at 200 to 400 m (Carreón-Freyre et al., 2005b). The E-W trending fault segments are cut by the N-S trending faults. To the south there is a normal fault inferred from the lineament of volcanic edifices such as the Cimatario volcano which is emplaced at the intersection with an N-S trending fault. The volcanic edifices play the role of watershed for the valley since the Miocene and controlled the deposition of the sediments filling the basin (< 5 Ma).

The central topographic depression is limited to the west by the N-S trending east dipping Balvanera fault for which a vertical throw of 150 m has been estimated (Carreón-Freyre et al., 2005b). The east boundary of the central depression is the N-S trending west dipping Cimatario fault characterized by a 60 m displacement. The asymmetry in the displacement of these graben flank faults is explained in terms of

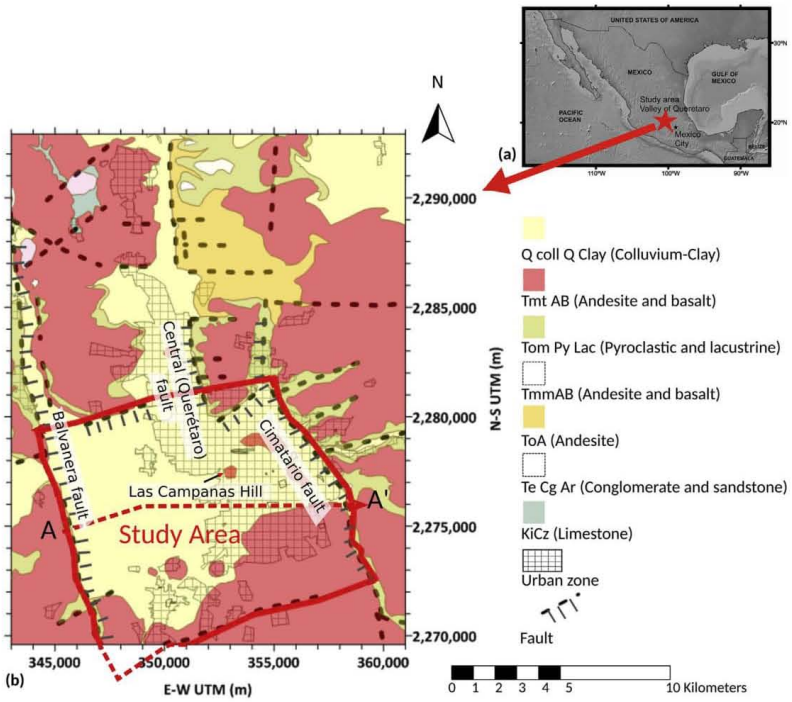

Fig. 2. (a) Location of the City of Querétaro in the Trans-Mexican Volcanic Belt. (b) Geological map of the Querétaro Valley, with the red line showing the simulation domain. The coordinate system is UTM 14N zone. Line A-A′ represents the trace of the geological section shown in Fig. 3. Modified after Ochoa-González et al. (2013). (For interpretation of the references to colour in this figure legend, the reader is referred to the web version of this article.)

the presence of the N-S trending west dipping Querétaro Fault, which is hidden by the sedimentary cover in the study area. The Cimatario and Querétaro faults overlap in the central depression producing a relay ramp in the zone among them. Carreón-Freyre et al. (2016) documented vertical displacements for the buried Central Fault of 56, 70, and 90 m at the north, central, and south sectors of the area, respectively, through the correlation of the lava plateau in lithological logs located at both sides of the fault trace,. Thus, the total vertical displacement accommodated by the Cimatario and Central faults is similar to the displacement in the Balvanera fault, bounding the basin westward, at least from the Miocene. There are several other minor buried faults, whose locations within the study area were identified by Pacheco et al. (2006) using gravimetric data measured transversally to the direction of the faults.

2.2. Stratigraphy

Six major geologic units compose the sedimentary-volcanic of the Querétaro Valley (Figs. 2 and 3). The volcanic are mainly fractured units and the sedimentary and pyroclastics rocks are mainly porous units. The surface Quaternary sequence is composed by lacustrine and/or colluvial deposits (Q Clay, Q Coll). The Cenozoic sequence includes a continental sedimentary unit with a predominance of conglomerates and sandstone (Tp Ar-Cg) below a predominantly volcanic rock sequence intercalated with thick pyroclastic and sedimentary deposits. The volcanic sequence comprises fissured basalts and lava flows from volcanoes (Tmt AB) with ages ranging from 12 to 5 My (Aguirre-Díaz and López-Martínez, 2001) and basalts of the Oligocene to early Miocene (Tmm AB). In between, the pyroclastic and lacustrine sequences in Querétaro consist of different grain-sized deposits of 80 m thick (Tom Py-Lac), this unit includes the Ezequiel Montes Pumice, an important stratigraphic marker dated between 7.5 and 5.6 My (Aguirre-Díaz and López-Martínez, 2001). This pyroclastic and lacustrine sequence is the main hydrogeological unit exploited recently in the City of Querétaro (Carrera-Hernandez et al. 2016). A third Andesitic and Basaltic unit characterized by a smaller fracturing degree than Tmm AB (To AB or To A) is reported in some wells.

Therefore, the hydrostratigraphic units described downwards from the land surface are: 1) Q Clay: Quaternary lacustrine, surficial clays and low-permeable relatively thin deposits; 2) Tp Ar-Cg: sediments and volcanic rocks representing the main porous unit; 3) Tmt AB: Andesitic and Basaltic representing a highly fractured unit; 4) Tom Py-Lac: pyroclastic and lacustrine deposits forming the second main porous unit; 5) Tmm AB: older Andesitic and Basaltic fractured unit underlying Tom Py-Lac; 6) To AB Andesitic and Basaltic less fractured unit; 7) Hydrogeological basement, for modeling purposes it is assumed that a low permeability and rigid material bounds the compressible sequence from which groundwater is withdrawn even if other porous/fractured materials likely exist below To AB (Carreón-Freyre et al., 2005b).

2.3. Physical properties

According to the stratigraphic sequence, the “static” model accounted in the study is composed of an alternate sequence of granular

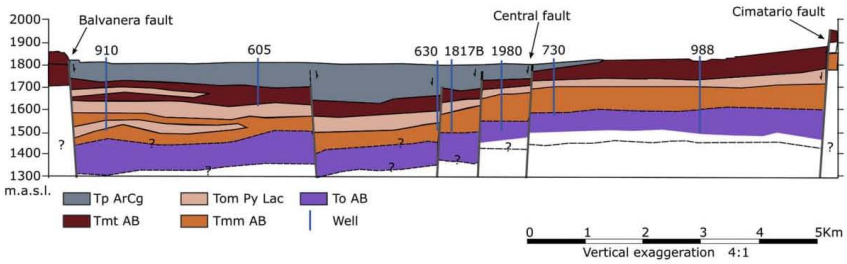

Fig. 3. West-east geological section A–A′ (see Fig. 2b) obtained by the correlation of lithologic well logs and highlighting the vertical dislocation between the main stratigraphic units by normal faulting (modified after Carreón-Freyre et al., 2005b).

and fractured volcanic and sedimentary materials. Granular sequences include compressible fine grain-size materials such as clays, silts, fine sands, and volcanic ashes (pumice), interbedded with stiff permeable volcanic materials such as fractured basalts and andesites.

The compression indexes (C_c) of the Q Clay formation were determined according to the ASTM D2435 method (2011) in the *Centro de Geociencias* at UNAM, C_c values were transformed in oedometric bulk compressibility (c_M) through the relationship:

$$c_M = \frac{C_c}{2.3(1+e)\sigma_v} \quad (1)$$

where $e = \frac{\varphi}{1-\varphi}$ is the reference void ratio, φ the porosity, and σ_v' the corresponding vertical effective stress. Fig. 4 shows the outcome of the two tests providing the minimum and maximum c_M values measured in the lacustrine materials. The range spans one order of magnitude, between 10^{-1} to $10^{-2}\,\mathrm{MPa}^{-1}$. The granular sequences Tp Ar-Cg are Tom Py-Lac are similarly composed by lacustrine, alluvial, and pyroclastic materials with variations in sedimentation sequence. The Tom Py-Lac sedimentary sequence was interrupted during the Oligocene by the deposition of fall ashes (pyroclastic) that were easy altered to clays. Therefore, it can be assumed that Tom Py-Lac has a higher clay content than Q Clay and Tp Ar-Cg. Because of the impossibility of coring and testing in the laboratory intact samples from the deep Tom Py-Lac unit, its c_M has been assumed to be 30% larger than that measured for the shallower fine-grained materials. The compressibility values of rocks were taken from the literature (Zhang, 2017). As described in section 5.1, c_M has been the key parameter involved in the model calibration. The calibrated c_M values are summarized in Table 1.

Other physical properties of interest include: a medium porosity φ equal to 0.4 and 0.2 for the granular and the fractured volcanic materials respectively; specific gravity of soil solids $G_s = 2.4 \times 10^3$; Poisson ratio $\nu = 0.3$; and water volumetric compressibility $\beta = 4.6 \times 10^{-4}\,\mathrm{MPa}^{-1}$.

The hydraulic conductivity along the vertical (K_h) and horizontal (K_v) directions, reported by Carrera-Hernández et al. (2016) were used in the model, they established a stratigraphic sequence for the Querétaro Valley consistent with the presented in this study. The K_h and K_v values used in the flow model are summarized in Table 1.

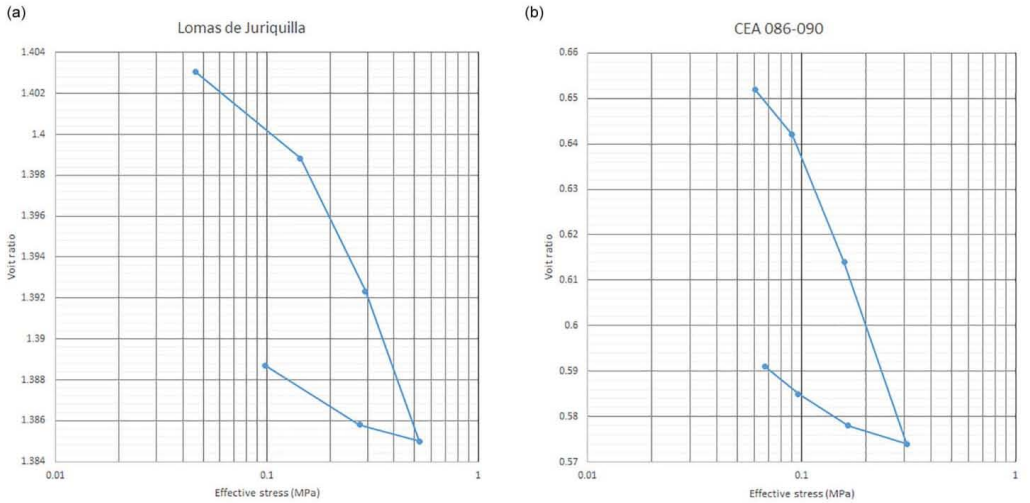

Fig. 4. Examples of oedometric test outcomes form two samples cored in the shallow Q Clay unit. These curves lead to the following values for the oedometric compressibility and specific storage: (a) $c_M = 1.13 \times 10^{-2}\,\mathrm{MPa}^{-1}$, $S_s = 1.1\mathrm{E}{-}04\,\mathrm{m}^{-1}$ and (b) $c_M = 9.2 \times 10^{-2}\,\mathrm{MPa}^{-1}$, $S_s = 0.9\mathrm{E}{-}04\,\mathrm{m}^{-1}$. The values represent the bounds of the variability range detected by the several oedometric tests carried out on samples cored from Q Clay. They have been obtained by extending the measured virgin section of the curve to an effective stress equal to 0.981 MPa, corresponding to a piezometric decline of 100 m, to derive a property value averaged over the stress range experienced by the porous medium because of the pressure decline.

Table 1
Hydraulic conductivity and calibrated geomechanical properties used in the model simulations.

Unit	K_h (m/day)	K_v (m/day)	c_M (MPa^{-1})	S_s (m^{-1})	E (MPa)	$c_M/c_{M,Qclay}$
Qclay	1.00	0.100	1.5×10^{-2}	1.5×10^{-4}	49	1
Tp Ar-Cg	1.00	0.100	1.5×10^{-2}	1.5×10^{-4}	49	1
Tmt AB	2.00	1.000	4.2×10^{-4}	5.0×10^{-6}	1786	0.03
Tom Py-Lac	0.10	0.010	2.0×10^{-2}	2.0×10^{-4}	37	1.34
Tmm AB	0.50	0.500	4.2×10^{-4}	5.0×10^{-6}	1786	0.03
To AB	0.06	0.006	2.1×10^{-4}	2.5×10^{-6}	3572	0.01
Base	0.01	0.010	2.0×10^{-6}	2.5×10^{-7}	364,371	0.0001

3. Hydrological evolution

3.1. Groundwater flow in faulted sequences

Groundwater flow in faulted aquifers has been characterized and modeled in the past using numerical models (Allen and Michel, 1999; Mayer et al., 2007). The presence of faults is simulated using different hydraulics properties relative to the surrounding materials, acting as a barrier (smaller permeability) or as a preferential flow-path (larger permeability), thus yielding a discontinuity in the piezometric levels between the two sides of a fault.

In Querétaro faulting strongly influence the groundwater system by compartmentalizing zones showing different piezometric values (Carreón-Freyre et al., 2005b). Previous numerical studies on the groundwater system (Ochoa-González et al., 2015; Carrera-Hernández et al., 2016) explicitly considered these faults and concluded that the truncation of the hydrostratigraphic units and the subsequent contrast of the hydraulic properties also contribute in the compartmentalization of the system.

3.2. Groundwater pumping and piezometric evolution

Groundwater withdrawal in Querétaro began during the early 1970s. According to the historical records of Conagua (2003), piezometric lowering occurred at an approximate rate of 3–5 m/yr. The piezometric level reached approximately 40 to 70 m below the land surface during the decade 1980–1990 when the shallow granular aquifer corresponding to Tmp Ar-Cg was exploited. From the 1990s to the 2000s, groundwater was pumped from the underlying Tmt AB volcanic unit. At that time, the average well depth varied between 150 and 200 m. The fractured aquifer was depleted over 2000–2010, and groundwater levels declined to the elevation of the second granular aquifer (Tom Py-Lac unit), i.e. between 80 and 120 m below the land surface.

The piezometric evolution versus time for some representative wells is provided in Fig. 5. Fig. 5a shows the well location and Fig. 5b the behavior of the drawdown from 1970 to 2012. Note that, because in Mexico the tube of water production wells is screened along its whole length, it is difficult to assign the recorded level to a specific aquifer. The majority of the wells are located along or near the faults and a few of them in the central part of the basin (Fig. 5a). The blue profiles in Fig. 5b are representative of the average piezometric behavior recorded in the Querétaro basin. The head drop measured in these wells was < 2 m/yr between 1970 and 1975 and grew to 3 m/yr afterward. Most of these wells are located to the West of the Central Fault, where ground ruptures are marked in Fig. 5a. In this area the Central Fault is believed to act as a boundary for the groundwater system and localizes the deformation associated with groundwater depletion (Carreón-Freyre et al., 2005b, 2016). A drawdown 5 to 10% smaller than the average was recorded for the wells colored in yellow in Fig. 5. Two of them (wells 0641 and 0641-A, close to each other) are located near a Tmt AB outcrop, the Cimatario volcano, in the southern part of the study area. Other two piezometers (wells 1010 and 0870) are placed near the Central Fault, and another one (well 0722) on the Cimatario Fault along the eastern border of the model. Conversely, the wells marked in green and grey in Fig. 5 are characterized by a drawdown rate significantly smaller and larger, respectively, than the average behavior. The reasons of these persistent differences are comprehensively discussed in Ochoa-González et al. (2015).

4. Modeling subsoil deformation due to groundwater pumping

Ground ruptures due to groundwater withdrawal were reported in Querétaro City since 1986 and strongly damaged the urban infrastructures (Trejo-Moedano and Martínez-Baini, 1991; Carreón-Freyre et al., 2005a). Fracturing and fault reactivation were related with the differential displacements caused by the thicknesses variations of the compressible layers (Rojas et al., 2002).

4.1. Modeling approach

The 3D poro-elasticity equations originally developed by Biot (1941) provide the coupled flow and deformation fields caused by groundwater pumping form aquifer systems. In the explicitly-coupled formulation, which is usually implemented in regional long-term analyses (e.g., Teatini et al., 2006), the flow equation is solved for the pressure independently of the stress equation, with the gradient of the pressure variations later integrated into the equilibrium equation as a known external source of strength. This simplification hypothesis is fully warranted in large-scale problems (Gambolati and Teatini, 2015).

The classical groundwater flow equation governing the hydrodynamics in an aquifer system reads:

$$\nabla(K\nabla h) = S_s\frac{\partial h}{\partial t} + q \tag{2}$$

where h is the hydraulic head, K the hydraulic conductivity, t is time, q the source/sink, and S_s the specific elastic storage. Linear finite elements (tetrahedra) and a weighted finite difference scheme are used by the groundwater flow simulator FLOW3D (Teatini et al., 2006) to solve Eq. (2) in space and in time, respectively.

The variation in time and space of the hydraulic head dh provided by the solution of Eq. (2) is converted in incremental pressure $p = \gamma_w dh$, with γ_w the specific weight of water, and used as forcing factor in the geomechanical model to compute the 3D aquifer-system deformation. The equilibrium equations governing the deformation of a mechanically isotropic medium read (e.g., Verruijt, 1969):

$$G\nabla^2 u_i + (G+\lambda)\frac{\partial \varepsilon}{\partial i} = \frac{\partial p}{\partial i}\ i = x, y, z \tag{3}$$

where u_i is the displacement component along the i-th coordinate direction, λ and G are the Lamè constant and the shear modulus of the porous medium, respectively, and ε is the volume strain. Finite elements using the same tetrahedral elements as the groundwater flow model are used in the SUB3D simulator (Teatini et al., 2006) to solve Eq. (3).

Well-known relations link the material properties in the flow and equilibrium equations (Teatini et al., 2006):

$$S_s = \gamma_w(c_M + \varphi\beta);\ c_M = \frac{1}{\lambda + 2G} = \frac{(1+\nu)(1-2\nu)}{E(1-\nu)};\ G = \frac{E}{2(1+\nu)} \tag{4}$$

with β the water volumetric compressibility, E the Young modulus, and ν the Poisson ratio. Explicitly coupling requires that c_M takes the same values in S_s and in the parameters E, λ, and G used in the geomechanical model. Notice that c_M is related to the compressibility index C_c provided by the usual graphical interpretation of oedometric tests through the relationship:

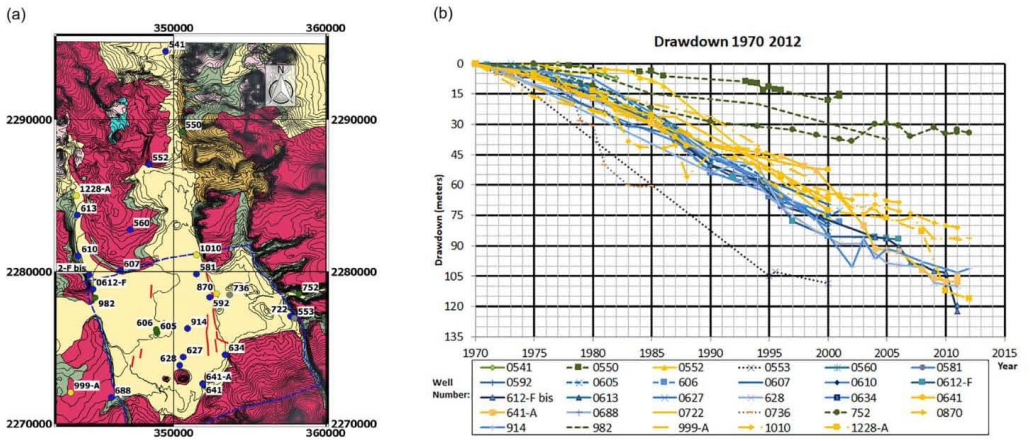

Fig. 5. (a) Geological map of the Querétaro Valley with the location of the monitoring wells. (b) Recorded drawdown from 1970 to 2012 in the wells of the Querétaro Valley. The colors of the piezometric profiles (blue, yellow, green, and grey) in (b) match those of the bullets used to mark to the corresponding well positions in (a). The blue lines and the red alignments in (a) represent the model boundaries and the trace of the ground ruptures, respectively. Modified after Ochoa-González et al. (2013). (For interpretation of the references to colour in this figure legend, the reader is referred to the web version of this article.)

$$c_M = \frac{C_c}{2.3(1+e)\sigma_v} \tag{5}$$

where $e = \frac{\varphi}{1-\varphi}$ is the reference void ratio and σ_v' the corresponding vertical effective stress.

Explicit failure mechanics due to groundwater pumping, e.g. using appropriate formulation such as the Interface Elements (Franceschini et al., 2016; Ye et al., 2018), is not addressed in the numerical approach used in this paper. However, the complete strain ε and stress $\boldsymbol{\sigma}$ fields can be computed by the 3D displacement field as follows:

$$\begin{bmatrix} \varepsilon_x \\ \varepsilon_y \\ \varepsilon_z \\ \varepsilon_{xy} \\ \varepsilon_{yz} \\ \varepsilon_{zx} \end{bmatrix} = \begin{bmatrix} \partial/\partial x & 0 & 0 \\ 0 & \partial/\partial y & 0 \\ 0 & 0 & \partial/\partial z \\ 0.5\partial/\partial y & 0.5\partial/\partial x & 0 \\ 0 & 0.5\partial/\partial z & 0.5\partial/\partial y \\ 0.5\partial/\partial z & 0 & 0.5\partial/\partial x \end{bmatrix} \bullet \begin{bmatrix} u_x \\ u_y \\ u_z \end{bmatrix} \tag{6}$$

$$\begin{bmatrix} \sigma_x \\ \sigma_y \\ \sigma_z \\ \tau_{xy} \\ \tau_{zy} \\ \tau_{zx} \end{bmatrix} = I \bullet \begin{bmatrix} 1-\nu & \nu & \nu & 0 & 0 & 0 \\ \nu & 1-\nu & \nu & 0 & 0 & 0 \\ \nu & \nu & 1-\nu & 0 & 0 & 0 \\ 0 & 0 & 0 & (1-2\nu)/2 & 0 & 0 \\ 0 & 0 & 0 & 0 & (1-2\nu)/2 & 0 \\ 0 & 0 & 0 & 0 & 0 & (1-2\nu)/2 \end{bmatrix} \bullet \begin{bmatrix} \varepsilon_x \\ \varepsilon_y \\ \varepsilon_z \\ \varepsilon_{xy} \\ \varepsilon_{yz} \\ \varepsilon_{zx} \end{bmatrix} \tag{7}$$

with $\frac{E}{(1+\nu)(1-2\nu)}$. The ruptures are more likely to develop and propagate where the tangential stress τ is relative large with respect to compression according for example to a Mohr-Coulomb failure criterion, and/or the normal stress component σ assumes negative/tensile values (Hernandez-Marin and Burbey, 2010).

4.2. 3D model set-up

The simulated domain is represented in Fig. 2, with boundaries following the principal geological structures (faults). The area encompasses the oldest part of Querétaro urban zone and the surrounding suburbs and farmland.

The top surface of the 3D domain is represented by the land surface. The analysis of 46 well logs with different depths and 11 gravimetric profiles (Carreón-Freyre et al., 2005b; Pacheco et al., 2006) allowed deriving the architecture of the geologic units and the location of the discontinuities caused by faulting, including faults not mapped in the surface but inferred from indirect methods (Fig. 3). The upper part of the Base unit constitutes the bottom boundary of the model. The model represents accurately the distribution of the main seven geological units (see Section 2.2) that compose the sedimentary-volcanic basin. Fig. 6a shows a horizontal view of the 3D grid that is composed of 267,385 nodes and 1,520,244 tetrahedra. Fig. 7 shows a perspective view of the 3D simulated domain. A number of 1 to 10 finite element layers are used to discretize each geologic unit along the vertical direction.

The boundary conditions are specified as follows. In the flow model, fixed head (i.e., "water-source") and no-flow conditions are prescribed along the lateral boundaries based on the geological setting (Fig. 6a), in particular the faults that can act as impermeable structures or water sources from larger depths, and the rocky outcrop distribution (Carreón-Freyre et al., 2005b; Ochoa-Gonzalez et al. 2015). The basement is assumed impermeable, and a negligible (null) recharge/efflux is assumed on the land surface based on the climatic conditions of the area (the yearly average precipitation is < 100 mm and the maximum temperature ranges between 20 °C in winter and 30 °C in summer). Standard Dirichlet conditions are assumed in the geomechanical model. The basement is assumed to be fixed, the horizontal displacements of the outer boundaries are precluded, and the top surface is left free to move both vertically and horizontally. The model is solved in term of piezometric drawdown and displacements from 1970, which is assumed as a reference equilibrated state for both the groundwater flow and the geomechanical models (Fig. 5b).

The time interval spanned by the simulations cover a period of 41 years (14,965 days), i.e. from 1970 to 2011. Groundwater withdrawal is carried out through the group of 123 wells distributed in the area (Fig. 6a). The time behavior of the pumping rates is available for the main 21 wells. Concerning the remaining 102 wells, their withdrawal rates have been assessed using the existing values in the year

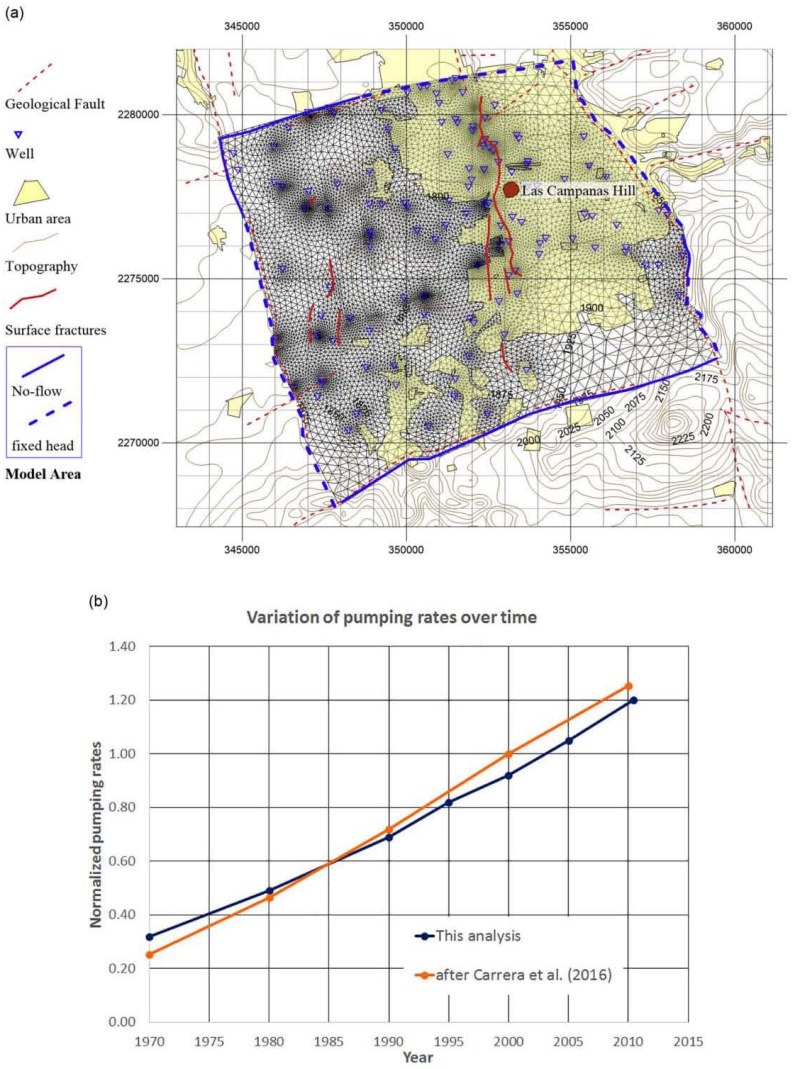

Fig. 6. (a) Horizontal projection of the 3D FE grid with the location of the main well fields. The blue lines correspond to major normal faults and are used to delimit the study area. The ground ruptures are represented by continuous red alignments and the topographic elevation by the brown curves. The boundary conditions for the flow model are indicated in the legend. (b) Comparison between the time behavior of the cumulative pumping rate normalized to the 2000 values as quantified in this study and used by Carrera-Hernández et al. (2016). (For interpretation of the references to colour in this figure legend, the reader is referred to the web version of this article.)

2000, with the temporal trend derived from the population growth in the City of Querétaro over the study period. The behavior vs time of the cumulative pumping rate obtained with this procedure is consistent with that reported in Carrera-Hernández et al. (2016) (Fig. 6b).

5. Modeling results

5.1. Model calibration

The groundwater flow and geomechanical models were initially calibrated using the available piezometric change and land subsidence records. Calibration by a trial-and-error procedure was focused on the soil compressibility c_M, while the hydraulic conductivity values

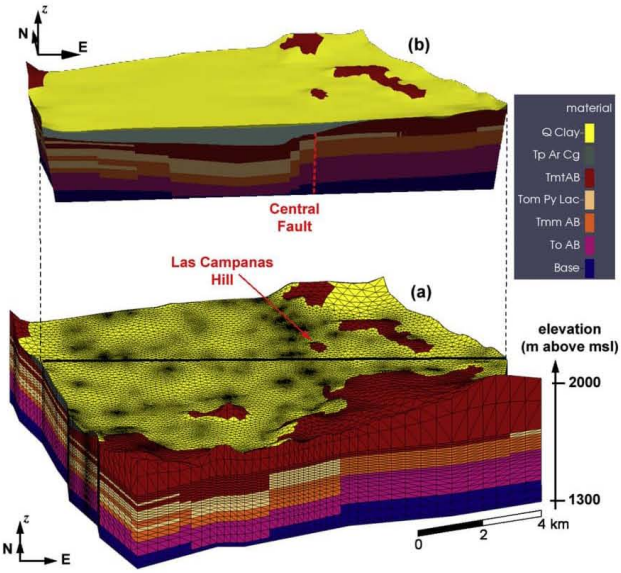

Fig. 7. (a) Perspective views of the 3D FE mesh used to carry out the flow and geomechanical simulations. (b) Vertical section of the 3D model domain along the black alignment shown in (a). The geologic units are highlighted by different colors. Note the graben-like structure between parallel normal faults and the largest Tp Ar-Cg thickness above the graben. Vertical exaggeration is 5.

previously calibrated by Carrera-Hernández et al. (2016) were used. Changes of c_M required to re-run the two models as it enters in the definition of both the specific storage (groundwater flow model) and Young modulus (geomechanical model), see Eq. (5).

The groundwater model was calibrated using the piezometric records provided in Fig. 5b and the maps of piezometric decline after Carreón-Freyre et al. (2005b). The piezometric evolution as computed by the model is shown in Fig. 8 where the maps of the head decline in 1980, 1990, 2007, and 2011 are presented. The decline peaked approximately 100 m in 2011, with a well-developed drawdown cone centered at 352′000 East and 2′278′000 North, UTM 14 N zone. Fig. 9 compares the measured and calculated drawdown versus time for one of the wells located in the critical area. The model fits satisfactorily the available measurements, particularly in relation to the main depletion cone located between 352′000–354′000 *E*-W and 2′276′000–2′280′000 N-S (dark red in Fig. 8). The largest drawdown

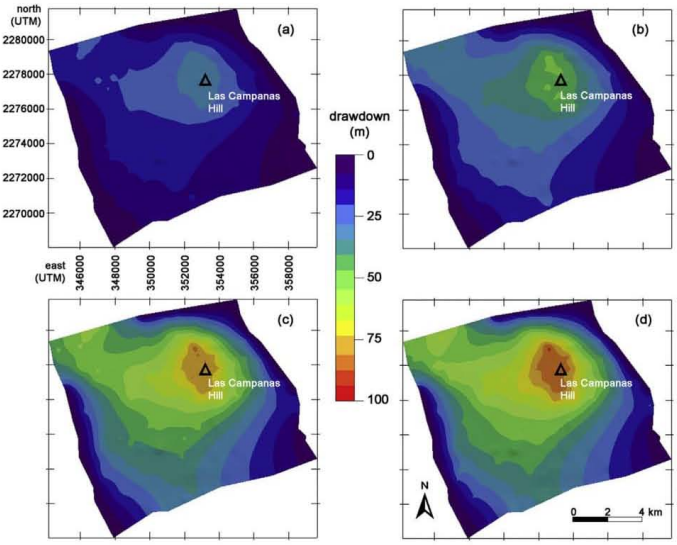

Fig. 8. Simulated piezometric drawdown from 1970 to (a) 1980 (10 years from the simulation inception), (b) 1990 (20 years), (c) 2007 (37 years), and (d) 2011 (41 years). The main depletion cone is located between 354,000–352,000 E-W and 2,278,000–2,276,000 N-S (dark red). The values refer to the shallowest layers. (For interpretation of the references to colour in this figure legend, the reader is referred to the web version of this article.)

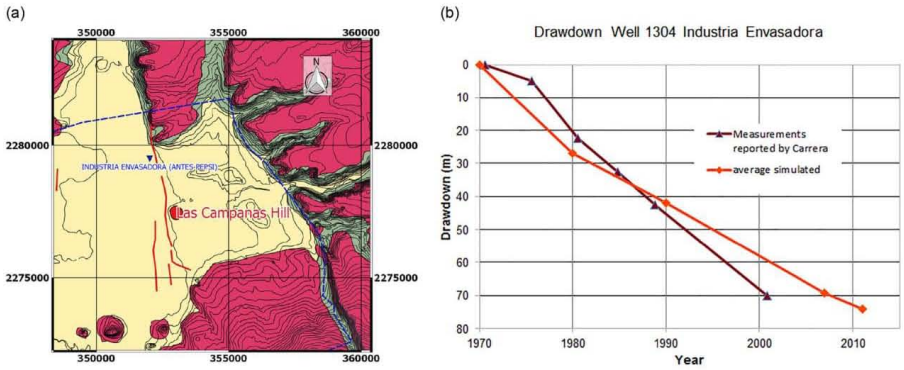

Fig. 9. Comparison between the computed and the measured drawdown at well No. 581. The location is provided in the map.

localized eastward of 352′000 E, in the east foot wall of the graben where the fractured units are located nearer to the land surface and the granular units are thinner.

Unfortunately, no long-term and extensive land subsidence records are available in the study area. The only available information has been obtained from Chaussard et al. (2014). They used SAR interferometry on a stack of ALOS images to quantify the average subsidence rates at the Querétaro Valley over the period from 2007 to 2011 (Fig. 10a). Fig. 10b shows the same amount as computed by the calibrated geomechanical model. To make the comparison straightforward, the u_x and u_z components of the simulated 3D displacement field were combined along the ALOS Line-of-Sight, which is characterized by an incident angle of 34.3°. The results match reasonably well the measurements, with a proper location of the main subsidence bowl and a maximum subsidence rate amounting to 4 to 5 cm/yr. In both the maps the subsidence extends mainly toward the western boundary of the simulated area.

Table 1summarizes the hydro-geomechanical parameters obtained from the calibration procedure. It is worth recalling that, because of the required consistency for the parameter values in the flow and geomechanical models, the calibrated c_M values allow the simultaneous match of the piezometric and subsidence measurements.

5.2. Outcome of the geomechanical model

The use of a 3D geomechanical model allows computing all the various components of the displacement, stress, and strain fields. In this section we provide a summary of relevant results on the land surface, on a plain at a specified depth, and along the vertical section shown in Fig. 7.

Fig. 11 shows the distribution of the land subsidence at 1980, 1990, 2007, and 2011. The maximum value amounted to approximately 2.8 m. The shape of the subsidence bowl differs from that of the piezometric decline (Fig. 8). These results provide evidence that land subsidence is not only related to the piezometric changes. The thickness and compressibility variability of the geologic units plays a major role. For example, the large drawdown close to the land surface within fractured volcanic rock (Tmt AB unit) in the surrounding of the Las Campanas Hill produced a relatively small land subsidence. This is because of the small specific elastic storage (yielding large drawdown) and deformability (yielding small land subsidence) of Tmt AB. Conversely, the thick granular sequences to the East of Central Fault (Tom Py-Lac and Tp Ar-Cg) mainly influence the geomechanical response of the system. The superposition of the ground rupture are with the computed subsidence maps shows that fractures developed where the maximum u_z gradient was computed.

The horizontal components u_x and u_y of the land displacement for

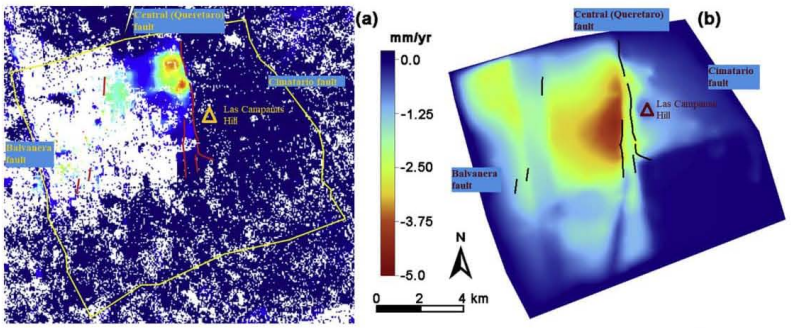

Fig. 10. Comparison between the average LoS displacement rate over the period between 2007 and 2011 (a) as measured by Chaussard et al. (2014) using SAR interferometry and (b) computed by the geomechanical model. Red (a) and black (b) lines correspond to mapped fractures in the study area, the yellow box in (a) represent the boundary of the simulated domain shown in (b). (For interpretation of the references to colour in this figure legend, the reader is referred to the web version of this article.)

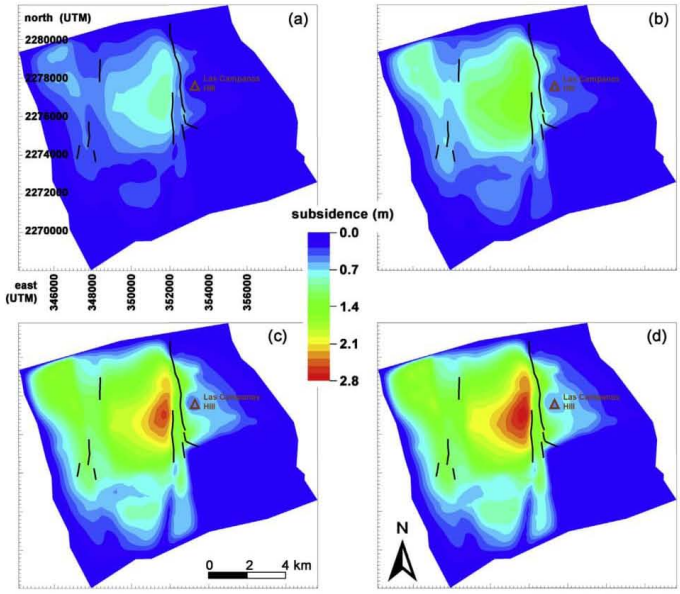

Fig. 11. Land subsidence as computed by the 3D geomechanical model in (a) 1980, (b) 1990, (c) 2007, and (d) 2011. The black alignments represent the trace of the observed ground fractures.

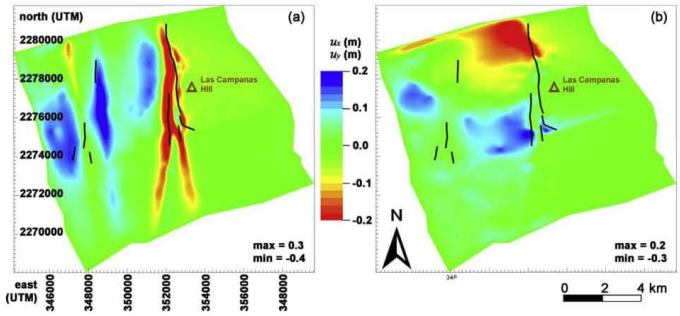

Fig. 12. (a) West-East u_x and (b) South-North u_y displacements as provided by the 3D geomechanical model at the land surface in 2011. The black alignments represent the trace of the observed ground fractures. Positive values mean eastward and northward movements in (a) and (b), respectively.

2011 are provided in Fig. 12. The two maps highlight the significant difference characterizing the pattern of the W-E and S-N displacements. The former are strongly influenced by the S-N geologic discontinuities, with the largest values assuming a band-shape located where the ground ruptures occurred. The latter develop in two large zones to the North and the South of the main subsiding bowl, with a smooth value distribution. Because of the lack of important geologic structures along the W-E direction, u_y is mainly controlled by the piezometric distribution, with movements toward the center of head drawdown.

Consistently with the available measurements (Fig. 10a), no displacement (both in the vertical and horizontal directions) takes place in the eastern portion of the study area because of the presence of the Cimatario Volcano system and the lack of compressible Tp Ar-Cg and Tom Py-Lac deposits (Fig. 7). Here a bifurcation and a slight change in direction were observed for the ground fractures (Fig. 11). The maximum values of the horizontal displacements are almost one order of magnitude smaller than the maximum land subsidence; however, the largest u_x and u_y developed where u_z is less than half of the maximum value.

The components of the displacement field along the vertical section traced in Fig. 7 are presented in Fig. 13b to d. The geological section with the trace of the Central Fault is added in Fig. 13a to help with the result interpretation. The figures confirm that u_x and u_z patterns are strongly influenced by the graben structure and the heterogeneous distribution of the compressible and stiff units.

Figs. 14 and 15 show the model results in term of stress variation (with respect to the natural stress regime) at the end of the simulation period. Fig. 14 provides the normal stress in the W-E direction, σ_x, on the land surface and on the plain at 1700 m above msl, (approximately 150–200 m below the valley surface); that approximately corresponds

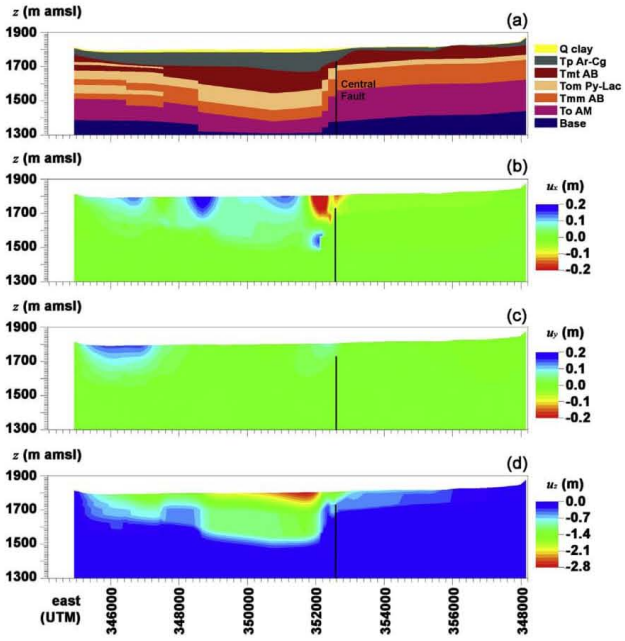

Fig. 13. (a) Geological model and (b) West-East, (c) South-North, and (d) vertical displacements as computed by the 3D geomechanical model in 2011 along the vertical section shown in Fig. 7. Positive values mean eastward, northward, and upward movements in (b), (c), and (d), respectively. The black line represents the trace of the Central Fault. The vertical exaggeration is 5.

to the boundary between the compressible To Ar-Cg and the stiff Tmt AB units. As expected, stress changes were negligible on the land surface because of the imposed traction-free condition. Conversely, large σ_x developed in depth, with an accumulation along the Central Fault. The distribution of the stress components σ_x, σ_z, and τ_{zy} along the analyzed vertical section (Fig. 7) is shown in Fig. 15. τ_{zy}, and secondarily σ_x, developed large values around the Central Fault and minor discontinuities on the western side of the graben. The horizontal stress accumulated within the stiff Tmt AB, which is overlain and underlain by the more compressible Tmt AB and Tom Py-Lac, respectively. The σ_z distribution is largely related to the pattern of the piezometric head decline. However, the geologic discontinuities strongly affect the σ_z pattern too.

Finally, Figs. 16 and 17 provide the model outcome in term of normal strain on the land surface and along the selected vertical section, respectively, as of 2011. Large (> 1‰) stretching ε_x values developed along the trace of the observed ground ruptures (Fig. 16a) and at depth along the Central Fault (Fig. 17b). Consistently with the u_y pattern (Fig. 12b), the normal strain along the S-N direction ε_y was negligible (Fig. 16b). In relation to the normal strain along the vertical direction ε_z, its pattern on the top layer resembles more the piezometric drawdown (Fig. 8d) than land subsidence (Fig. 11d), with the exception where Tmt AB outcrops (Fig. 16c). Note for example the "red dot", meaning zero deformation, corresponding to the Las Campanas Hill, in the center of the most compacting zone. Fig. 17c provides a clear picture of how deformation almost exclusively occurred in the granular units, which are approximately 2 orders of magnitude more compressible than the volcanic formations (Table 1). The vertical displacements

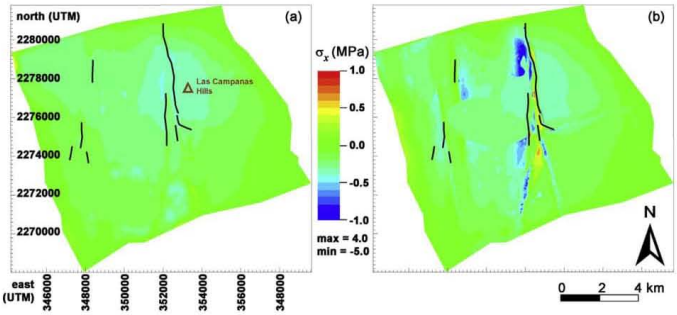

Fig. 14. West-East normal stress σ_x in 2011 as provided by the 3D geomechanical model at (a) the land surface and (b) an elevation of 1700 m above msl. Negative values mean compression, positive mean traction. The black alignments represent the trace of the observed ground fractures.

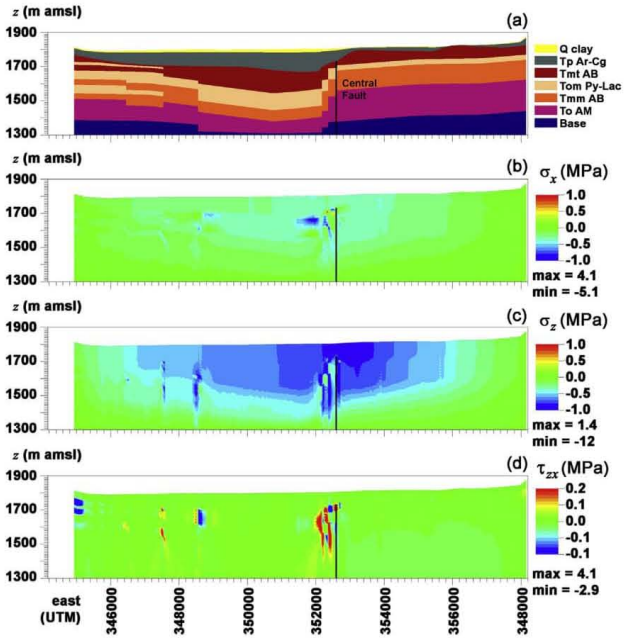

Fig. 15. (a) Geological model and (b) West-East normal stress σ_x, (c) vertical normal stress σ_z, and (d) tangential stress τ_{zx} as computed by the 3D geomechanical model in 2011 along the vertical section shown in Fig. 7. Negative values in (b) and (c) mean compression, positive traction. The black line represents the trace of the Central Fault. The vertical exaggeration is 5.

shown in Fig. 13d are the integral along z of the vertical strain (Fig. 17c) which depends on the drawdown and the compressibility of the geologic units. In the eastern part of the study area (Fig. 17c, coordinate < 348′000 E, UTM 14 N zone), where the Tom Py-Lac unit is interbedded, there are a higher thickness of granular material (Fig. 17a) and the model shows a secondary subsidence bowl (Fig. 11).

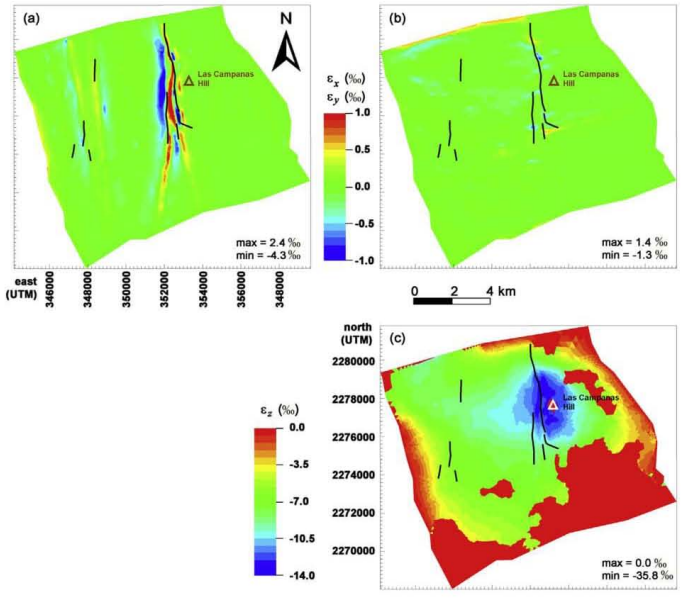

Fig. 16. (a) West-East, (b) South-North, and (c) vertical strain at the land surface in 2011. Blue (negative) colour represents squeezing. Red (positive) colour represents stretching in (a) and (b), or null strain in (c). The black alignments represent the trace of the observed ground fractures. (For interpretation of the references to colour in this figure legend, the reader is referred to the web version of this article.)

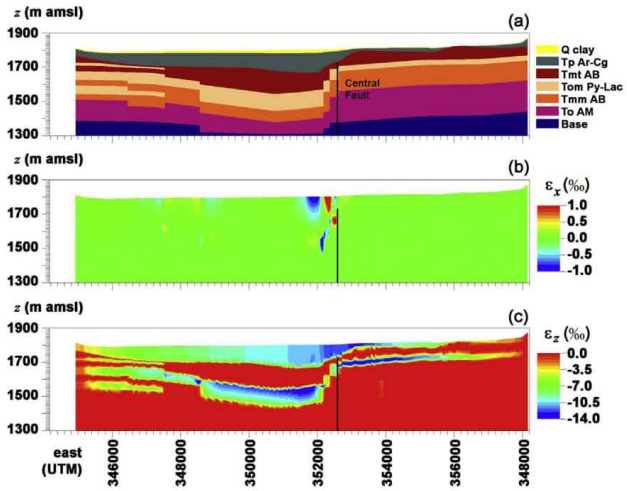

Fig. 17. (a) Geological model, (b) West-East strain, and (c) vertical strain as computed by the 3D geomechanical model in 2011 along the vertical section shown in Fig. 7. Negative values in (b) and (c) mean squeezing, positive stretching. The black line represents the trace of the Central Fault. The vertical exaggeration is 5.

6. Discussion

This paper presents a modeling investigation on the relationship between the heterogeneous distribution of the geomechanical properties and the differential deformation and stress fields in a subsiding basin, with specific reference to the Querétaro volcano-sedimentary sequences where extensive groundwater depletion is ongoing since the early 1970s. This is a complex issue that has not been addressed with detail in the literature.

The obtained results highlight the importance of using 3D geomechanical simulators when the subsiding basin is characterized by a complex geologic setting. One-dimensional modeling approaches properly describe deformation in the vertical direction and are appropriate to simulate granular multi-aquifer systems with a tabular setting. In Shanghai, for example, where the hydrogeological setting is characterized by flat clayey and sandy alluvial layers, Ye et al. (2016) showed that the main features of the deformation field are limited to the vertical direction. The use of 3D models is particularly appropriate to relate the localization of deformation with the stress fields. Our results show that thickness variations of fractured volcanic and granular units directly affect the pressure changes in the deep layers and the distribution of the displacement and deformation at the surface.

Moreover, Quaternary displacements on the N-S and E-W trending fault systems were proposed in the past (Alaniz-Alvarez et al., 2001; Zuñiga et al., 2003). Although there is not available information in their magnitude and timing, the Quaternary displacements in buried faults below the study area may have contributed to the presence of discontinuities and fractures in the sedimentary sequence. Differential compaction due to groundwater exploitation caused land subsidence in the hanging wall adjacent to the Central Fault (Chaussard et al., 2014) and vertical slip along the fractures traces producing a fault scarp. In the Central Fault the scarp formed by the vertical displacements reached up to 2 m in height over the last 30 years. The fractures and the regional extensional faults are characterized by the same geometry.

Displacements were examined in trench excavations at two sites confirming that in the surface the fault and associated fractures slipped previously within the last 25 ka, nevertheless it was assumed that most of the displacement was accommodated in the clayey layers (Carreón-Freyre et al., 2016). This suggests that compaction of unconsolidated sediments resulting from water extraction enhanced the displacement in the Central Fault, where the vertical component of the displacement in the near surface strata is > 1.0 m. This amount is equivalent to the surface subsidence recorded during the last ~ 30 years.

Slip of the fault planes may have occurred not only at the surface but also at depth. Carreón-Freyre et al. (2016) have documented the sudden rupture of groundwater extraction wells along faults or stratigraphic contacts, at depths ranging from 70 to 150 m. The evidences suggest that at different depths the faults can be in a critical stress state and any perturbation of the system equilibrium, such as pore pressure depletion, may result in vertical and horizontal displacements of the discontinuities. Consistently with the results obtained for other faulted basins (e.g., Hernandez-Marin and Burbey, 2010), the modeling output confirms this possibility and suggests that the presence of geologic discontinuities has an important role in the localization of stress changes during aquifer exploitation (Fig. 15). Another effect of the long-term fault displacements is the juxtaposition of high compressibility materials (Tom Py-Lac) and stiffer layers (Tmt AB) in the direction perpendicular to the fault plane (Fig. 17).

Finally, the model outputs suggest that the areas most affected by land subsidence are not necessarily associated with the major withdrawn, as mentioned by Bell et al. (2002). Vertical sections of the displacement and strain fields (Figs. 13 and 17) allow for a better understanding of how groundwater depletion and hydrogeological setting combine in causing different subsidence amounts. Local piezometric and deformation measurements alone cannot suffice to explain the overall recorded subsidence.

7. Conclusions

Overexploitation of groundwater resources in faulted sedimentary-volcanic basins poses severe problems to the safety of structures and infrastructures located in urban areas. Large land subsidence may develop because of the presence of very compressible alluvial and pyroclastic materials and significant differential displacements may affect the land surface because of the heterogeneous distribution of granular compressible and fractured rocky deposits. Ground ruptures may easily

occur because of fault reactivation and stress and strain accumulation along discontinuity surfaces.

Geomechanical modeling of such occurrences cannot be effectively carried out adopting the 1D vertical approach traditionally used in land subsidence studies. In this work a complete 3D model is used to understand the geomechanical processes caused by groundwater pumping in one of these basins, specifically the Querétaro Basin in Mexico. Although based on a continuous approach, which is not capable to quantify fault and rupture opening and slippage, the proposed model gives us the possibility to provide a clear picture of the 3D displacement, stress, and strain fields caused by groundwater pumping.

The major outcomes can be summarized as follows:

- land subsidence is accompanied by significant horizontal displacements of the land surface. The horizontal movements orthogonal to the discontinuity planes concentrate precisely in correspondence of the fault trace, where ground ruptures are observed;
- both the normal and shear components of the stress field changes accumulate along the discontinuity surfaces at depth. This result provides evidence that large piezometric declines can be a key factor triggering the reactivation of faults;
- significant normal strains, in particular stretching, develop on the land surface above the faults where ground rupture are more likely to occur.

To the authors knowledge, this is the first modeling study that allows making such inferences in a real three-dimensional setting. The same modeling approach can be profitably used in the future to cast light to the geomechanical processes that are affecting several other basins similar to the Querétaro Basin in Central Mexico, Iraq, Pakistan, China, and South-western USA. Geomechanical modeling studies follow the damage occurrences and are usually used to plan possible mitigation strategies. Unfortunately, land subsidence and ground rupture cannot be recovered. Taking inspiration from the outcome assessed by this study, we hope that in the near future geomechanical models will also be used proactively, i.e. to develop effective plans of sustainable use of the groundwater resources to avoid the occurrence of subsidence and ground rupture hazards.

Acknowledgments

This paper is a contribution to the International Geoscience Programme (IGCP) Project641 – Mechanisms, Monitoring and Modeling Earth Fissure generation and Fault activation due to subsurface Fluid exploitation. The funding of the Comisión Nacional del Agua (Project SGT-OCLSP-QRO-13-EP-085-RF-CC) to D. Carreón-Freyre and of the Consejo Nacional de Ciencia y Tecnología (CONACYT) to G. Ochoa-González are acknowledged.

References

Aguirre-Díaz, G.J., López-Martínez, M., 2001. The Amazcala caldera, Querétaro, central Mexican Volcanic Belt, México. Geology and geochronology. J. Volcanol. Geotherm. Res. 111, 203–218.

Alaniz-Alvarez, S.A., Nieto-Samaniego, A.F., Reyes-Zaragoza, M.A., 2001. Estratigrafía y deformación extensional en la región San Miguel de Allende-Querétaro, México (Stratigraphy and extensional deformation in the San Miguel de Allende-Querétaro region, Mexico). Rev. Mex. Cienc. Geol. 18 (2), 129–148.

Allen, D.M., Michel, F.A., 1999. Characterizing a faulted aquifer by field testing and numerical simulation. Ground Water 37, 718–728.

ASTM, 2011. 2435/2435M Standard Test Methods for One-Dimensional Consolidation Properties of Soils Using Incremental Loading. (15 pp.).

Bell, J.W., Amelung, F., Ramelli, A.R., Blewitt, G., 2002. Land subsidence in Las Vegas, Nevada, 1935–2000: new geodetic data show evolution, revised spatial patterns, and reduced rates. Environ. Eng. Geosci. 8 (3), 155–174.

Biot, C., 1941. General theory of three-dimensional consolidation. J. Appl. Phys. 12 (2), 155–164.

Burbey, T.J., 2006. Three-dimensional deformation and strain induced by municipal pumping, part 2: numerical analysis. J. Hydrol. 330 (3–4), 422–434.

Cabral-Cano, E., Dixon, T.H., Miralles-Wilhelm, F., Diaz-Molina, O., Sanchez-Zamora, O., Carande, R.E., 2008. Space geodetic imaging of rapid land subsidence in Mexico City. Geol. Soc. Am. Bull. 120 (11 – 12), 1556–1566. https://doi.org/10.1130/B26001.1.

Carreón-Freyre, D., 2010. Land subsidence processes and associated ground fracturing in Central Mexico. In: Carreón-Freyre, D., Cerca, M., Galloway, D.L. (Eds.), Land Subsidence, Associated Hazards and the Role of Natural Resources Development (Proceedings of EISOLS 2010, Querétaro, México). Red Book Series Publication 339. IAHS Press, CEH Wallingford. UK, pp. 149–157 ISBN 978-1-907161-12-4. ISSN 0144-7815.

Carreón-Freyre, D., Cerca, M., Luna-González, L., Gámez-González, F., 2005a. Influencia de la estratigrafía y estructura geológica en el flujo de agua subterránea del Valle de Querétaro. Rev. Mex. Cienc. Geol. 22 (1), 1–18.

Carreón-Freyre, D., Cerca-Martínez, M., Hernández-Marín, M., 2005b. Propagation of fracturing related to land subsidence in the Valley of Querétaro, Mexico. In: Proc. 7th Int. Symp. on Land Subsid. (SISOLS 2005, Shanghai, China). vol. 1. pp. 155–164 ISBN 7-5323-8209-5.

Carreón-Freyre, D., Cerca, M., Ochoa-Gonzalez, G., Teatini, P., Zuñiga, F.R., 2016. Shearing along faults and stratigraphic joints controlled by land subsidence and hydraulic gradient in the Valley of Querétaro, Mexico. Hydrogeol. J. 24 (3), 657–674.

Carrera-Hernández, J.J., Carreón-Freyre, D., Cerca, M., Levresse, G., 2016. Groundwater flow in a transboundary fault-dominated aquifer and the importance of regional modeling: the case of the city of Querétaro, Mexico. Hydrogeol. J. 24 (2), 373–393.

Chaussard, E., Wdowinski, S., Cabral-Cano, E., Amelung, F., 2014. Land subsidence in central Mexico detected by ALOS InSAR time-series. Remote Sens. Environ. 140, 94–106.

Conagua, 2003. Plan de manejo integrado del Acuífero del Valle de Querétaro (Integrated management plan of the aquifer of the Valley of Queretaro). In: Technical Report. Qro. Comisión Nacional del Agua, Querétaro, Mexico (150 pp.).

Franceschini, A., Ferronato, M., Janna, C., Teatini, P., 2016. A novel Lagrangian approach for a stable numerical simulation of the mechanics of faults. J. Comput. Phys. 314, 503–521.

Galloway, D.L., Burbey, T., 2011. Review: regional land subsidence accompanying groundwater extraction. Hydrogeol. J. 19, 1459–1486.

Galloway, D.L., Bawden, G.W., Leake, S.A., Honegger, D.G., 2008. Land subsidence hazards. In: Baum, R.L. (Ed.), Landslide and Land Subsidence Hazards to Pipelines. US Geol. Surv. Open-File Rep. 2008–1164, Chap. 2.

Gambolati, G., Teatini, P., 2015. Geomechanics of subsurface water withdrawal and injection. Water Resour. Res. 51, 3922–3955. https://doi.org/10.1002/2014WR016841.

Hernandez-Marin, M., Burbey, T.J., 2010. Controls on initiation and propagation of pumping-induced earth fissures: Insights from numerical simulations. Hydrogeol. J. 18 (8), 1773–1785.

Hoffmann, J., Galloway, D.L., Zebker, H.A., 2003. Inverse modeling of interbed storage parameters using land subsidence observations, Antelope Valley, California. Water Resour. Res. 39 (2), 1031. https://doi.org/10.1029/2001WR001252.

Hung, W.-C., Hwang, C., Liou, J.-C., Lin, Y.-S., Yang, H.-L., 2012. Modeling aquifer-system compaction and predicting land subsidence in central Taiwan. Eng. Geol. 147–148, 78–90.

INEGI, 2011. Censo Nacional de Población, 2010, México. Instituto Nacional de Estadistica y Geografia. National Institute of Statistics and Geography.

López-Quiroz, P., Doin, M.P., Tupin, F., Briole, P., Nicolas, J.M., 2009. Time series analysis of Mexico City subsidence constrained by radar interferometry. J. Appl. Geophys. 69 (1), 1–15.

Mahmoudpour, M., Khamehchiyan, M., Nikudel, M.R., Ghassemi, M.R., 2016. Numerical simulation and prediction of regional land subsidence caused by groundwater exploitation in the southwest plain of Tehran, Iran. Eng. Geol. 201, 6–28.

Mayer, A., May, W., Lukkarila, Ch., Diehl, J., 2007. Estimation of fault-zone conductance by calibration of a regional groundwater flow model: Desert Hot Springs, California. Hydrogeol. J. 15, 1093–1106.

Ochoa-González, G.H., Teatini, P., Carreón-Freyre, D., Gambolati, G., 2013. Modeling the deformation of faulted volcano-sedimentary sequences associated to groundwater withdrawal in the Queretaro Valley, Mexico. In: Piantadosi, J. (Ed.), MODSIM 2013 Adapting to Change: The Multiple Roles of Modelling. The Modelling and Simulation Society of Australia and New Zealand Inc. Publ., pp. 2737–2743 ISBN 978-0-9872143-3-1.

Ochoa-González, G.H., Carreón-Freyre, D., Cerca, M., López-Martínez, M., 2015. Assessment of groundwater flow in volcanic faulted áreas. A study case in Querétaro, Mexico. Geophys. Int. 54 (3), 199–220.

Pacheco, J., Arzate, J., Rojas, E., Arroyo, M., Yutsis, V., Ochoa-González, G., 2006. Delimitation of ground failure zones due to land subsidence using gravity data and finite element modeling in the Querétaro valley, México. Eng. Geol. 84, 143–160.

Rojas, E., Arzate, J., Arroyo, M., 2002. A method to predict the group fissuring and faulting caused by regional groundwater decline. Eng. Geol. 65, 245–260.

Sutter, M., Martínez, M.L., Legorreta, O.Q., Martínez, M.C., 2001. Quaternary intra-arc extension in the central Trans-Mexican volcanic belt. Geol. Soc. Am. Bull. 113 (6), 693–703.

Teatini, P., Ferronato, M., Gambolati, G., Gonella, M., 2006. Groundwater pumping and land subsidence in the Emilia- Romagna coastland, Italy: Modeling the past occurrence and the future trend. Water Resour. Res. 42, W01406. https://doi.org/10.1029/2005WR004242.

Trejo-Moedano, A., Martínez-Baini, A., 1991. Agrietamiento de suelos zona de Querétaro. Agrietamiento de Suelos, Soc. Mex. de Mec. de Suelos, A. C, pp. 67–73.

Verruijt, A., 1969. Elastic storage of aquifers. In: De Wiest, R. (Ed.), Flow Through Porous Media. Elsevier, New York, pp. 331–376.

Xu, S., Nieto-Samaniego, A.F., Alaniz-Alvarez, S.A., Cerca-Martinez, L.M., 2011. Structural analysis of a relay ramp in the Querétaro Graben, central Mexico: Implications for relay ramp development. Rev. Mex. Cienc. Geol. 28 (2), 275–289.

Yang, Y., Song, X.F., Zheng, F.D., Liu, L.C., Qia, X.J., 2015. Simulation of fully coupled finite element analysis of nonlinear hydraulic properties in land subsidence due to groundwater pumping. Environ. Earth Sci. 73, 4191–4199.
Ye, S., Luo, Y., Wu, J., Yan, X., Wang, H., Jiao, X., Teatini, P., 2016. Three-dimensional modeling of land subsidence in Shanghai, China. Hydrogeol. J. 24 (3), 695–709.
Ye, S., Franceschini, A., Zhang, Y., Janna, C., Gong, X., Yu, J., Teatini, P., 2018. A novel approach to model earth fissure caused by extensive aquifer exploitation and its application to the Wuxi case, China. Water Resour. Res. 54. https://doi.org/10.1002/2017WR021872.
Zhang, L., 2017. Evaluation of rock mass deformability using empirical methods - a review. Undergr. Space 2, 1–15.
Zuñiga, F.R., Pacheco, J.F., Guzmán-Speziale, M., Aguirre-Dıaz, G.J., Espındola, V.H., Nava, E., 2003. The Sanfandila earthquake sequence of 1998, Querétaro, Mexico: activation of an undocumented fault in the northern edge of central Trans-Mexican Volcanic Belt. Tectonophysics 361 (3), 229–238.

DISCUSIÓN

La geometría de los modelos numéricos presentados en este trabajo se construyó con base en la amplia información disponible cartográfica, litológica, piezométrica y geofísica. La cantidad de información permitió construir un modelo geométrico tridimensional que pretende integrar la complejidad del sistema acuífero en la parte central del graben de Querétaro. Los resultados obtenidos muestran que la morfología y/o geometría del sistema natural tiene un rol significativo en la distribución del abatimiento piezométrico y de la subsidencia del terreno, por lo que determina la distribución de esfuerzos en el sistema. El considerar el fallamiento regional en el modelo tridimensional permitió analizar el comportamiento hidráulico de las unidades hidroestratigráficas y registrar los cambios de niveles piezométricos.

Durante el desarrollo del trabajo de investigación los valores que se consideraron de conductividad hidráulica, almacenamiento y compresibilidad se fueron modificando al aumentar la comprensión del sistema e integrando nuevos datos. Los valores utilizados en el último modelo podrían cambiar al integrar más información sobre cambios en los niveles piezométricos. Una línea de trabajo a seguir sería la construcción de modelos a diferentes escalas para analizar el sistema bajo diferentes condiciones de frontera. Esto permitiría comprender mejor el funcionamiento regional y el local del sistema acuífero.

En el Capítulo 2 se presenta una simulación bajo las condiciones locales del norte del graben de Querétaro, considerando de manera explícita las estructuras geológicas mayores. Los resultados de ese modelo permitieron documentar una mayor sensibilidad de la simulación a la conductividad hidráulica de la falla El Nabo debió a la localización de los pozos simulados. El estudio de flujo de agua subterránea utilizando el análisis de derivadas en el mismo capítulo sugiere que hay dos sistemas diferentes de flujo en la zona norte del graben de Querétaro, uno relacionado con las calizas y lutitas de secuencias profundas (mayores a 500) y uno que transporta agua a través de los distintos sistemas de fallamiento. La diferencia de temperaturas medidas durante la prueba de bombeo en las cercanías de El Nabo también sugiere la coexistencia diferentes sistemas de flujo. En el mismo capítulo se reporta la presencia de un dique magmático emplazado en la falla de El Nabo, este emplazamiento podría haber generado mayor fracturamiento incrementado la conductividad hidráulica de la falla. Además, se presentan gradientes hidráulicos perpendiculares a los planos de falla y gradientes dentro de las mismas (generados en la simulación). Los primeros pueden ser provocados por la diferencia de carga hidráulica de las unidades adyacentes en ambos lados de la falla y los segundos pueden estar asociados a un flujo interno dentro de las fallas que funcionarían como canales. Lo anterior puede explicar por qué en algunas zonas de falla de la Ciudad de Querétaro se presenta una mayor localización de pozos de extracción de agua. También abre diferentes líneas de investigación sobre el comportamiento hidráulico de las fallas, si son canalizadoras de diferentes tipos de flujo (por ejemplo, una entrada de un flujo regional al sistema acuífero) o si podrían canalizar agua de acuíferos adyacentes o del mismo sistema, pero en una parte externa al modelo, simulado como condición de frontera (ej. alturas piezométricas fijas).

En el Capítulo 3 se estudió la relación entre los gradientes hidráulicos y el cizallamiento en pozos de extracción. Se estudiaron las variaciones locales en el estado de esfuerzos, su relación con los gradientes podría ser tema de un modelo hidráulico/mecánico local, especialmente configurado para simular la fuerza inercial del agua sobre la fase sólida de las unidades.

La variación de las propiedades de almacenamiento y compresibilidad reflejan principalmente la diferencia entre materiales granulares y fracturados, los granulares muestran una mayor capacidad de almacenamiento y por lo tanto más deformabilidad que las rocas fracturadas más rígidas. La capacidad de almacenamiento y compresibilidad de los materiales granulares también presenta diferentes magnitudes.

Los valores obtenidos de las propiedades físicas de los materiales geológicos: conductividad hidráulica, compresibilidad, almacenamiento y módulo elástico se analizaron en el Capítulo 4. Los resultados muestran que la conductividad hidráulica no depende del tipo de material, granular o fracturado, el material más permeable fue la unidad Andesitas y Basaltos del Mioceno Tardío (Tmt AB), seguido por la unidad de Areniscas y conglomerados (TP-Ar-Cg), después la unidad volcánica fracturada del Mioceno Medio (TmmAB) y los valores menores fueron de la unidad granular de piroclastos y lacustres (Tom Py-Lac) con un valor diez veces menor que el mayor. Para los valores de compresibilidad y almacenamiento si se observó una clara relación con la consideración de un material granular o fracturado, los granulares presentan el mismo orden de magnitud, así como los fracturados. La diferencia entre unos y otros es de dos órdenes de magnitud. Los resultados se observan en la tabla siguiente:

Unidad	K_h **(m/día)**	K_v **(m/día)**	c_M **(MPa^{-1})**	S_s **(m^{-1})**	E **(MPa)**	c_M / $c_{M,Qclay}$
Qarcilla (granular)	1.00	0.100	1.5×10^{-2}	1.5×10^{-4}	49	1
Tp Ar-Cg (granular)	1.00	0.100	1.5×10^{-2}	1.5×10^{-4}	49	1
Tmt AB (fracturado)	2.00	1.000	4.2×10^{-4}	5.0×10^{-6}	1786	0.03
Tom Py-Lac (granular)	0.10	0.010	2.0×10^{-2}	2.0×10^{-4}	37	1.34
Tmm AB (fracturado)	0.50	0.500	4.2×10^{-4}	5.0×10^{-6}	1786	0.03
To AB (fracturado)	0.06	0.006	2.1×10^{-4}	2.5×10^{-6}	3572	0.01
Basamento	0.01	0.010	2.0×10^{-6}	2.5×10^{-7}	364371	0.0001

Los parámetros físicos utilizados en el modelo del Capítulo 4 permitieron simular las deformaciones verticales y horizontales, así como los abatimientos y relacionar los fracturamientos con áreas de mayores esfuerzos y deformaciones. Los desplazamientos horizontales perpendiculares a fallas coinciden con la ubicación de las fracturas, así como también los esfuerzos de tensión generados. Cabe recordar que la distribución de esfuerzos y deformaciones junto con la variación de los espesores de las unidades determinan la distribución de la subsidencia, es decir, el hundimiento observado en la superficie depende de la propagación de deformación desde subsuelo.

Los resultados presentados muestran también que diferentes esfuerzos se generan en materiales con diferentes compresibilidades a ambos lados de las fallas, lo que puede provocar deformación diferencial y a su vez dar lugar a desplazamientos verticales entre las unidades granulares. De acuerdo a la distribución de esfuerzos simulada, también se podrían generar desplazamientos en contactos estratigráficos con buzamiento variable, no necesariamente vertical. Un posible efecto a largo plazo de estos desplazamientos es la yuxtaposición de materiales de alta y baja compresibilidad y de diferentes conductividades hidráulicas. Las secuencias fluviolacustres someras presentan un desplazamiento vertical de aproximadamente 1 m en superficie, magnitud equivalente a a la subsidencia regional registrada durante los últimos 30 años, los desplazamientos relativos podrían poner en contacto diferentes unidades. Las simulaciones realizadas permitieron analizar también concentraciones de esfuerzos a profundidades entre 70 y 150 m que coinciden con localización de cizallamiento de pozos reportada por la Comisión Estatal de Aguas.

Los modelos realizados permitieron distinguir variaciones verticales y horizontales en la evolución de la deformación y fracturamiento de las secuencias granulares. Se debe recordar que el carácter elástico lineal de los modelos presentados no permite estimar variaciones del abatimiento con el tiempo. En la simulación presentada en el Capítulo 4 se calcula un abatimiento piezométrico mayor al observado durante los primeros 15 años (de acuerdo con en el pozo que se utilizó de comparación), para este intervalo la diferencia de niveles piezométricos medido y simulado fue de aproximadamente 10 m, sin embargo, al final de la simulación el abatimiento medido fue mayor por aproximadamente la misma magnitud de 10 m. Las diferencias mencionadas se deben a que la respuesta de un modelo lineal no varía con el tiempo o el nivel de esfuerzos, cuando en los materiales granulares si la porosidad disminuye también disminuirá su capacidad de almacenamiento y su compresibilidad. El nivel calculado por el modelo coincide con la observación un poco antes de los 20 años de simulación (de 41 totales) debido probablemente a los cambios en la porosidad que va sufriendo el sistema al irse deformando. En un inicio el medio geológico granular tendria mayor capacidad de almacenamiento, que disminuye al incrementarse el abatimiento.

CONCLUSIONES

En el trabajo de investigación desarrollado se simuló el comportamiento hidráulico y mecánico de la parte central del sistema del Acuífero Valle de Querétaro, también denominado graben de Querétaro por sus condiciones estructurales. De acuerdo al modelo conceptual de "acuífero multicapa en compartimentos" propuesto por Carreón Freyre y colaboradores (2005) se propone que las fallas geológicas delimitan compartimentos entre los cuales el abatimiento puede ser propio a cada uno de ellos. Los abatimientos calculados y medidos difieren en no más de 10 metros para un periodo de simulación de 41 años.

Los resultados obtenidos muestran que el abatimiento de los niveles piezométricos, así como la configuración de los gradientes del agua subterránea, están controlados por el sistema de fallas y por la distribución espacial de las unidades volcánicas y sedimentarias. Este control estructural fue ser integrado en los modelos, las fallas son representadas como un truncamiento de las unidades hidroestratigáficas.

En las zonas de falla los gradientes hidráulicos pueden ser perpendiculares a sus planos principales, principalmente generados por la diferencia piezométrica entre los "compartimentos" hidráulicos que delimitan. La simulación presentada en el Capítulo 2 sugiere que puede haber una componente de los gradientes interna a la falla y con orientación paralela a su plano, funcionando como un canal preferencial de flujo. El análisis de abatimientos por medio de derivadas presentado en el mismo capítulo y la variación de las temperaturas durante la prueba de bombeo sugieren que hay dos sistemas de flujo diferentes en ese lugar, uno relacionado con la unidad formada por calizas y lutitas y otro flujo transportado a través de las fallas. El segundo podría ser un flujo de tipo regional.

Aun cuando no se modelaron las posibles entradas de flujos a través de las fallas, la observación en campo sugiere que algunas zonas de influencia de la falla permiten la entrada de flujo de modo que se han construido varios pozos de extracción. Queda como tema de investigación el comportamiento de los distintos sistemas de flujo para averiguar si provienen de un flujo regional de mayor profundidad, de acuíferos adyacentes o de otras partes del mismo sistema. Los dos últimos pueden estar incluidos en el modelo por medio de las condiciones de frontera laterales (ej. alturas piezométricas fijas).

La información del comportamiento de las unidades hidroestratigráficas y de las fallas como elementos del modelo permitió la calibración de estos modelos, pero se requiere un número de observaciones acorde al número de unidades; por ejemplo, observaciones piezométricas dentro de cada unidad hidroestratigrafica. Aún con la calibración de los modelos, los valores de conductividad hidráulica, almacenamiento y compresibilidad se va construyendo conforme se entiende el sistema y se pueden integrar datos, por lo tanto, se deben concebir como parámetros que pùeden mejorar su ajuste.

Las deformaciones calculadas simulan una compactación diferencial a ambos lados de las fallas generando un desplazamiento relativo vertical entre unidades, en contactos estratigráficos se podrían inducir deslizamientos horizontales entre unidades. Hubo coincidencia espacial entre los esfuerzos normales de tensión calculados y las zonas de fractura. Asimismo, se calcularon deformaciones a profundidades entre 70 y 150 m de profundidad, que pueden estar asociadas al

cizallamiento de pozos de extracción de agua y a las variaciones de gradientes hidráulicos calculados a profundidad.

Se han observado desplazamientos en la superficie, con su componente mayor en capas de arcillas recientes, cuyo componente vertical es de aproximadamente un metro equivalente al hundimiento de la superficie registrado durante los últimos 30 años. Los movimientos verticales calculados son equivalentes a las observaciones del desplazamiento diferencial en planos de falla y con el hundimiento de la superficie medido con percepción remota (Chaussard et al 2014).

La realización del modelo geomecánico en tres dimensiones permitió analizar la distribución de los campos de esfuerzos, y estudiar el comportamiento de las diferentes unidades hidroestratigráficas y su influencia en la localización abatimientos y las deformaciones, distinguiendo variaciones verticales y horizontales.

El modelo numérico hidromecánico utilizado permitió documentar que la deformación y el abatimiento son inversamente proporcionales. Como es de esperar, las unidades granulares son menos susceptibles al abatimiento por su mayor capacidad de almacenamiento, pero más deformables; en cambio las unidades fracturadas son más susceptibles a disminuciones piezométricas pero presentan una mayor rigidez.

El desarrollo de los modelos numericos presentados permitió documentar como las discontinuidades geológicas de distinta magnitud tienen un rol importante en la localización de los esfuerzos, que pueden resultar en el desplazamiento de discontinuidades o en la compactación diferencial a ambos lados de las fallas geológicas mayores. La variación de los espesores de las diferentes unidades también determina las condiciones de abatimiento, así como la `ropagación de la deformación hacia la superficie. En el análisis se consideró el rol de la deformación de las unidades más profundas.

En un trabajo posterior se podría simular la respuesta no lineal del sistema ya que una disminución del tamaño de los poros o fracturas y genera menor capacidad de almacenamiento y un abatimiento mayor conforme el fenómeno evoluciona.

AGRADECIMIENTOS

Información: CONAGUA Dirección local Queretaro, CEA Queretaro, Ing. Javier Gámez González, Ing. Ignacio Ortiz Villaseñor, Ing. Ignacio Barrón. Al Consejo Nacional de Ciencia y Tecnología (CONACYT).

Referencias:

Alaniz-Álvarez, S. A., Nieto-Samaniego, Á. F., Reyes-Zaragoza, M. A., Orozco-Esquivel, M. T., Ojeda-García, Á. C., & Vassallo, L. F. (2001). Estratigrafía y deformación extensional en la región San Miguel de Allende-Querétaro, México. *Revista Mexicana de Ciencias Geológicas*, *18*(2), 129-148.

Allenaan, D. M., & Michel, F. A. (1999). Characterizing a faulted aquifer by field testing and numerical simulation. *Groundwater*, *37*(5), 718-728.

Biot, M. A. (1941). General theory of three-dimensional consolidation. *Journal of applied physics*, *12*(2), 155-164.

Caine, J. S., Evans, J. P., & Forster, C. B. (1996). Fault zone architecture and permeability structure. *Geology*, *24*(11), 1025-1028.

Castle, R. F., Yerkes, R. O. y Riley, F. S. 1969. "A linear relationship between liquid production and oil-field subsidence: Tokyo", Internat. In *Symposium on Land Subsidence, Proc., I ASH and A ISH-UNESCO Pub* (No. 89, pp. 162-171).

Carreón-Freyre, D., Cerca, M., Luna-González, L., & Gámez-González, F. J. (2005). Influencia de la estratigrafía y estructura geológica en el flujo de agua subterránea del Valle de Querétaro. *Revista Mexicana de Ciencias Geológicas*, *22*(1), 1-18.

Carreon F. D., (2010). Land subsidence processes and associated ground fracturing in Central Mexico. *IAHS-AISH Publication*, *339*, 149-157.

Carreón-Freyre, D., Cerca, M., Ochoa-González, G., Teatini, P., & Zuñiga, F. R. (2016). Shearing along faults and stratigraphic joints controlled by land subsidence in the Valley of Queretaro, Mexico. *Hydrogeology Journal*, *24*(3), 657-674.

Chaussard, E., Wdowinski, S., Cabral-Cano, E., & Amelung, F. (2014). Land subsidence in central Mexico detected by ALOS InSAR time-series. *Remote sensing of environment*, *140*, 94-106.

Doherty, J. (2005). PEST Model Independent Parameter Estimation, User manual: Watermark numerical computing. 336 p.

Galloway, D. L., & Burbey, T. J. (2011). Regional land subsidence accompanying groundwater extraction. *Hydrogeology Journal*, *19*(8), 1459-1486.

Galloway, D. L., & Sneed, M. (2013). Analysis and simulation of regional subsidence accompanying groundwater abstraction and compaction of susceptible aquifer systems in the USA. *Boletín de la Sociedad Geológica Mexicana*, *65*(1).

Harbaugh, A. W., Banta, E. R., Hill, M. C., & McDonald, M. G. (2000). MODFLOW-2000, The U. S. Geological Survey Modular Ground-Water Model-User Guide to Modularization Concepts and the Ground-Water Flow Process. *Open-file Report. U. S. Geological Survey*, (92), 134.

Hoffmann, J., Leake, S. A., Galloway, D. L., & Wilson, A. M. (2003). MODFLOW-2000 ground-water model--User guide to the subsidence and aquifer-system compaction (SUB) package (No. USGS-03-233). Geological Survey Washington DC.

Hwang, J. M., & Wu, C. M. (1969). “Land subsidence problems in Taipei Basin, in Tison”. L. J., ed. *Land Subsidence, Vol. 1*. Internat. Assoc. Sci. Hydrology, Pub. 88, p. 21-734

Ochoa-González, G. H., Teatini, P., Carreon-Freyre, D., & Gambolati, G. (2013). Modeling the deformation of faulted volcano-sedimentary sequences associated to groundwater withdrawal in the Queretaro Valley, Mexico. In *MODSIM*.

Ochoa-González, G. H., Carreón-Freyre, D., Cerca, M., & López-Martínez, M. (2015). Assessment of groundwater flow in volcanic faulted areas. A study case in Queretaro, Mexico. *Geofísica internacional*, *54*(3), 199-220.

Ochoa-González, G. H., Carreón-Freyre, D., Franceschini, A., Cerca, M., & Teatini, P. (2018). Overexploitation of groundwater resources in the faulted basin of Querétaro, Mexico: A 3D deformation and stress analysis. *Engineering geology*, *245*, 192-206.

Pacheco, J., Arzate, J., Rojas, E., Arroyo, M., Yutsis, V., & Ochoa, G. (2006). Delimitation of ground failure zones due to land subsidence using gravity data and finite element modeling in the Querétaro valley, México. *Engineering Geology*, *84*(3-4), 143-160.

Rafini, S., & Larocque, M. (2012). Numerical modeling of the hydraulic signatures of horizontal and inclined faults. *Hydrogeology Journal*, *20*(2), 337-350.

Rojas, E., Arzate, J., & Arroyo, M. (2002). A method to predict the group fissuring and faulting caused by regional groundwater decline. *Engineering Geology*, *65*(4), 245-260.

Teatini, P., Ferronato, M., Gambolati, G., & Gonella, M. (2006). Groundwater pumping and land subsidence in the Emilia-Romagna coastland, Italy: Modeling the past occurrence and the future trend. *Water Resources Research*, *42*(1).

Terzaghi, K., 1923. “Die Berechnug der Durchlassigkeit des Tones aus dem Verlauf der hydromechanischen Spannungserscheinungen.” Sitzungsber. Akad. Wiss.(Wien). Math.-Naturwiss. *Kl., Abt. Iia*, *132*, 125-138.Wadachi, K., 1940. “Ground sinking in West Osaka” (second rept.) Rept. Disaster Prevention Research Institute, No. 3.

Trejo-Moedano, A., & Martinez-Baini, A. (1991). Agrietamientos de suelos en la zona de Querétaro. *Agrietamientos de Suelos. Sociedad Mexicana de Mecánica de Suelos, México*, 67-74.

UNESCO 1984. “Guidebook to studies of land subsidence due to ground-water withdrawal” Prepared for the International Hydrological Programmed Working Grpup 8.4, Joseph F. Poland. ISBN 92-3-102213-X

Xu, S., Samaniego, Á. F. N., Álvarez, S. A. A., & Martínez, L. M. C. (2011). Structural analysis of a relay ramp in the Queretaro Graben, central Mexico: Implications for relay ramp development. *Revista mexicana de ciencias geológicas*, *28*(2), 275-289.